The role of hemocytes in formation of the cardiac extracellular matrix

Danielle F. MacDuff

A thesis

Submitted to the School of Graduate Studies in Partial Fulfillment of the Requirements for the Degree Master of Science

McMaster University, Master of Science (2019), Hamilton, Ontario (Biology)

Title: The role of hemocytes in formation of the cardiac extracellular matrix

Author: Danielle MacDuff, BSc Molecular Biology and Genetics, University of Guelph

Supervisor: Dr. J. Roger Jacobs

Number of pages: 1-120

Abstract

Cardiovascular disease is a leading cause of death worldwide. Changes in the cardiac extracellular matrix (ECM) are associated with cardiac pathologies such as cardiomyopathy and cardiac hypertrophy. The ECM is a dynamic scaffold of proteoglycans, fibrous proteins, and glycoproteins that sheathes and protects many organs and tissues, including the heart, by attenuating mechanical stress. Misregulation of ECM proteins triggers changes in matrix stiffness, which can lead to age-associated and congenital heart defects. ECM rigidity is also important to the migration of cells, such as hemocytes, the invertebrate blood cells. In the embryo, hemocytes also perform fibroblast functions, through the deposition of the ECM proteins Collagen and Laminin. Hemocytes are hypothesized to be critical for ECM assembly, and by extension, for heart development. The consequences of impaired hemocyte function in the embryo and during larval growth are unknown and are the focus of this research. Using *Drosophila melanogaster* as a model, I used genetic tools to manipulate hemocyte survival and motility to assess their role in ECM organization and structure around the heart. Concerted gene knockdown and confocal microscopy techniques were employed to evaluate the effects of altered hemocyte abundance and motility on hemocyte behaviour and resulting changes to the ECM. Here I provide evidence to support a role for hemocytes in the turnover of a vital ECM protein, the Type IV Collagen Viking. I also developed a novel protocol to photobleach and observe fluorescence recovery in intact, living larvae using confocal microscopy. Recovery of fluorescence of GFP tagged ECM is a measure of the rate of ECM protein turnover during development or growth. This novel technique has allowed for assessment of recovery of Viking-GFP after photobleaching in vivo, as a measue of Viking protein turnover at the

cardiac ECM. This new technique can be employed to determine the turnover of other major ECM proteins. Combining hemocyte impairment with photobleaching provides the opportunity to observe innate protein turnover at the ECM in real time, both in normal and hemocyte-deprived matrices. Recovery of Viking-GFP fluorescence was also observed in hemocyte-deprived conditions. My findings reveal gradual recovery of Viking-GFP at the cardiac ECM in controls, and potentially slower recovery in hemocyte-impaired conditions. These observations suggest a role of hemocytes in ECM protein turnover. This work will help reveal the role of hemocytes in organizing the cardiac ECM and provides a novel technique for the *in vivo* assessment of ECM protein turnover. Ultimately, this research sheds light on how hemocyte function affects overall structure of the cardiac ECM and contributes to an enhanced understanding of how changes in this ECM influence predisposition to and progress of cardiac disease.

Acknowledgments

I would like to begin by thanking my supervisor and mentor, Dr. Roger Jacobs for agreeing to take me on as a student despite my ignorance of fly biology, and for his endless patience and undying support throughout the past two years. Thank you for always pushing me to think critically and for assuring me of my decision to pursue a career in science. I would also like to extend my gratitude to my committee member Dr. Ana Campos for her constructive criticism, attention to detail, and for being an inspiration to me as a fellow woman in science. Thank you to Dr. Jonathon Stone for consenting to act as chair for my MSc defense on such short notice.

Thank you also to members of the Jacobs lab, both past and present, particularly Duygu and Chris, for their welcoming attitude, resolute patience, and vital advice upon my joining the lab. A special thank you to Duygu for her guidance and expertise as well as for pioneering the work on hemocytes, and for giving me the opportunity to build on it. and I would like to thank undergraduate students Sam, Courtney, Mae, and Gurkamal for their help with running the lab, especially in keeping our flies alive and well. We couldn't have done it without you!

To Rachel and Katie, I would be remiss not to thank you for everything you've done. I was fortunate enough to begin this journey with you both and could never express my gratitude for your patience and thoroughness in teaching me the basics of fly pushing, and for being incredible team members in all things lab and otherwise. Thank you to Rachel for joining me (often at a moment's notice) in exploring new breweries and trying weird beers. Thank you to Katie for your calming presence and for coming along with Rachel and I on our beer excursion (even though I know you don't really like beer).

Lastly, but not the least, I would like to thank my family and friends for their encouragement and feigned interest in listening to my ceaseless ramblings about how cool microscopes and genes are. Thank you in particular to my parents Monique and Duncan for being my first and most important teachers in life. Thank you for your endless supply of love and encouragement, and for continuously inspiring me to be a better person. A final thank you goes to my partner and best friend, Karishma. I don't have the words to thank you for all you've done to help me keep my head above water. Thank you for being my therapist during my times of despair, thank you for always knowing what to say and what to do. Thank you for reminding me that life is a lot more fun if you make everything an adventure. I wouldn't be where I am without you.

Table of contents

List of figures

List of tables

List of abbreviations

DSHB	Developmental studies Hybridoma bank
DV	Dorsal vessel
ECM	Extracellular matrix
FRAP	Fluorescence recovery after photobleaching
Loh	Lonely heart
Lox	Lysyl oxidase
MMP	Matrix metalloproteinase
NGS	Normal goat serum
PBS	Phosphate buffered saline
PBST	Phosphate buffered saline with 0.3% Triton-X-100
PC	Pericardial cell
Prc	Pericardin
TIMP	Tissue inhibitor of matrix metalloproteinase
Loh	Lonely heart
Prc	Pericardin
Vkg	Viking
yw	*yellow white*

Chapter 1: Introduction

Cardiovascular disease is a leading cause of pathology and death worldwide. Understanding the mechanisms underlying these illnesses is instrumental to developing new drugs and technologies to better manage and treat diseases such as cardiac hypertrophy, dilated cardiomyopathy, and heart failure, among others (Badylak et al., 2009; Mouw et al., 2014). Several of these cardiovascular conditions arise from changes in the composition of the cardiac extracellular matrix (ECM), a network of myriad proteins that surround and protect the heart (Hughes & Jacobs, 2017). Misregulation of the cardiac ECM can have a profound impact on the heart's ability to function properly and can drastically alter an organism's quality of life and longevity (Rotstein & Paululat, 2016; Sessions et al., 2017). Of equal importance to heart integrity is the deposition and assembly of the ECM by various cell types during development, such as vertebrate fibroblasts, or hemocytes, the insect blood cells (Matsubayashi et al., 2017; Sánchez-Sánchez et al., 2017). Hemocytes have functions similar to both vertebrate macrophages and fibroblasts, and as a result perform vital immune and developmental tasks (Matsubayashi et al., 2017; Olofsson & Page, 2005). For instance, hemocytes are responsible for the targeting and destruction of foreign particles in the larva, and embryonically have also been shown to deposit key ECM proteins (Sánchez-Sánchez et al., 2017). The significance of hemocyte action in laying down the ECM at the larval stage, however, remains unexplored, and will be examined herein through the lens of the classic model organism *Drosophila melanogaster*.

The fruit fly may seem an unlikely model for the study of heart disease, but is relevant owing to the striking conservation of its genome at the sequence and functional

level compared to higher order vertebrates, including humans (Hughes & Jacobs, 2017). The availability of genetic tools for the targeted manipulation of gene expression make *Drosophila* amenable to studies of development and disease (Bodmer & Frasch, 2010; Ocorr et al., 2007).

This thesis will explore the relationship between hemocyte behavior and the integrity of the cardiac ECM. This work can be divided into two fundamental inquiries: first, we examined the role of hemocytes in deposition and organization of two major ECM proteins; Collagen IV (Viking in *Drosophila*) and Pericardin, a *Drosophila*-specific Collagen IV-like protein. To impair hemocyte function, genetic tools were used to induce apoptosis in these cells, as well as to impair hemocyte secretion and motility. The consequent effects on the cardiac ECM were then visualized microscopically. Manipulating hemocyte function to modify their behavior contributes to understanding their role in forming and shaping the ECM. However, what if hemocytes appear not to be significant in laying down the cardiac ECM in the *Drosophila* larva? Are other cell types responsible? Could it be ECM self-assembly? The latter was proposed over three decades ago but has yet to be thoroughly examined (Yurchenco & Furthmayr, 1984). ECM self-assembly can be defined as the interaction between ECM molecules to form and organize a complex and functional matrix without major input from cells thought to deposit it.

The second topic I explored is the innate turnover of proteins at the cardiac ECM through recovery of the fluorescently tagged ECM protein Viking, after photobleaching. Little is known about the rate of protein turnover at the ECM. Protein turnover is defined as a balance between protein degradation and synthesis of new protein (Hinkson & Elias, 2011). Even less is known about the role of hemocytes in ECM protein turnover. Here I

sought to understand the implications of hemocyte behaviour on Vkg recovery after photobleaching of the ECM. Fluorescence recovery after photobleaching (FRAP) is a microscopy technique commonly used in molecular biology to study the *in vivo* dynamics of protein diffusion in a cell. A major challenge was to adapt this technique and develop a novel protocol for the *in vivo* bleaching of intact third instar larvae, which has never been reported in the literature. FRAP was performed both in control larvae and in hemocyte-deprived animals to compare the recovery of Vkg-GFP when hemocyte function is impaired.

Heart development and disease is undeniably one of the most relevant and pressing health concerns of our time. It is vital to understand the molecular mechanisms that underlie development and pathology of this crucial organ in order to provide better care for those suffering from heart defects and disorders. Research using simple genetic models such as *Drosophila melanogaster* is the first step toward furthering our comprehension of cardiogenesis and heart pathology throughout development, and over time, will help develop better tools and technologies to prevent and treat cardiac illnesses.

1.1 The *Drosophila* dorsal vessel (DV)

The *Drosophila* heart, or dorsal vessel (DV) is a tubular structure located beneath the dorsal epidermis (Lehmacher et al., 2012). The *Drosophila* heart is divided into two sections; the anterior aorta and the posterior heart chamber (Rotstein & Paululat, 2016). A pair of intracardiac valve cells separates the aorta, which is narrow in luminal diameter and does not develop incurrent openings at embryonic and larval stages, from the heart chamber, which has a much wider luminal diameter (Lehmacher et al., 2012; Zaffran et al., 1995). At the larval stage, seven pairs of alary muscles arise from myoblasts, connecting

the heart to the epidermis, thereby creating a flexible heart suspension system (Bataillé et al., 2015; LaBeau et al., 2009; Rizki, 1978). Only four pairs of posterior alary muscles remain in the adult (Rizki, 1978). The DV is flanked by two cell types: the large pericardial cells (PCs), and cardiomyocytes (Ivy et al., 2015; Zaffran et al., 1995). Embedded within the cardiac extracellular matrix (ECM), PCs eventually differentiate into the distinct cell types nephrocytes or wing hearts (Das et al., 2008; Ivy et al., 2015; Tögel et al., 2008; Tutor et al., 2014). They are also key members of the *Drosophila* excretory systems, along with garland cells and Malpighian tubules (Rotstein & Paululat, 2016). PCs are responsible for the endocytosis of effete cells, extracellular debris, and macromolecules (Ivy et al., 2015; Weavers et al., 2009). These cells have also been shown to filtrate hemolymph, similar to mammalian reticuloendothelial cells (Tutor et al., 2014; Zhang et al., 2013; Zhuang et al., 2009). Lastly, PCs of the embryo express and secrete ECM proteins, thus contributing to the formation of the basement membrane (BM), a thin layer of ECM found around organs as well as between the epithelia and endothelia (Drechsler et al., 2013).

There are three types of cardiomyocytes: contractile cardiomyocytes that line the heart chamber (Jagla et al., 1997; Schaub et al., 2015), intracardiac valve cells that are bilaterally located at the valves separating the heart chambers (Lehmacher et al., 2012), and ostia, found at inflow openings of the heart (Molina & Cripps, 2001). Contractile cardiomyocytes work together to produce the peristaltic movement of the heart wall that pumps hemolymph into the cardiac lumen. At the embryonic and larval stages, 104 cardiomyocytes comprise the heart tube, but only 84 remain in the adult (Sellin et al., 2006). This is the result of histolysis and remodeling that occurs during metamorphosis (Sellin et al., 2006).

In early development, the DV resembles the mammalian heart before the latter undergoes cardiac looping (Bataillé et al., 2015). Cardiogenesis begins in the embryo, where two bilateral rows of cardiomyocytes migrate toward each other to form the lumen, which together with ostial and pericardial cells, forms the heart tube (Bataillé et al., 2015; Ivy et al., 2015; Rotstein & Paululat, 2016). A beating heart marks the end of embryogenesis, where cardiomyocytes begin to contract, pushing hemolymph from the posterior heart chamber into the aorta, where it leaves the heart tube and fills the open body cavity (Rotstein & Paululat, 2016). Although heart formation takes place in embryogenesis, the larval stage of the *Drosophila* life cycle is a critical time for growth at both the organismal and cellular levels (Rotstein & Paululat, 2016). In fact during larval development the organisms increases roughly five times in size (Bogatan et al., 2015). Growth of the heart is unique in that it retains the same number of cells it had in embryogenesis: maturation occurs through cell growth, as opposed to proliferation (Bataillé et al., 2015; Zaffran et al., 1995). Cardiomyocytes increase in size and elongate and they form more myofibrils and also cause the lumen diameter to expand (Zaffran et al., 1995). Heart development in the larva is mirrored by substantial remodelling of the cardiac ECM (C. J. R. Hughes & Jacobs, 2017). During pupation, the heart undergoes distinct differentiation processes that differentiate the larval heart from the adult heart. To name a few: the formation of new ostia, which are incurrent openings (Molina & Cripps, 2001; Wasserthal, 2007), differentiation of other cardiac valves (Lehmacher et al., 2012; Sellin et al., 2006) and of the ventral longitudinal muscle (VLM) layer underneath the heart tube (Schaub et al., 2015; Shah et al., 2011). Other processes include remodeling of the terminal heart chamber and the formation of neuronal innervations (Dulcis & Levine, 2003).

Conservation exists between invertebrates and vertebrates with regard to the molecular mechanisms underlying cardiogenesis as well as function of proteins such as Collagens, Laminins, and Integrins (Cammarato et al., 2007; Wolf et al., 2006). Often, mutations in *Drosophila* orthologue proteins sequences produce phenotypes that parallel those seen in mammalian cardiac dysfunctions (Viswanathan et al., 2014). This provides the opportunity to expresses mutant forms of human cardiac proteins in the fly to model heart disease (Cammarato et al., 2007; Wolf et al., 2006).

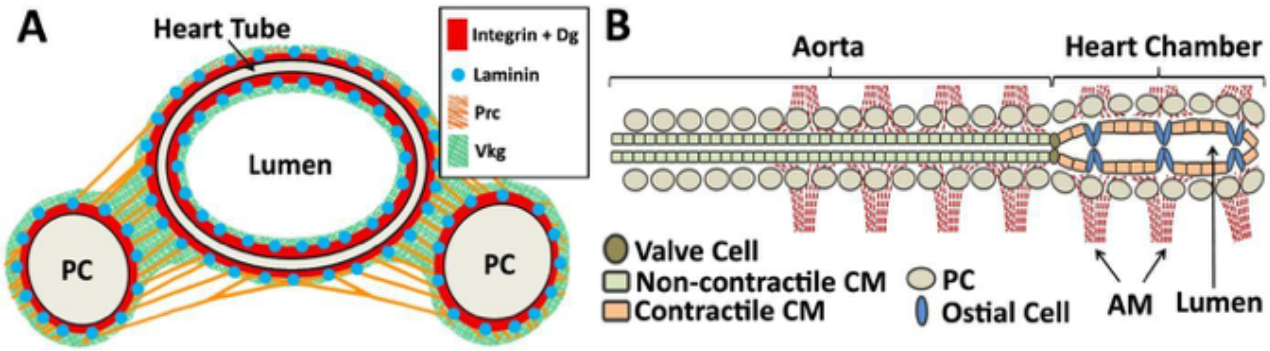

Figure 1.1: Schematic of the *Drosophila* heart. (**A**) Cartoon cross sectional view of the heart flanked by pericardial cells. The transmembrane receptors Integrin and Dystroglycan (Dg) are located along the luminal domain and at the abluminal surfaces of the heart. Laminin is ubiquitous. Vkg (Collagen IV) is found along the basal lamina. Vkg also localizes at lower levels inside the heart lumen. Prc is absent from the heart lumen. Dorsal at top. (**B**) Longitudinal view of the aorta and heart proper, divided by valve cells. Non-contractile cardiomyocytes comprise the aorta. The wider heart chamber is formed by contractile cardiomyocytes and non-contractile ostial cells. Anterior at left. AM: alary muscle; CM: cardiomyocyte. (Adapted from Hughes and Jacobs, 2017).

1.2 The extracellular matrix (ECM)

Extracellular matrices are essential to the structure and function of many organs, including the heart (Badylak et al., 2009). In general, ECMs have important roles in regulating the development, function and homeostasis of all eukaryotic cells (Lu et al., 2011; Mecham, 2001; Mouw et al., 2014; Rozario & DeSimone, 2010). They connect to and protect the intercellular regions between these organs and their tissues, and act as scaffolds to organize cells, transfer tension, and regulate repercussions of mechanical stress (Hughes & Jacobs, 2017). ECMs therefore provide physical support for cells, participate in separating and maintaining differentiated tissues and organs by modulating the concentration of growth factors and receptors, as well as the level of hydration and the pH of the local environment (Mouw et al., 2014). These diverse and physiologically crucial functions are possible due to the ECM's complex composition and organization .

1.2.1 ECM composition

The primary constituents of the ECM are water, proteins and polysaccharides (Mouw et al., 2014). However, the composition and topology of ECMs vary depending on tissue-specific needs established in early development (Frantz et al., 2010). Tissue specificity arises from unique ECM compositions and topographies created by biochemical and biophysical interactions of cells that make up tissues and their microenvironment (Mouw et al., 2014; Naba et al., 2012). For example, the ECMs surrounding tendons, ligaments and cartilage are rich in Collagens and thus are very fibrillar, which allows for the transmission and absorption of tensile forces while avoiding damage (Birk et al., 1997; Wang, 2006). In contrast, the basal lamina is a layer of the basement membrane comprised of interconnected Collagen IV and VII polymers, as well as Laminins bound to Nidogen

glycoproteins and heparan sulphate proteoglycans (HSPGs) (Martin & Timpl, 1987). The basal lamina is usually assembled near cell surfaces and is comprised of cell-adherent sheet-like layers that act to regulate communication between cells within a tissue, and cells with their environment (Yurchenco, 2011). In addition to its function as a site for cell adhesion, this ECM also plays the role of protecting tissues form biochemical and biophysical stresses (Hay, 1993; Yurchenco, 2011). A third class of ECM are the proteoglycan-rich matrices of the brain. Proteoglycan-rich ECM is also located in cartilage and in the CNS and are far less organized that ECMs of other tissues. Instead, proteoglycan-rich ECMs such as that in the brain are often characterized by amorphous protein aggregates, similar to the proteoglycan component of cartilage _. Fibrous proteins such as Collagen and Fibronectic are found in the brain ECM but do not make up the majority of its constituents. Most of the brain ECM is comprised of hyaluronic acid, proteoglycans, and GAGs (Mouw et al., 2014). Like all types of ECM, the brain ECM serves to provide structural support for cells of the organ. However, the brain ECM is unique in that it is also critical to the formation of perineuronal nets (PNNs) and is therefore essential to brain function (Kwok et al., 2011; Wang & Fawcett, 2012). PNN formation is synced with termination of plasticity in the developing brain, which is known as the 'critical period (Kwok et al., 2011; Wang & Fawcett, 2012). On the other hand, composition of the ECM around neurons, including matrix stiffness and density, can hinder their growth at the end of development (Yamaguchi, 2000).

Although there exist specialized ECMs for different tissues, two main classes of macromolecules comprise the ECM: fibrous proteins (including collagens and elastins) and glycoproteins (including fibronectin, proteoglycans (PGs) and laminin) (Mecham, 2001).

The most important fibrous proteins are collagens and elastins, which are considered structural proteins (Frantz et al., 2010). The glycoproteins Laminins, their Integrin receptors, as well as the vertebrate-specific Fibronectin are classified as specialized proteins (Wiradjaja et al., 2010). PGs, which include the proteins Perlecan (Trol in *Drosophila*), and mammalian proteins Collagen XVIII and Agrin serve more diverse roles by aiding in structural support and allowing for matrix flexibility (Frantz et al., 2010; Rienks et al., 2014). They also make up the basement membrane, a thin layer of ECM. Collagens constitute a significant portion of the ECM and are the most abundant in the body (Mouw et al., 2014). The composition of an ECM can change for various reasons. Stimuli from the environment such as physical force or injury can cause remodeling of the ECM, which helps maintain tissue homeostasis and represents a response to physical stress and disease (Bonnans et al., 2014; Humphrey et al., 2014; Jakeman et al., 2014; Lu et al., 2011; Mouw et al., 2014). ECM remodeling will be observed later in this chapter.

1.2.2 Collagen

Collagen arises from Procollagen, which undergoes processing in the ER and Golgi apparatus, before being packaged into secretory vesicles and cleaved in extracellular space to allow assembly of collagen fibres (Mouw et al., 2014). Stable supramolecular collagen is formed through the crosslinking of collagen molecules by the enzyme lysyl oxidase (Hulmes, 2002; Hulmes, 2008; Myllyharju & Kivirikko, 2004). Fibrillar Collagen is characterized by a triple helix three-dimensional structure that arises from multiple levels of coiling to form fibrils and leads to distinct mechanical properties within the ECM (Mouw et al., 2014). The structure and biophysical properties of Collagen are also modified by incorporation of proteoglycans into Collagen fibrils (Myllyharju & Kivirikko, 2004). This

results in various fibril compositions and structures that differ at tissue and stage-specific levels (Wess, 2005). Different collagen fibrils are therefore amenable to unique biochemical, biomechanical, and structural functions (Wess, 2005; Wu & Crane, 2019). The complex self-assembly results in a multi-ordered collagen structure possessing binding sites for other proteins and cells (Wu & Crane, 2019). The dynamic assembly and organization of collagen is key to the mechanical integrity of the ECM (O'Leary et al., 2011).

1.2.3 Proteoglycans

Proteoglycans constitute the foundation of higher order ECM structures surrounding cells (Mouw et al., 2014). The hallmark characteristic of proteoglycans is their ability to bind water and therefore provide the ECM with hydration and compressive resistance due to the presence of glycosaminoglycans (GAGs) (Mouw et al., 2014). As a result proteoglycans are found in high concentrations in cartilage and neural ECM (Bandtlow & Zimmermann, 2000; Knudson & Knudson, 2001). GAG types include heparin sulfate, chondroitin sulphate, dermatan sulfate, hyaluronan and keratin sulfate (Cui et al., 2013; Deepa et al., 2006; Simon Davis & Parish, 2013; L. Zhang, 2010). Different proteoglycans have specialized roles in ECM integrity. Heparan sulfate proteoglycans (HSPGs) for example are abundant in the basement membrane (Mouw et al., 2014). They have highly negative charges that permit their binding to proteins such as Laminin, Fibronectin and cell surface receptors such as Syndecan (Bishop et al., 2007; Johnson et al., 2004; Wade et al., 2014). Due to their distinct and widespread binding affinities, proteoglycans are important in regulating cell growth and migration (Bishop et al., 2007; Maeda et al., 2011).

1.2.4 Laminins

Laminins are a group of glycoproteins that are abundant in certain mesenchymal compartments, as well as in the basal lamina, a layer of the basement membrane within the ECM that is secreted by epithelial cells (Mouw et al., 2014). They are made up of alpha, beta, and gamma chains that exist in a great number of heterotrimeric conformations (Timpl & Brown, 1994). The interactions of other proteins with the modular domains of laminins control cell-cell communication through cell surface receptors like Integrins and Dystroglycan and other ECM proteins such as Nidogens (Entactins), Perlecans and Collagens (Timpl & Brown, 1994).

1.2.5 Fibronectin

Fibronectin is a large secreted ECM protein that is assembled into fibrillar structures around cells, and is found exclusively in vertebrates (Singh, Carraher, & Schwarzbauer, 2010). Type I, II, and, III structural modules comprise each fibronectin subunit, and contain binding motifs to mediate binding between fibronectin and cell surface receptors such as integrins, Collagen, and Gelatin (Kreis & Vale, 1999; Singh et al., 2010).

1.2.6 ECM assembly and organization

Understanding assembly of ECM macromolecules into functional 3D structure is necessary to comprehend cellular differentiation, tissue morphogenesis, and physiological remodeling (Lu et al., 2011; Rozario & DeSimone, 2010). The specialized composition and organization of ECM vary from tissue to tissue. For example, the ECM of tendons, which have highly mechanical function and must withstand physical strain, is rich in fibrillar collagen (Wu & Crane, 2019). On the contrary, the basal lamina is an ECM that is non-fibrillar and protein-rich (Mouw et al., 2014). It is made via the cell-adherent layering of

ECM molecules in a sheet-like conformation (Kalluri, 2003; Martin & Timpl, 1987; Paulsson, 1992). It provides support for epithelial, endothelial, muscle and fat cells, the CNS, and the Schwann cells of peripheral nerves (Kalluri, 2003; Martin & Timpl, 1987; Paulsson, 1992). The basal lamina therefore serves to protect tissues from biochemical and biophysical stressors, as well as regulate communication between cells within a tissue and cells with their environment (Yurchenco, 2011). The basal lamina is not to be used interchangeably with the basement membrane, which includes the basal lamina and the reticular lamina (Sanes, 2003). Conception of the reticular lamina is directed by connective tissue cells, such as fibroblasts (Sanes, 2003). Conversely, the basal lamina is primarily secreted by cells of the tissue it surrounds (Yurchenco, 2011). This raises the issue of ECM 'self-assembly' and whether this concept takes place across species.

The process of ECM assembly is well conserved between species. First, ECM ligands such as Laminin, are secreted by cells that comprise the template for the basal lamina (BL). These ligands can then bind their transmembrane receptors such as integrins and dystroglycans (Hynes, 1992). As such, the meshwork-forming proteins Laminin and Collagen IV become anchored and form the basis of the ECM (Rotstein et al., 2018). Interactions between these proteins generates a the dynamic meshwork that is the ECM, which is then reinforced by Nidogen (Kohfeldt et al., 1998). Nidogen also allows for the binding of additional proteins to the matrix, such as Perlecan (Kohfeldt et al., 1998; Timpl, 1996). Different ECMs comprise variations in the quantity, identity, assembly, and organization of ECM macromolecules. This results in differences in the abilities of ECM molecules self-assemble based on interactions with other ECM components, to bind different growth factors and chemokines, as well as to variations in the formation of

adhesive surfaces. In fact, ECM components are seldom found as individual units but rather as supramolecular structures with a range of identities and abundances. The different ECMs macromolecules are thus vital to the signaling that determines cell behaviour, to the physical support of cells, as well as to the balance between ECM flexibility and rigidity (Rowe & Weiss, 2008; Schaefer & Schaefer, 2010; Rotstein & Paululat, 2016).

1.2.7 The cardiac ECM

Like all other ECMs, the cardiac ECM is a dynamic network that serves to support and protect one of the body's most important organs: the heart. A few ECMs types have been explored in the previous section, however the emphasis in this section is specifically on the vertebrate cardiac ECM. It comprises many of the structural proteins described earlier such as Laminin, Collagen, Fibronectin, and Elastin, as well as several non-structural glycosylated proteins, namely glycoproteins, proteoglycans, and glycosaminoglycans (Rienks et al., 2014).

ECM integrity depends on protein composition as well as on the organization of those proteins. The quantity and arrangement of ECM proteins varies based on tissue-specific needs and fluctuates with age and pathology. An important characteristic of the cardiac ECM is elasticity, which is needed to allow flexibility during heart contractions (Rotstein et al., 2018). Another important biomechanical characteristic of the heart ECM is its ability to withstand the incessant forces produced by heart contractions throughout the organism's life (Pelouch et al., 1993). ECM is found in all tissues of the vertebrate heart, though composition of these ECM types within the heart change in a spatial and temporal-dependent manner as they develop, remodel, and mature (Lockhart et al, 2011). The specific functions of many ECM molecules has not yet been revealed, but several of them

have implication in congenital heart disease in both animals models and humans (Rienks et al., 2014). These disorders include cardiodilation, arrhythmia, cardia bifida, and myocardial infarction among many others (Hughes & Jacobs, 2017).

1.3 *Drosophila melanogaster* as a model

The fruit fly is a popular model of pathology and development due to its short generation time, ease of culture, and established genetic tools (Hughes & Jacobs, 2017). Many gene families, such as Integrins, have fewer members in *Drosophila* than they do in humans or mice, which enables targeted manipulation of specific genes or gene families (Ezkurdia et al., 2014).

There is also remarkable genetic conservation of organ development, including the heart, between *Drosophila* and vertebrates (Ocorr et al., 2007). Another benefit of using *Drosophila* to study heart development and function is the capacity to conduct live imaging. Fluorescence microscopy can be used to observe the internal structures of larvae, as well as cardiogenesis in the embryo, through the translucent cuticle (Bogatan et al., 2015; Raza & Jacobs, 2016), and optical coherence tomography (OCT) allows visualization of more opaque components (Bogatan et al., 2015; Wolf et al., 2006).

Mammalian models of disease present many challenges due to complexity of protein interactions and functions, and well as redundancy (Hughes & Jacobs, 2017). In humans it can also be difficult to understand heart disease for this reason. Because the *Drosophila* genome encodes fewer proteins it is easier to observe effects of manipulating protein function and the resulting impact on heart function (Bier, 2005; Bodmer & Frasch, 2010).

1.3.1The *Drosophila* cardiac ECM

This work focuses on the cardiac ECM of *Drosophila melanogaster,* which is similar in function and composition to mammalian ECMs (Sessions et al., 2017). The ECM of the *Drosophila* heart is a three dimensional network of structural and non-structural proteins that sheathes the heart (Hughes & Jacobs, 2017). However there exist major differences in the *Drosophila* cardiac ECM; such as the fact that it connects the beating heart to the epidermis through specialized alary muscles (Rotstein & Paululat, 2016; Volk et al., 2014). The fly ECM also comprises the *Drosophila* and heart-specific protein Pericardin and its receptor Lonely heart (Loh) (Drechsler et al., 2013; Rotstein et al., 2018; Frantz et al., 2010). Pericardin is a type IV collagen-like protein secreted by pericardial nephrocytes and adipocytes into the hemolymph (Drechsler et al., 2013). The adaptor protein Loh, found exclusively at the surfaces of the heart and chordotonal organs, acts to recruit Prc to the cardiac ECM, where Prc immediately begins to form a stable network (Drechsler et al., 2013; Rotstein et al., 2018). In fact, recent research has suggested that the role of Prc in the cardiac ECM is to provide the heart with structural integrity, as opposed to contributing to tissue flexibility (Rotstein et al., 2018). Loss of either Prc or Loh leads to heart collapse and dissociation of the PCs and alary muscles with the heart. As a result the organism experiences diminished fitness and a reduced lifespan (Drechsler et al., 2013).

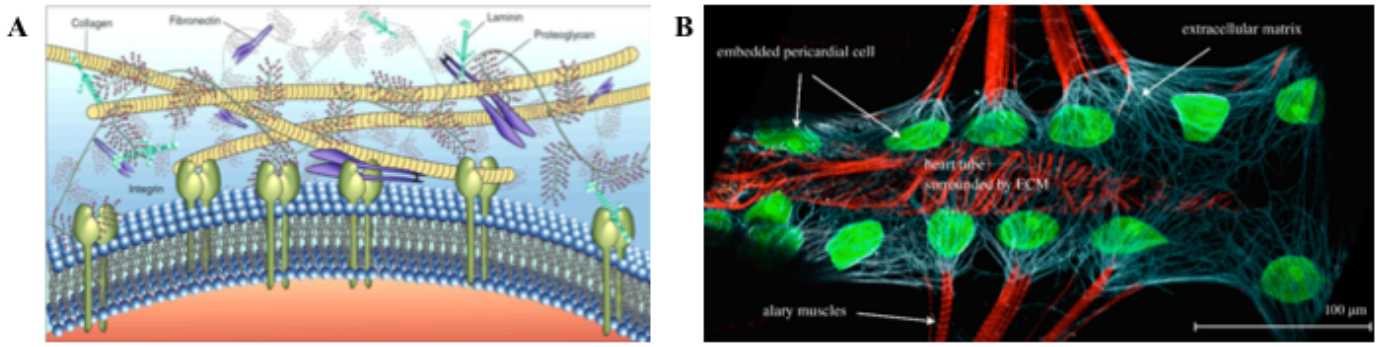

Figure 1.2: Composition and structure of the *Drosophila* ECM. (**A**) Protein composition of the ECM. Collagen, Laminin, Fibronectin, and Proteoglycans are all major constituents of the ECM. Fibronectin is only found in the vertebrate ECMs. (Adapted from John Wiley and Sons, 1999). (**B**) Dissected and fixed image of the *Drosophila* larval cardiac ECM. The heart tube (muscle, in red) is flanked by pericardial cells (green) and is sheathed by ECM (light blue). (Adapted from Rotstein and Paululat, 2016)

1.3.2 ECM remodeling

ECM remodeling in vertebrates and invertebrates occurs as a normal part of development as well as with age, ischemia, and pressure overload and stems from changes in the deposition and degradation of ECM proteins (Heymans, 2006; Sessions et al., 2017). It is an adaptive response to mechanical stress or hormonal stimulus that leads to changes in ECM composition and heart function (Rienks et al., 2014). Remodeling of the ECM can be defined as the balance between at least two phenomena: protein synthesis and concurrent protein degradation (Frantz et al., 2010; Stamenkovic, 2003). Several different protease families are involved in this process, most famously matrix metalloproteinases (MMPs) and their inhibitor, tissue inhibitor of matrix metalloproteinases (TIMPs) (Hughes & Jacobs, 2017; Wiradjaja et al., 2010). Together these enzymes act to maintain a balance of protein synthesis and degradation, which is essential for normal development (Hughes & Jacobs, 2017). Another important enzyme in ECM homeostasis is Lysyl oxidase (LOX), a secreted copper-dependent amine oxidase (Kim et al., 2014). Once secreted by migratory cells such as fibroblasts, LOX acts to crosslink ECM Collagens as well as the vertebrate protein Elastin (Frantz et al., 2010). Crosslinking results in increased ECM stiffness and promotes integrity and robustness of the overlying tissue (Wang et al., 2017).

Misregulation of ECM regulator enzymes MMPs, TIMPs, and LOX, as well as ECM proteins such as, Viking (Drosophila Collagen type IV), Laminin, their cell surface receptor Integrin, and Pericardin can lead to cardiac disorders such as systolic heart failure (SHF), dilated cardiomyopathy (DCM), and hypertrophy (Wiradjaja et al., 2010; Frantz et al., 2010). Overexpression of LOX can also favour the cell migration through stiffening of the ECM, a characteristic of many cancers (Wang et al., 2017). Furthermore, the age-

associated increase of collagen deposition leads to a type of fibrosis, the pathological stiffening of the ECM that decreases the heart's ability to contract (Hughes & Jacobs, 2017; Wiradjaja et al., 2010). Differential regulation of collagens, therefore, leads to altered physiology of cardiac muscle, such as stiffening, as well as heart dysfunction (Hein et al., 2002; Lieber et al., 2004). Furthermore, upregulation of BM proteins produces a thickened BM and consequently a more rigid ECM, thereby obstructing heart contractility (de Castro Brás et al., 2014). On the other hand, cardiac-specific knockdown of ECM proteins Pericardin, Laminin A, and Collagen IV (Viking in *Drosophila*) in *Drosophila* has been shown to ameliorate heart contractility and circumvent age-related heart tube restriction (Kim et al., 2016). Decreased LanA expression is associated with general maintenance of contractile velocity over time and lengthening of lifespan (Sessions et al., 2017).

ECM composition is not only important in early development, but throughout the life of an organism. This research centers on ECM formation at the third instar stage in *Drosophila* larvae as this is a time of tremendous growth for both the heart and the organism as a whole. Despite the importance of understanding how the proteins are produced and crosslinked to form a network, little is known about ECM assembly and organization at this stage. Turnover of matrix proteins is another key to uncovering the mechanisms of matrix maintenance in vivo and will be explored throughout this work. ECM protein composition and homeostasis are relevant to heart performance but are also vital to the migration of various cell types during cancer metastasis and development, including hemocytes, the *Drosophila* blood cells.

1.4 Hemocytes

Hemocytes are insect blood cells that, like vertebrate macrophages, are integral to the immune response (Gyoergy et al., 2018). Another function of hemocytes, and the reason they are of interest to this research, is their secretion of ECM proteins (Cevik et al., 2019; Sánchez-Sánchez et al., 2017). This behaviour has been observed in the embryo but has never been reported for larval hemocytes. In our lab, larval hemocytes have been observed in close association with the heart, providing some evidence for a relationship between immune function and circulation (Cevik, 2016; Sigle and Hillyer, 2018). The deposition of cardiac ECM proteins by hemocytes may also help explain their relationship with the larval heart (Cevik, 2016; Cevik, Acker, Arefi, et al., 2019). Impairing hemocyte function can lead to severe developmental defects, including unstable ECM networks and consequent failure to develop normal tissues. Because hemocytes have been shown to deposit the ECM proteins Collagen IV, Laminin, and Papilin in the developing embryo, they may also have a hand in cardiac ECM formation and integrity in larvae (Olofsson & Page, 2005).

1.4.1 Hemocyte lineages

In *Drosophila*, there are three types of hemocytes, each with distinct functions. Plasmatocytes, which account for most circulating hemocytes, phagocytose small particles and are capable of differentiating into another hemocyte type, crystal cells (Honti et al., 2014; Letourneau et al., 2016). Crystal cells represent close to 5% of circulating hemocytes and direct the melanisation of invaders, working together with lamellocytes, the largest and rarest of the hemocytes (Krzemien, Oyallon, Crozatier, & Vincent, 2010; Lamiable et al., 2016). Lamellocytes are flat cells specialized to encapsulate and neutralize large items such

as parasitic wasp eggs, and generally only appear under conditions of immune stress (Lamiable et al., 2016; Letourneau et al., 2016; Nappi & Vass, 1998). Plasmatocytes have also been shown to deposit the ECM proteins Collagen, Laminin, and Papillin in the Drosophila embryo, and will therefore be the focus of this research (Gyoergy et al., 2018; Honti et al., 2014). Hemocytes are therefore critical components of the cellular immunity, wound healing, and embryonic development. Moving forward, hemocytes and plasmatocytes will be used interchangeably.

1.4.2 Hematopoiesis

Hematopoiesis is defined as the production of blood cells, or in this case, hemocytes, which originate from a progenitor cell type known as prohemocytes in the head mesoderm (Krzemien et al., 2010). Hematopoiesis occurs in two waves during development, the first of which occurs in early embryogenesis (Gyoergy et al., 2018; Letourneau et al., 2016; Matsubayashi et al., 2017). Embryonic plasmatocytes and crystal cells are produced and circulate in the hemolymph, undergoing directed migration to colonize the embryo (Honti et al., 2014). At the larval stage, these cells accumulate in 'hematopoietic pockets' (HPs), segmentally repeated niches for sessile hemocytes located dorsally between the epidermis and the muscle of the body wall between segments A1-A7 (Leitão & Sucena, 2015; Makhijani et al., 2017). HPs are found at the lateral midline and at the second and third instar stages, form 'stripes' that reach toward the dorsal midline (Makhijani et al., 2011).

The larval lymph gland is where the second wave of hematopoiesis occurs (Gyoergy et al., 2018). The lymph gland is attached to the anterior end of the heart and grows with it throughout development (Lebestky, 2000; Mandal et al., 2004; Rizki, 1978;

Tepass et al., 1994). The lymph gland is an organ that exists only at the larval stage, and is occupied by both differentiated and undifferentiated hemocytes (Cevik et al., 2019; Honti et al., 2014; Letourneau et al., 2016; Nappi & Vass, 1998). *Drosophila melanogaster* is a fantastic genetic model to study how cell lineages respond to physiological cues that regulate differentiation and proliferation owing to the well-defined genetic markers of hemocyte types (Cevik et al., 2019).

1.4.3 Hemocyte association with the heart

In our lab, hemocytes have also been shown to associate with the heart and follow the movement of its contractions (Cevik, 2016; Cevik et al., 2019). These aggregate on the inner foldings of the heart BM, close to the ostia and pericardial cells (Cevik et al., 2019). Hemocyte numbers in these clusters augment in anticipation of pupariation, but decrease again prior to pupa formation (Cevik et al., 2019). Due to the varying and unstable number of hemocytes at these pericardial pockets, they are not thought to be sites for hematopoiesis, but rather hubs allowing differentiation and release based on developmental or immune demands (Cevik et al., 2019).

The *Drosophila* heart is strikingly similar in morphology and function to that of the mosquito. In the adult African malaria mosquito *Anopheles gambiae* sessile hemocytes surrounding the abdominal ostia of the heart, termed periosteal hemocytes, are known to accumulate and phagocytose pathogens (King & Hillyer, 2012; Sigle & Hillyer, 2016). An increase in hemocyte number is observed at the ostia upon bacterial infection (Sigle & Hillyer, 2018). Hemocyte aggregation is not observed along the cardiac aorta however, as it is devoid of ostia (Sigle & Hillyer, 2018). This supports the idea of a close relationship between immune function and circulation (Sigle & Hillyer, 2018).

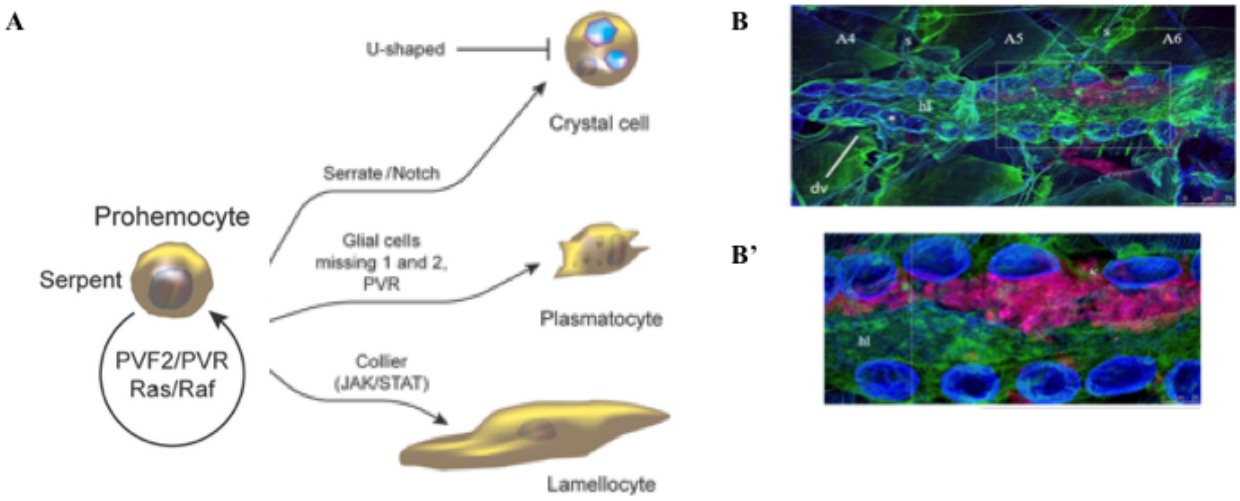

Figure 1.3: *Drosophila* hemocytes lineages. (**A**) The three distinct hemocytes lineages: crystal cells, plasmatocytes, and lamellocytes. All originate from the progenitor 'prohemocyte' cells. (Adapted from Lemaitre, 2007). (**B**) Hemocytes (pink) cluster tightly and associate with the heart. They can be seen between and around pericardial cells (blue) and within the Viking (Collagen IV) network. (**B**') Close-up of boxed area in B). This work examines the role of hemocytes in ECM formation and integrity. Green = Viking (Collagen IV) (Adapted from Cevik, 2016).

1.4.4 Hemocyte migration and deposition of ECM proteins

Cell migration is important for a number of processes such as embryonic development and cancer metastasis. Embryonic hemocytes are known to deposit ECM proteins such as Collagen IV and Laminin as they migrate over the matrix (Matsubayashi et al., 2017; Olofsson & Page, 2005; Sánchez-Sánchez et al., 2017). In turn, cell migration is dependent on the protein composition of the ECM. In fact, hemocytes deposit Laminin in track-like formations to favour their own migration through the embryo (Sánchez-Sánchez et al., 2017). This positive feedback loop is also important in maintaining the directional persistence and integrity of lamellipodia, cytoplasmic protrusions used by hemocytes for directed migration and adhesion (Sánchez-Sánchez et al., 2017). In the embryo, hemocytes are thus the most important contributors of ECM as their migration is vital to the even distribution of proteins Laminin A (LanA), Collagen IV (ColIV), and Perlecan (Perl), but to varying degrees (Matsubayashi et al., 2017). For instance, a 2017 study showed that in the embryo, 70% of Collagen IV, 50% of Perlecan, and only 30% of Laminin A comprising the BM were deposited by hemocytes (Matsubayashi et al., 2017). Laminin A is expressed in the mesoderm and is consequently present in early embryogenesis, although the majority of Laminin production occurs later in development (Matsubayashi et al., 2017). Also in embryo, hemocytes have been shown to deposit Laminin in 'track' formations as well as fibrillar meshes covering the ventral nerve chord (VNC) that they then use for their own migration (Sánchez-Sánchez et al., 2017). These Laminins are also essential for the formation and stability of lamellipodia, cytoplasmic protrusions formed and used by hemocytes, among other cell types, for migration and adhesion (Sánchez-Sánchez et al., 2017). At the larval stage, the fat body is the most

significant producer of ECM proteins, particularly Collagen IV and Perlecan (Mouw et al., 2014). Deposition of proteins is undeniably critical to ECM formation; though it is also important to consider the assembly and organization of these proteins. The function of larval hemocytes may therefore be more important to the organization of ECM proteins, rather than protein secretion (Mouw et al., 2014). To summarize, the majority of our understanding of hemocyte migration and ECM deposition comes from studying *Drosophila* embryos because they permit easy visualization of hemocyte behaviour *in vivo* (Ghosh, et al., 2018). Thus, the question of how ECM proteins are linked and assembled at later developmental stages remains.

1.5 Proteins of interest

Hemocytes are known to secrete ECM proteins in the *Drosophila* embryo, and in turn they depend on the macromolecular composition of the ECM for their migration. In parallel, altering hemocyte function during development has been shown to cause defects in the formation of the ECM. This kind of functional manipulation is possible due to the expansive genetic toolkit available for the tissue-specific and temporal control of gene expression. These tools can be used to explore the importance of hemocytes in establishing and maintaining the ECM. Here I have used the Gal4-UAS system to upregulate *reaper,* a gene that produces a pro-apoptotic protein causing cell death and to knock down the gene *shibire,* which is important in hemocyte motility and secretion.

Hemocytes are also similar in many ways to fibroblasts: vertebrate cells that are involved in wound healing and depositing ECM (Alberts et al., 2002; Wang et al., 2017). Fibroblasts, like hemocytes, also have to capacity to differentiate into other cell types of the connective tissue cell family (Alberts et al., 2002). This research therefore will help

bridge the gap between our understanding of vertebrate fibroblasts and invertebrate hemocytes and will provide insight into how these cell types construct and organize the ECM throughout development.

1.5.1 Reaper (*rpr*)

Reaper (*rpr*) is a *Drosophila* pro-apoptotic gene that promotes apoptosis through inhibition of the Death-associated inhibitor of apoptosis 1 (Diap1) protein (K. White et al., 1994). *rpr*, along with its fellow apoptosis-activating genes *head involution defect* (*hid*), and *grim* establish the pattern of embryonic programmed cell death (PCD), a normal process in tissue homeostasis throughout development and growth (Oppenheim, 1991; Truman, 1984). On the other hand, misregulation of PCD has implication in human pathologies such as AIDS, cancer, and many neurodegenerative diseases (Chen et al., 1996; Gougeon et al., 1993).

In *Drosophila*, embryonic deletions in *rpr, hid,* and *grim* produce a block in programmed cell death, whereas upregulation of *rpr* is known to induce extensive PCD (Bangs & White, 2000; E. White, 1996). Although no vertebrate homologues for these genes have been discovered, *rpr, hid,* and *grim* have been shown to induce caspase-dependent apoptosis in various vertebrate systems (Clavería et al., 1998; Evans et al., 1997; McCarthy & Dixit, 1998). Using the Gal4-UAS system, I have overexpressed *rpr* in hemocytes. I anticipated survival of few to no hemocytes in *rpr* overexpression samples compared to controls. Because hemocytes have been shown to deposit ECM proteins in the embryo, it was expected that the ECM in *rpr* overexpression samples would be disrupted when compared to controls.

1.5.2 Dynamin (*shi*)

The *Drosophila* gene *shibire* encodes protein *Drosophila* Dynamin (dDyn), which performs many of the same functions as the mammalian GTPase Dynamin (Dyn) (Chen et al., 2007; van der Bliek & Meyerowitz, 1991). In *Drosophila, shibire* transcripts are expressed early in embryogenesis and in various tissue, suggesting a role in development of the organism (Guha et al., 2003). In fact, null *shi* mutations in *Drosophila* zygotes are lethal and result in neural hyperplasia (Poodry, 1990).

The Dyamin protein is most known for its implications in endocytosis. This was discovered in *Drosophila* synaptic vesicles using a temperature-sensitive mutant *shi* allele that produces a block of endocytosis at 29°C (van der Bliek & Meyerowitz, 1991). This resulted in paralysis caused by depletion of the intracellular pool of releasable transmitter vesicles through inhibition of membrane cycling (van der Bliek & Meyerowitz, 1991). Membrane cycling is a dynamic endo/exocytic activity that causes plasma membrane proteins to be kept in a polarized state (Jones, Caswell, & Norman, 2006). Polarization of plasma membrane proteins is required for directed migration, and helps establish the direction of movement (Jones et al., 2006). Dynamin has also been shown to influence dynamic of cytoskeletal filaments, which maintain cell shape, allow cellular motility, are required for cell division, and mediate vesicle trafficking (Menon & Schafer, 2013). The mechanism through which Dynamin influences the cytoskeleton is independent of its role is vesicle recycling but is nonetheless reliant on GTPase (Gu et al., 2010).

In hemocytes, dDyn-dependent and independent endocytosis have been observed in temperature sensitive *shibire* mutants (Guha et al., 2003). Impairing *shi* function in hemocytes using the shi^{ts} allele as well as a *shi-RNAi* line can contribute to understanding

the function of dDyn in these cells. Because *shi* is implicated in endocytosis and membrane cycling, it is thought that knocking down its function in hemocytes will hinder their migration as well as their ability to secrete ECM proteins.

1.6 Project outline

The first objective of this work was to observe the effects of reducing hemocyte motility and secretion on the integrity of the cardiac ECM. Hemocytes have been shown to deposit core ECM proteins in the *Drosophila* embryo and may potentially do so in larvae as well. Furthermore, hemocytes may act to place or pattern ECM deposition, as suggested by the actions of cross-linkers like lysyl oxidase (*lox*) or proteases like MMP2. I posited that upon manipulating the expression of the apoptosis-inducing gene *rpr* as well as *shi,* a gene implicated in endocytosis and cell motility, hemocytes would experience reduced ability to migrate toward and associate with the heart. I also hypothesized that upon blocking endocytosis hemocytes would not deposit ECM proteins, assuming they possess this function in larvae, leading to abnormal deposition of ECM proteins, or to changes in ECM organization compared to wildtype. A hemocyte specific driver, *hemolectin* (*hml-gal4*) was used to drive the expression of proteins of interest.

The second objective concerns turnover of the cardiac ECM. We know that protein turnover occurs at the cardiac ECM as a part of growth, and also as a result of aging and/or pathology. This has never been observed *in vivo* – until now. I have developed an approach to observe the recovery of fluorescently tagged ECM proteins following photobleaching in living third instar larvae. Fluorescence recovery after photobleaching (FRAP) was originally developed to determine the kinetics of protein diffusion *in vivo* and is most commonly used at the cellular level; in the lipid bilayer for instance. I have generated a

protocol for the photobleaching of live, anesthetized larvae, using confocal microscopy. The challenge of developing this technique was to adapt it for the photobleaching of extracellular protein through several tissue layers, as opposed to photobleaching a fluorescently labelled protein within a single cell. In traditional FRAP, recovery of fluorescence is primarily attributed to diffusion of unbleached molecules into the bleached region. (Pincet et al., 2016). In this case, recovery of fluorescence is interpreted as incorporation of newly synthesized protein. Once developed, I combined photobleaching with impairment of hemocyte motility, adhesion, and secretion. If hemocytes are important to the turnover of ECM proteins, I expect recovery of VKG-GFP in hemocyte-impaired larvae compared to VKG control animals. Recovery of fluorescence was observed exclusively at the third instar developmental stage.

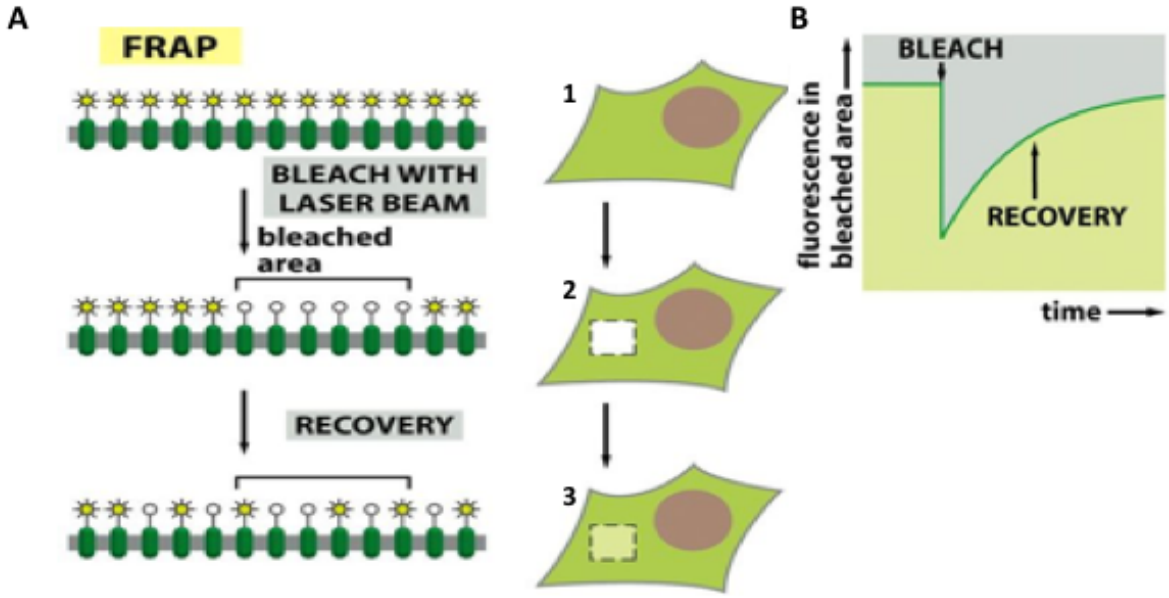

Figure 1.4: Fluorescence recovery after photobleaching schematic. **(A)** Traditional photobleaching uses fluorescent microscopy to observe the kinetics of protein diffusion *in vivo*. Here it is used to assess natural turnover of ECM proteins. **1)** A pre-bleach image taken with a confocal microscope. **2)** An ROI is selected and photobleached by high-intensity laser. It is important that regions outside of the ROI are not also photobleached. **3)** Recovery of fluorescence is observed as probes that are still fluorescing move into the region of interest to replace their bleached counterparts. Recovery observed from FRAP over long periods could be the result of normal protein turnover, lateral diffusion, or from injury triggered protein deposition. **(B)** A fluorescence recovery curve can be generated to track the recovery of fluorescence, in this example exponential, within an ROI over time. (Adapted from Garland Science Molecular Biology of the Cell, 2008 and Ishikawa-Ankerhold, 2012).

Chapter 2: Methods

2. 1 Stocks used

Table 2.1: List of *Drosophila* stocks used.

Stock	Chromosome	Use	Source
w[1118]; P{w[+mC]=Hml-Gal4.Delta}2, P{w[+mC]=UAS-2xEGFP}AH2	II	Hemocyte-specific driver (*Hml-Gal4*)	Bloomington (30140)
HmldsRed, Vkg-GFP/Cyo; Hml-Gal4/TM3	II, III	Used in photobleaching experiments to impair and visualize hemocytes	Made by Duygu Cevik
yw		Wildtype control	Bloomington (6598)
UAS-rpr	X	*rpr* overexpression	Bloomington (5823)
UAS-shi^{ts}	III	Expression of *shi* temperature-sensitive allele	Bloomington (44222)
yw; UAS-Shi RNAi		Expression of *shi RNAi*	Bloomington (28513)
Vkg^{cc0079} GFP trap	II	Fluorescent Vkg protein used photobleaching experiments	(Morin et al., 2001)

The crosses below depict how the genotypes assayed were acquired:

Hml-Gal4, UAS-GFP x UAS-shi RNAi

Hml-Gal4, UAS-GFP x UAS-shi^{ts}

Hml-Gal4, UAS x UAS-rpr

2.2 Stock maintenance

All flies were kept on yeast fly food at room temperature, unless indicated otherwise. Flies were flipped every two weeks. Rachel Andrews, Katie Perry, and I contributed equally to making the food.

2.3 Collection of larvae for dissection

Crosses were set up in pairwise vials at room temperature. Vials were either left at room temperature or moved to 18°C or 29°C after one day at room temperature. Low temperature shifts were used to reduce potentially toxic transgene expression at early developmental stages, and higher temperatures to achieve optimal levels of transgene expression. Control crosses were left at room temperature until the development of L3 larvae. Vials shifted to 18°C were again shifted to 29°C after four days at 18°C, or until the L2 stage. Vials moved directly from room temperate to 29°C remained there until the L3 stage. Wandering L3 larvae were selected for dissection.

2.4 Dissections

The protocol for larval dissections was adapted from (Vogler & Ocorr, 2009). Larvae were immobilized dorsal side down with tungsten pins magnetically adhered to a dissection plate. A small incision was made at the anterior end of the larva using fine iridectomy scissors to deflate the larva. A longitudinal incision was then made from the initial anterior cut to the posterior end of the larva along the ventral midline. The cuticle was then pinned down to expose the larval contents. The intestines and fat bodies were then removed, taking care not to detach the heart. Lastly, the dissection was fixed in the plate, in 4% paraformaldehyde for five minutes before being transferred to the same solution on ice.

2.5 Immunolabelling

Immunolabeling protocol was adapted from the outline of Alayari et al. (2009). All steps took place at room temperature unless indicated otherwise. Following dissection, samples were fixed with 4% parafolmaldehyde in PBS for 15 minutes in a 48-well plate. No more

than six samples were placed in the same well. Samples were then washed on a shaker in PBST (0.3% Triton in PBS) three times for ten minutes. Following the washes, samples were blocked with 10 µl NGS in 150 µl of PBT for 30 minutes. Dissections were then immunolabelled with 5 µl of primary antibody in 150 µl of PBST overnight with shaking at 4°C. The next day the samples were again washed three times with PBST as described. Samples were then immunolabelled with 1 µl secondary antibody and 2 µl Phalloidin (Alexa Fluor, Thermofisher) in 150 µl PBT for one hour. Samples were subsequently washed with PBT three times as described. A final wash with PBS followed, after which samples were placed in 50% glycerol in PBS for three hours at 4°C. Samples were then transferred to 70% glycerol in PBS until imaging.

Table 2.2: Antibodies used for immunolabeling. All antibodies were diluted in 1x PBST. 647 Phalloidin was added with secondary antibodies. Secondary antibodies were obtained from Thermofisher and were used at 1 in 150.

1° antibody/conjugated marker	Concentration used (from stock solution)	Supplier	2° used
Pericardin	1/30	DSHB (EC11)	Alexa 546 α-mouse
Viking	1/30	DSHB (CF.6G11)	Alexa 546 α-mouse
647 Phalloidin	1/75	Thermofisher	N/A

2.6 Confocal imaging

Confocal imaging was performed on a Leica SP5 confocal microscope. Frontal stack images were taken at 200Hz with a step size of 1 um. The Leica LAS AF software was used to generate 3D projections of stacks taken. This applied to heart, hemocyte, and ECM protein stacks. Heart stacks were taken at 20X magnification; hemocyte, Prc, and

Vkg stacks were taken at 63x magnification, zoom 1, 2, and 4. The pinhole size used for images at 20X was 60 μm, and for images at 63X, 95 μm.

2.7 Hemocyte volume measurement

The ImageJ plugin Volumest was used to determine hemocyte volume, as outlined in Cevik (2016). First, a stack was imported into ImageJ. The scale bar and distance between images in the stack were then set to calibrate the image. The region of interest (ROI) for hemocyte quantification was selected, which includes cropping the image such that areas outside of the ROI were not considered for quantification. Virtual transverse cross sections were constructed by reslicing the cropped stack. From there, the Volumest plugin was launched to measure total volume covered by hemocytes located underneath the ECM layers of the DV. The settings for Volumest were as follows: slice thickness=1μm, # steps = 1, grid width = 3 μm, object type = irregular. The Brown-Forsythe and Welch ANOVA tests (C.I. 95%) were performed to determine statistical difference in hemocyte volumes between controls and experimental groups.

2.8 Photobleaching

Below is the protocol developed for photobleaching of intact third instar larvae, including anesthesia, mounting, imaging, and bleaching.

Part 1: Anesthesia

Chloroform immobilization was performed as described by former lab members who pioneered the technique (Cevik et al., 2019).

Part 2: Mounting

1. Before anesthetization, make a mounting slide. To do this, use double-sided tape to adhere one 18x18 or 22x22 mm, 1.5mm thick coverslip on either side of a roughly

1cm space. Add another piece of double-sided tape to each of these coverslips and place a second coverslip on the tape. This creates a divot into which a larva can be placed without getting crushed.

2. Place anesthetized larva dorsal side up on the mounting slide, between the columns of coverslips.
3. Add a very thin strip of halocarbon oil to a fresh 1.5 mm coverslip.
4. Place the coverslip on the mounting slide, over the larva such that the halocarbon oil should lightly coat the larva to prevent it from drying out. Avoid contact between halocarbon and the larval anterior or posterior spiracles. If spiracles are immersed, the larva will drown.
5. Use tape to secure the coverslip to the microscope slide by gently taping down the left and right edges to the mounting slide. Be careful not to roll or squash the animal.

<u>Part 3: Imaging and bleaching</u>

1. Add a small drop of immersion oil to the outside coverslip before imaging.
2. First bring the larva into focus under BF, at 20X to make sure that it is immobile, but that its heart is beating. The heart beat is often very slow or barely perceptible as a result of chloroform anesthesia.

Pre-bleach stack

1. Set total laser power to 30%. Visible laser (488 and 543 in this case) power can be adjusted depending on intensity of fluorescence.
2. Use the confocal settings described for confocal imaging, including ‘Bidirectional X’ for faster scanning.

3. Take a pre-bleach stack of the heart. This stack will likely be larger than a stack in a dissected sample, owing to the additional tissue layers.
4. Obtain a 3D projection of the pre-bleach stack. Try to position the heart such that the segment A7 is in the center of the image.

Bleaching stack

1. Pull up the 3D projection of the pre-bleach stack.
2. Select the "ROI Scan" function on the main acquisition page.
3. Select 'ROI' box. Draw an ROI on the 3D projection using the square icon on the right screen. You can save this ROI and load the same one later. To save an ROI or load a saved ROI, right click on the image and select either 'Save ROI' or 'Load ROI'. A saved ROI, when loaded, will appear on the middle of the screen, so be sure to have the region you want to bleach in the appropriate position. In this case, the ROI should be placed within segment A7.
4. Select 'laser power' underneath the visible laser box. This is a shortcut to turning up the Argon laser only. Argon is the laser used to visualize GFP. Turn this up to 80% using the sliding bar.
5. With the ROI box selected, turn up visible 488 laser to 100%. During bleaching, only the 488 nm laser should be activated in order to exclusively bleach GFP. If another wavelength is needed to image hemocytes (543 nm), turn it off during the bleaching period.
6. Select "ROI configuration". Select all lasers that apply. In this case, only GFP is being bleached, and thus only 488 should be selected.

7. Select “Backgound”. Turn visible laser down to 0%. This change will only apply to the background during the bleaching period. The purpose of turning off the background laser intensity relative to the ROI to be bleached is to avoid photobleaching of off-target regions and to focus the laser beam onto the ROI.
8. Select “3D”. This allows you to select the depth of bleaching. If your stack is 75 steps, then enter 1 to 75 to bleach through all steps in your stack.
9. Before bleaching, zoom in 12x using either the wheel on the palette in front of the keyboard or the acquisition setting on the LAS software. Make sure the region you are zooming in on is where the ROI is. This helps to focus the unattenuated laser beam onto the ROI.
10. Click “Start” to image this stack. A 3D projection for this stack does not need to be generated because it only serves the purpose of bleaching the ROI. The ROI will light up much brighter than the surrounding areas as the stack is imaged.

Post-bleach stack

1. Turn the Argon laser back down to 30% and the visible laser back down to its pre-bleach value.
2. Take a post-bleach stack at 1x zoom, as done for the pre-bleach stack. Obtain a 3D projection. This is t=0 post-bleach. You can take stacks at downstream timepoints as well to assess recovery of fluorescence.
3. Re-image the larvae either 12h or 24h post-bleach by anesthetizing and mounting as described. Only one stack per sample is necessary to observe and determine recovery of fluorescence.

4. It is helpful to take snapshots of pre- and post-bleach projections with the ROI box delineating the bleached area. To do so, pull up the 3D projection and load the ROI used, as described. Right click on right screen and select "Snapshot". This is useful to visualize the tissue before and after photobleaching.
5. To quantify loss and recovery of fluorescence, a graph and table representing fluorescence intensity can be found under Quantify→Graphs/Stats. The ROI must be selected to acquire quantification measurements.

2.9 Quantification of fluorescence recovery after photobleaching

Recovery of fluorescence was quantified using fluorescence intensity measured in grey Each pixel is assignment a grey value, from 0 to 255. 0 is black and 255 is white. Using the LAS AF software, average grey values were obtained for bleached and unbleached regions, then compared to determine recovery of fluorescence.

Chapter 3: Results

Hemocytes are known to deposit ECM in the *Drosophila* embryo. The aim of this research was to understand more about hemocyte function at the larval stage of development, which so far has not been thoroughly studied. To do this, genetic manipulation was used to limit the number of hemocytes, as well as to impair endocytosis and cell motility. There are several ways to qualitatively and quantitatively determine the effects of perturbing hemocyte function. I observed hemocyte localization, hemocyte volume at the heart, hemocyte shape and clustering patterns, as well as organization of two major ECM proteins Prc and Vkg.

Table 3.1: Outline of genetically induced hemocyte impairments.

Objective	Mechanism	Genotype
Induce hemocyte apoptosis	Hemocyte-specific overexpression of *rpr*	*Hml-Gal4 x UAS-rpr*
Block endocytosis in hemocytes	*shi* knockdown via *shi RNAi*	*Hml-Gal4 x UAS-Shi RNAi*
Block endocytosis in hemocytes	*shi* knockdown at 29°C via the temperature sensitive allele shi^{ts}	*Hml-Gal4 x* shi^{ts}
Generate wildtype control	N/A	*Hml-Gal4 x yw*

3.1 Functionally impaired hemocytes fail to accumulate at discrete pockets near the *Drosophila* heart

In order to assess the impact of disturbing normal behaviour on hemocyte localization, I observed hemocyte accumulation at defined patches along the dorsal and lateral midlines and compared them to control samples. Genetic manipulation of hemocyte survival (*rpr*) and motility (*shi*) was performed to perturb this pattern. The driver line *Hml-Gal4* was crossed to *UAS-rpr*, *UAS-shi RNAi* or *UAS-*shi^{ts} to drive either overexpression of

the pro-apoptotic gene *rpr* or to decrease *shi* expression in hemocytes only (Table 3). Progeny of these crosses were raised according to two separate temperature treatments: crosses were set up at room temperature then shifted a day later to either 18°C or 29°C. The temperature shift served the purpose of minimizing the effects of hemocyte impairment (18°C) at early developmental stages, and subsequently to exacerbate the effect (29°C) at the onset of L3. Vials at 18°C were again shifted to 29°C after four days. Four days is typically required for maturation to second instar (L2) from embryogenesis at 18°C. This temperature shift was used to minimize the effect of either *rpr* overexpression or impaired expression of *shi* from embryogenesis to L2. The shift to 29°C from early L2 to L3 was designed to augment the impact of hemocyte impairment without affecting embryogenesis. The other temperature treatment consisted of raising larvae at 29°C from embryogenesis to L3. The effects of impairing hemocyte survival and motility on hemocyte localization and distribution were then compared between temperature treatments. The *Hml-Gal4* line was outcrossed to a 'wildtype' yellow-white (*yw*) strain and raised at room temperature as a control.

When the apoptosis-inducing gene *rpr* was overexpressed in hemocytes, third instar larvae exhibited defective clustering of hemocytes as well as fewer hemocytes along the dorsal midline (Fig.3.1 A-B') compared to controls (Fig.3.1 C-C'). This phenotype was more severe in larvae raised at 29°C (Fig.3.1 B-B') throughout development relative to temperature shifted individuals (Fig.3.1 A-A'), suggesting that embryonic hemocyte function contributes to larval phenotypes. Hemocyte clustering in larvae expressing either shi^{ts} (Fig.3.2 C-D') or *shi-RNAi* (Fig.3.2 A-B') was also disrupted compared to controls (Fig.3.2 E-E'). There appear to also be fewer hemocytes present at the dorsal midline in

these larvae relative to wildtype individuals. However, the effect of impairing *shi* expression on hemocyte numbers and clustering along the dorsal midline was not as pronounced as in *rpr* overexpression experiments. Hemocyte numbers were not quantified due to their characteristic tight clustering. This behaviour makes it difficult to identify separate cells in a cluster. One potential method to quantify hemocyte presence along the dorsal midline is to calculate the volume occupied by hemocytes in experimental and control samples (Cevik, 2016; Cevik et al., 2019).

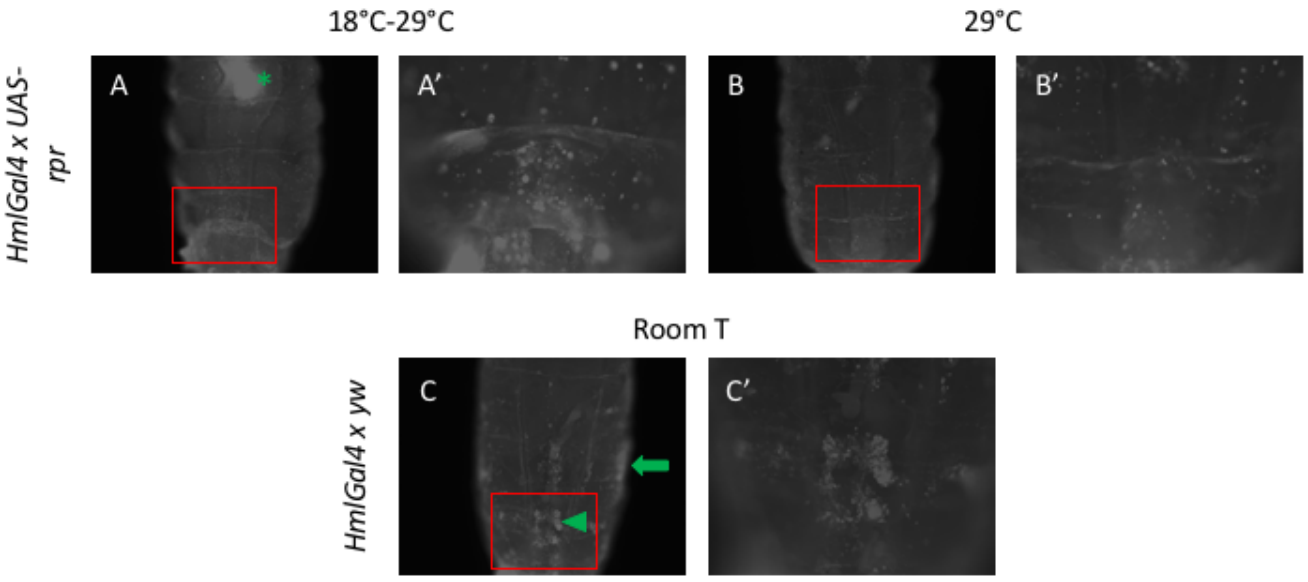

Figure 3.1: Hemocytes fail to accumulate at discrete pockets along dorsal and lateral midlines when *rpr* is overexpressed. (A, A') Hemocytes do not form defined dorsal patches in temperature shifted *rpr* overexpression larvae. **(B, B')** The *rpr* overexpression phenotype is more pronounced when larvae were raised at 29°C throughout development. **(C-C')** Hemocyte clusters along the 'dorsal stripe' (arrowhead) are clearly seen in control larvae. Hemocyte clusters are also found laterally around the chordotonal organs (arrow). Hml-Gal4 x *yw* is a wildtype controlling for genetic background. To control for the level of *rpr* expression, the following cross Hml-Gal4 x UAS-*rpr* raised at 18°C should be performed. Prime (') panels were imaged at 10x magnification and represent enlarged areas (red boxes) of their non-prime counterparts, imaged at 4x. The asterisk indicates the lymph gland. Anterior at top. Third instar larvae were anesthetized with chloroform and imaged dorsal side up using an Olympus fluorescence microscope. n=10 for all genotypes and temperature treatments.

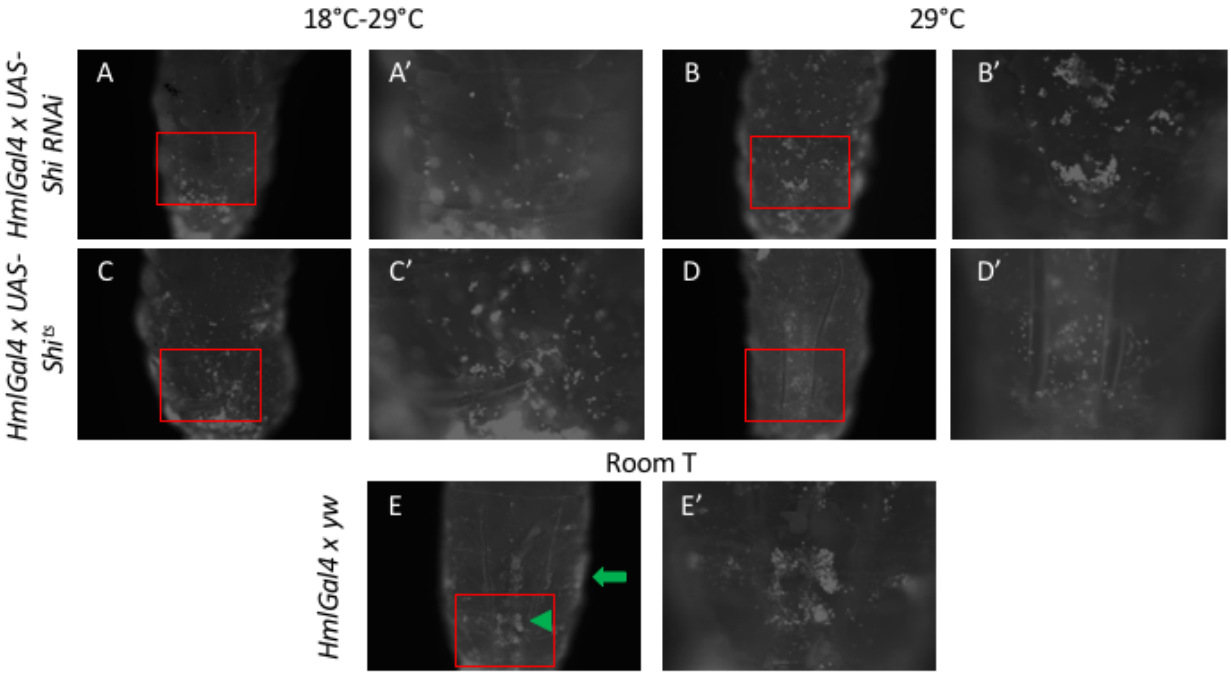

Figure 3.2: Hemocytes fail to accumulate at discrete pockets along dorsal and lateral segments when expression of *shi* is disrupted. (**A, A'**) Hemocytes do not form defined dorsal or lateral patches in temperature shifted *shi-RNAi* larvae. **(B, B')** Clustering is not impaired with hemocyte-specific expression of *shi-RNAi* in larvae raised at 29°C. The *shi* knockdown phenotype is less pronounced when larvae were raised at 29°C throughout development. **(C, C')** Hemocytes are abundant when the shi^{ts} allele is expressed but fail to cluster in patches as they do in wildtype individuals. **(D, D')** Fewer hemocytes are seen in shi^{ts} larvae raised at 29°C. The clustering defect is also more pronounced at this temperature. Hemocyte clusters along the 'dorsal stripe' (arrowhead) are clearly seen in control larvae. Hemocyte clusters are also found laterally around the chordotonal organs (arrow). Prime (') panels were imaged at 10x magnification and represent enlarged areas (red boxes) of their non-prime counterparts, imaged at 4x. Anterior at top. Third instar larvae were anesthetized with chloroform and imaged dorsal side up using an Olympus fluorescence microscope. n=10 for all genotypes and temperature treatments

3.2 Hemocyte-specific functional impairment does not lead to heart tube defects but does disrupt ECM proteins Prc and Vkg

I hypothesized that, if larval hemocytes are important to ECM and heart integrity, defects in heart tube formation would be observed, along with disrupted organization of ECM proteins upon manipulation of hemocyte survival or motility. To manipulate hemocyte function and observe the consequences on the heart and its ECM, larvae were first raised as described in the previous section then dissected and immunolabelled for two important ECM proteins; Prc and Vkg. Imaging was subsequently performed via confocal microscopy to generate three dimensional projections of the heart and of Prc and Vkg networks. Hemocytes were also imaged the same way. As such, hemocyte-impaired larvae were assayed for gross defects in heart morphology, abnormal ECM protein arrangement, and differences in hemocyte abundance, shape, and association with the heart.

3.2.1 Hemocyte-specific induction of apoptosis or impairment of membrane cycling does not result in heart formation defects

Hemocyte-impaired third instar larvae were imaged to observe differences in formation of the heart tube itself and its supporting musculature. No gross defects in heart morphology or structure were observed upon overexpression of *rpr,* knockdown of *shi,* or expression of the shi^{ts} allele when compared to controls (Fig.3.3-3.6). The heart tube, alary muscles connecting the heart to the epidermis, and surrounding body wall muscles were visualized with fluorescently conjugated phalloidin, a bicyclic peptide that stains F-actin.

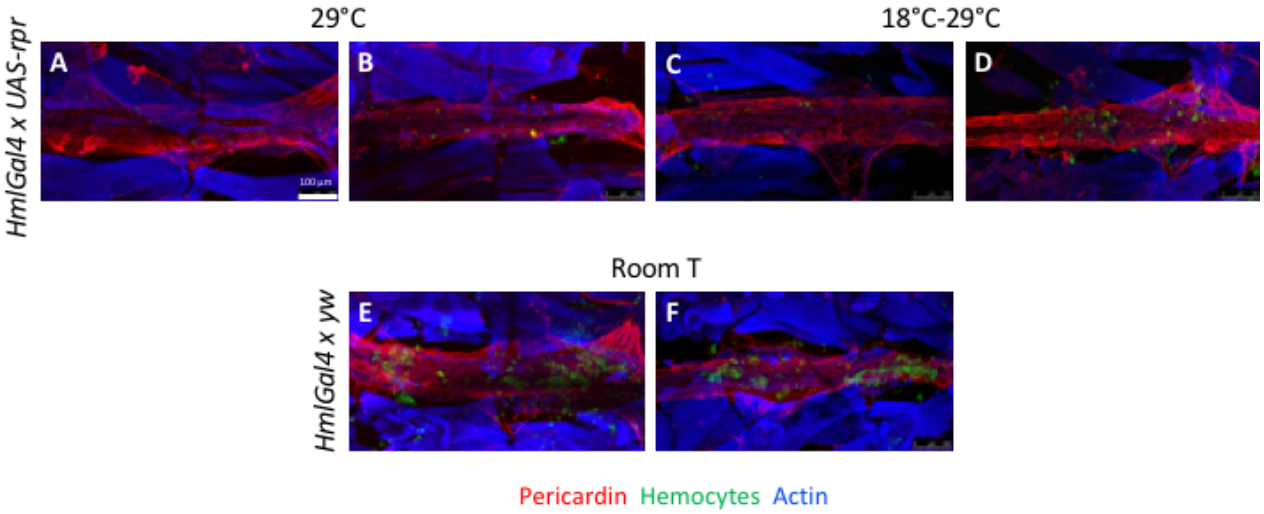

Figure 3.3: Hemocyte-specific overexpression of *rpr* may lead to a thinner heart tube as well as disruption of Prc density and organization. (A-B) Heart dissections from *Hml-Gal4 x UAS-rpr* third instar larvae raised at 29°C. **(C-D)** Heart dissections from *Hml-Gal4 x UAS-rpr* temperature shifted third instar larvae. Prc fibers density and abundance appears reduced in *rpr* overexpression samples raised at 29°C (A-B) and to a lesser extent in temperature shifted animals (C-D) relative to control (E-F) samples. In panel B the heart tube also appears much thinner relative to controls and may indicate partial collapse. Prc fiber organization also appears most disrupted in larvae raised at 29°C, and potentially in temperature shifted individuals to a lesser degree. Hemocytes from all *rpr* overexpression samples are smaller and rounder relative to control cells. This change in cell shape is typical of apoptotic cells (Saraste and Pulkki, 2000). They also exhibit clustering defects and do not associate with the heart as they do in wildtype controls. **(E-F)** Heart dissections from *Hml-Gal4 x yw* larvae raised at room temperature. A complex and dynamic arrangement of Prc fibers is generally observed. Hemocytes are found in clusters and in association with PCs and the heart tube. Images taken on a Leica SP5 confocal microscope at 20X. Expression of *UAS-shi^{ts}* or *UAS-shi RNAi* was driven with the hemocyte specific driver *Hml-Gal4*.

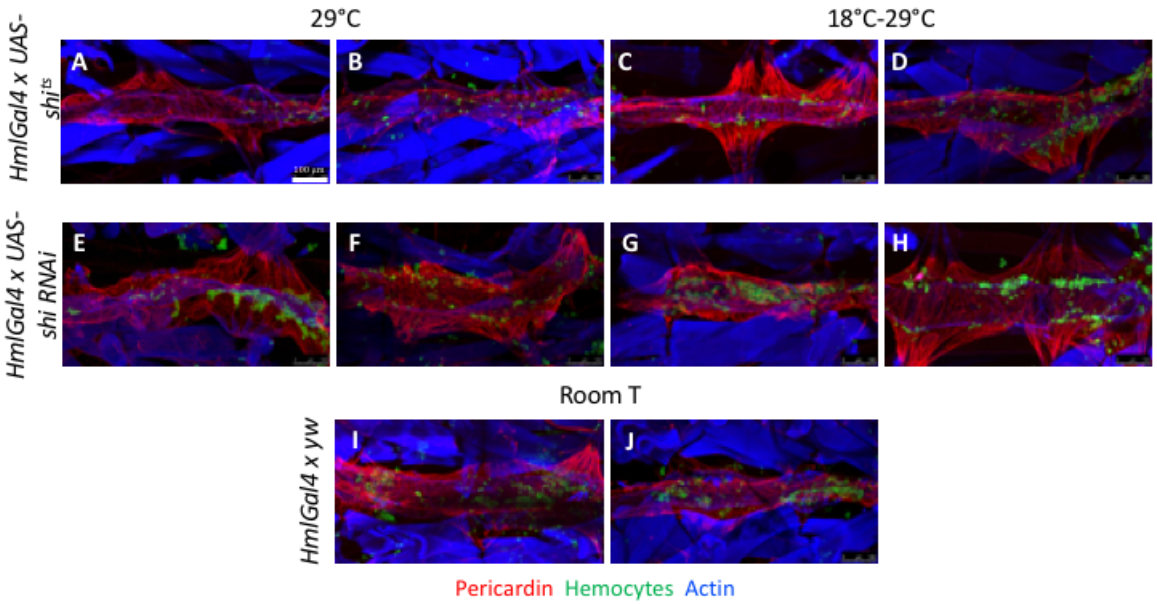

Figure 3.4: Hemocyte-specific knockdown of *shi* does not lead to defects in heart formation but may disrupt Prc organization. (A-B) Heart dissections from *Hml-Gal4 x UAS-shi^{ts}* third instar larvae raised at 29°C. **(C-D)** Heart dissections from *Hml-Gal4 x UAS-shi^{ts}* temperature shifted third instar larvae. **(E-F)** Heart dissections from *Hml-Gal4 x UAS-shi RNAi* third instar larvae raised at 29°C. **(G-H)** heart dissections from *Hml-Gal4 x UAS-shi RNAi* temperature shifted third instar larvae. Prc distribution is sparser in *shi RNAi* larvae raised at 29°C and potentially to a lesser degree in temperature shifted animals relative to controls. Otherwise the Prc network of *shi RNAi* impaired larvae appears similar to that seen in wildtype animals. No gross morphological Prc network defects are observed in *shi^{ts}* animals raised at either temperature. Hemocytes associate more closely in temperature shifted larvae from both *shi* impairments relative to both controls (I-J) and to animals raised at 29°C (A-B, E-F). Hemocytes tend to dissociate from each other more in *shi* impaired temperature shifted larvae relative to those raised at 29°C and compared to controls. Hemocytes are also more abundant in temperature shifted larvae and tend to cluster more tightly than they do in control animals. Larger hemocytes can be seen in *shi RNAi* larvae compared to control cells. **(I-J)** Heart dissections from *Hml-Gal4 x yw* larvae raised at room temperature. A complex and dynamic arrangement of Prc fibers is generally observed. Hemocytes are found in clusters and in association with PCs and the heart tube. Images taken on a Leica SP5 confocal microscope at 20X. Expression of *UAS-shi^{ts}* or *UAS-shi RNA*i was driven with the hemocyte specific driver *Hml-Gal4*. n=10 for all genotypes and temperature treatments assayed.

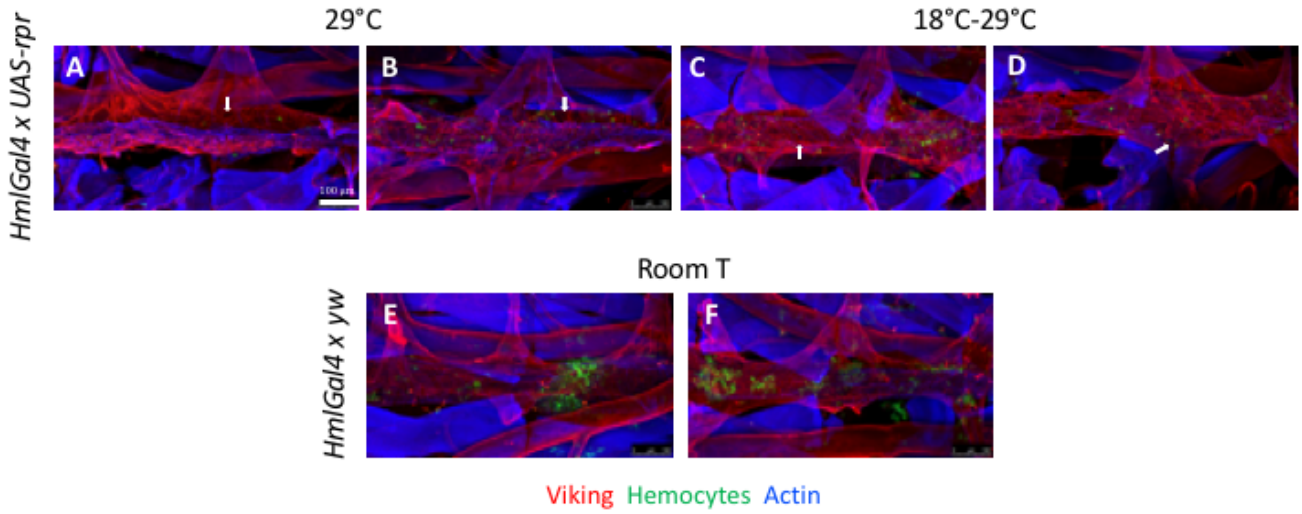

Figure 3.5: Hemocyte-specific overexpression of *rpr* does not lead to significant defects in heart formation but does appear to disrupt Viking distribution. (A-B) Heart dissections from *Hml-Gal4 x UAS-rpr* third instar larvae raised at 29°C. **(C-D)** Heart dissections from *Hml-Gal4 x UAS-rpr* temperature shifted third instar larvae. The presence of holes (arrows) in the Vkg network is more prominent in larvae overexpressing *rpr* from both temperature treatments. Vkg distribution also appears less uniform over the heart compared to controls (E-F) in animals raised at 29°C as well as temperature shifted larvae. The abundance of hemocytes is severely reduced in *rpr* overexpression samples, particularly in those raised at 29°C. **(E-F)** Heart dissections from *Hml-Gal4 x yw* larvae raised at room temperature. A relatively uniform distribution of the Vkg protein can be seen in these animals. Images taken on a Leica SP5 confocal microscope at 20X. Expression of *UAS-rpr* was driven with the hemocyte specific driver *Hml-Gal4*. n=10 for all genotypes and temperature treatments.

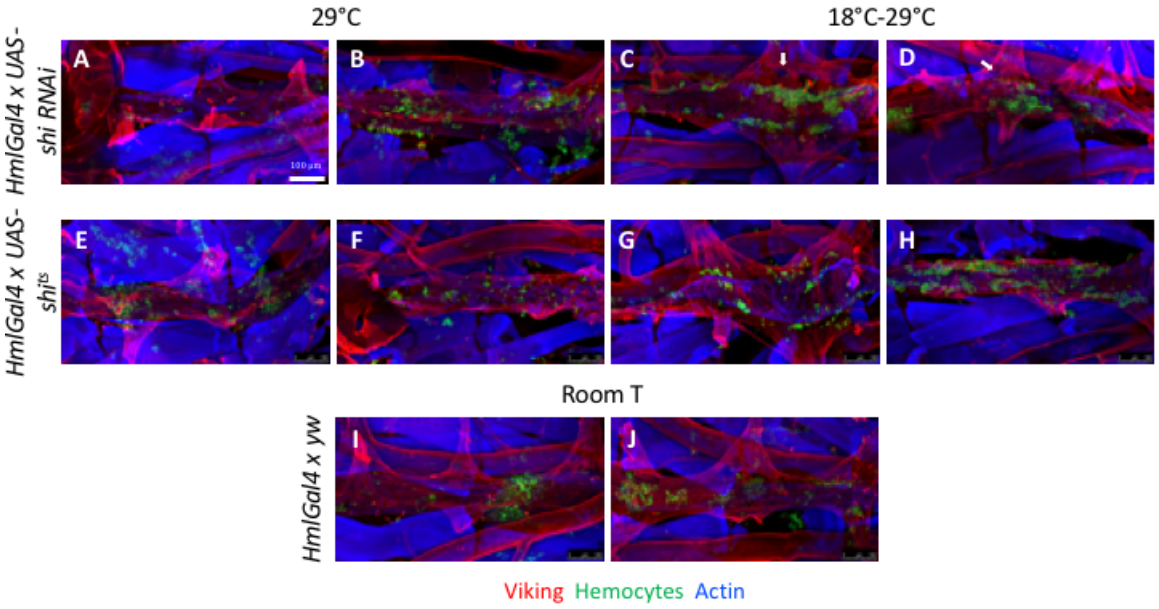

Figure 3.6: Hemocyte-specific knockdown of *shi* does not lead to significant defects in heart formation but may disrupt Viking distribution. (A-B) Heart dissections from *Hml-Gal4 x UAS-shi RNAi* third instar larvae raised at 29°C. **(C-D)** Heart dissections from *Hml-Gal4 x UAS-shi RNAi* temperature shifted third instar larvae. **(E-F)** Heart dissections from *Hml-Gal4 x UAS-shi^{ts}* third instar larvae raised at 29°C. **(G-H)** Hear dissections from *Hml-Gal4 x UAS-shi^{ts}* third instar temperature shifted larvae. The presence of holes (arrows) or tears in the Vkg network is more prominent in larvae expressing *shi RNAi* or *shi^{ts}* from both temperature treatments compared to controls. The formation of Vkg aggregates is pronounced in *shi RNAi* larvae raised at 29°C and to a lesser degree in temperature shifted animals. Distribution and abundance of Vkg protein appear most disrupted in animals raised at 29°C relative to controls. The phenotypes described are subtler in temperature shifted larvae. Hemocytes associate more closely in temperature shifted larvae from both *shi* impairments relative to both controls and to animals raised at 29°C. Larger hemocytes can be seen in *shi RNAi* larvae compared to control cells. **(I-J)** Heart dissections from *Hml-Gal4 x yw* larvae raised at room temperature. A relatively smooth distribution of the Vkg protein can be seen in these animals. Images taken on a Leica SP5 confocal microscope at 20X. Expression of *UAS-rpr* was driven with the hemocyte specific driver *Hml-Gal4*. n=10 for all genotypes and temperature treatments.

3.2.2 Hemocyte-specific induction of apoptosis or impairment of membrane cycling results in some disruption of the Prc network

Pericardin is a heart-specific *Drosophila* Collagen IV-like protein that constitutes a significant portion of the cardiac ECM. A Prc antibody was used to observe the distribution of this protein at the cardiac ECM in control and hemocyte-impaired samples. High variation in Prc fiber thickness and organization even in control (wildtype) samples was observed (Fig.3.7-3.9). In some cases, there appeared to be more laterally, rather than obliquely oriented fibers. Several samples from the *shi RNAi* test group, particularly those raised at 29°C, appeared to have more taught fibers relative to other groups. Taught fibres were frequently oriented in a similar direction, so that fibre intersections were more often at obtuse angles, and further apart than normal networks. In wildtype samples, fibres were encountered in all orientations, with the majority of frequent fibre crossings at more acute angles. A range of fiber widths is also observed in control samples (e.g. Fig.3.7 C-C''), as is normal. There may be some disruption in Prc fiber density and organization in *rpr* overexpression samples. Organization appears especially different in *rpr* overexpression samples raised at 29°C. When *rpr* was overexpressed in hemocytes, the Prc network appears sparser for both temperature treatments compared to controls. When *shi-RNAi* was expressed in hemocytes, Prc fibers appeared sparser compared to controls in larvae raised at 29°C. This may also be true for *shi-RNAi* sampled temperature shifted but is seen less frequently (Fig.3.9A-A''; B-B''). Similar observations apply to shi^{ts} samples compared to wildtype (Fig.3.8). Occasionally clumping of Prc fibers was seen (Fig.3.8 A-A'') but most individuals did not exhibit this phenotype. A technique for the objective quantification of Pericardin fiber thickness as well as abundance has not yet been developed. Quantification

of these parameters will provide concrete evidence of differences between Prc fiber characteristic under normal and hemocyte-impaired conditions. One potential objective method is blind scoring, whereby fibers are randomly selected for measurement and compared between samples. Another, and likely simpler quantification method that could be used to assess Prc fiber thickness is stereology. Stereological techniques use systematic sampling to generate quantitative and unbiased data (Cakmak & Ragbetli, 2019.; McNeal et al., 2016). These methods will be discussed further in the discussion.

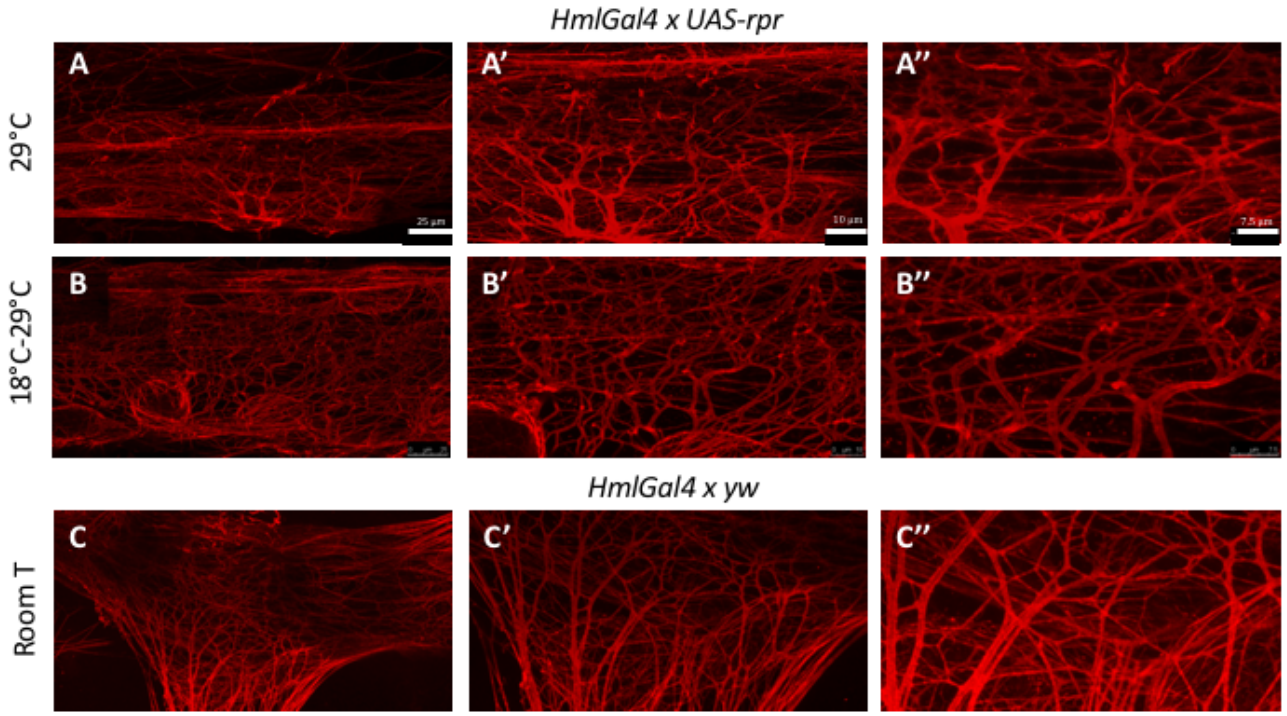

Figure 3.7: Hemocyte-specific expression of *rpr* leads to disrupted organization of the Pericardin network. (A) Prc network from *Hml-Gal4 x UAS-rpr* third instar larvae raised at 29°C. Fiber density, or abundance, often appears reduced in these animals. Organization of Prc fibers is disrupted, particularly in larvae raised at 29°C. Fibers frequently appear less straight, more lobular, and less cable-like relative to Prc networks from control animals (C). **(B)** Prc network from *Hml-Gal4 x UAS-rpr* temperature shifted third instar larvae. The organization and density of Prc fibers in these larvae is similar to those observed in larvae raised at 29°C, but to a lesser extent. **(C)** Prc network from *Hml-Gal4 x yw* wildtype control raised at room temperature. Prc fibers naturally vary with regard to thickness, length, abundance, and directional orientation. Images taken on a Leica SP5 confocal microscope at 63X. Prime (‘) and double prime (‘’) images are 2x and 4x enlarged from the non-prime panels, respectively. Expression of *UAS-rpr* was driven with the hemocyte specific driver *Hml-Gal4*. n=10 for all genotypes and temperature treatments.

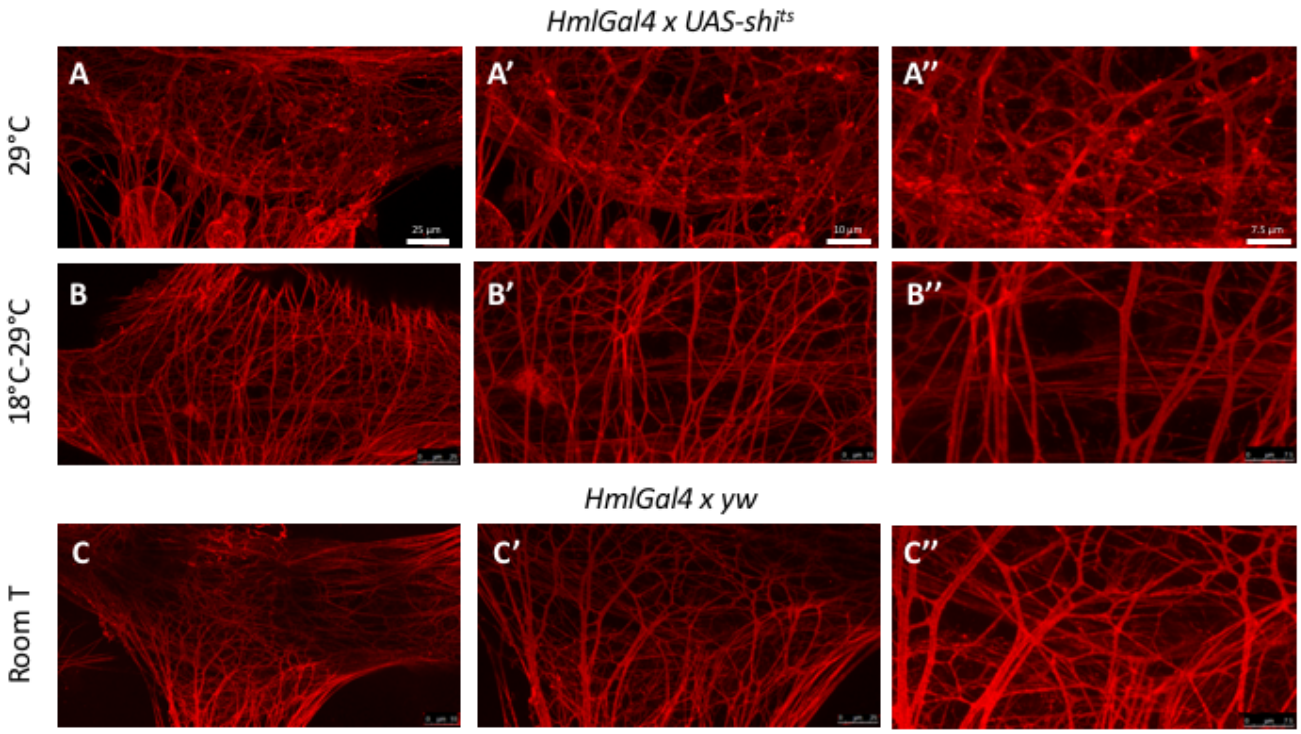

Figure 3.8: Hemocyte-specific expression of the *shi^{ts}* allele does not leads to gross defects in Pericardin network organization. (A) Prc network from *Hml-Gal4 x UAS-shi^{ts}* third instar larvae raised at 29°C. In this group, there was substantial variation in Prc fiber thickness, orientation, and density with no pattern observed between categories. Occasionally clumping as shown in (A-A'') was observed in these individuals. The Prc networks were similar to those found in wildtype animals. **(B)** Prc network from *Hml-Gal4 x UAS-shi^{ts}* temperature shifted third instar larvae. In some samples Prc fibers were more sparsely distributed. In other samples the Prc appeared normal and indistinguishable from controls. **(C)** Prc network from *Hml-Gal4 x yw* wildtype control raised at room temperature. Prc fibers naturally vary with regard to thickness, length, abundance, and directional orientation. Images taken on a Leica SP5 confocal microscope at 63X. Prime (') and double prime ('') images are 2x and 4x enlarged from the non-prime panels, respectively. Expression of *UAS-shi^{ts}* was driven with the hemocyte specific driver *Hml-Gal4*. n=10 for all genotypes and temperature treatments.

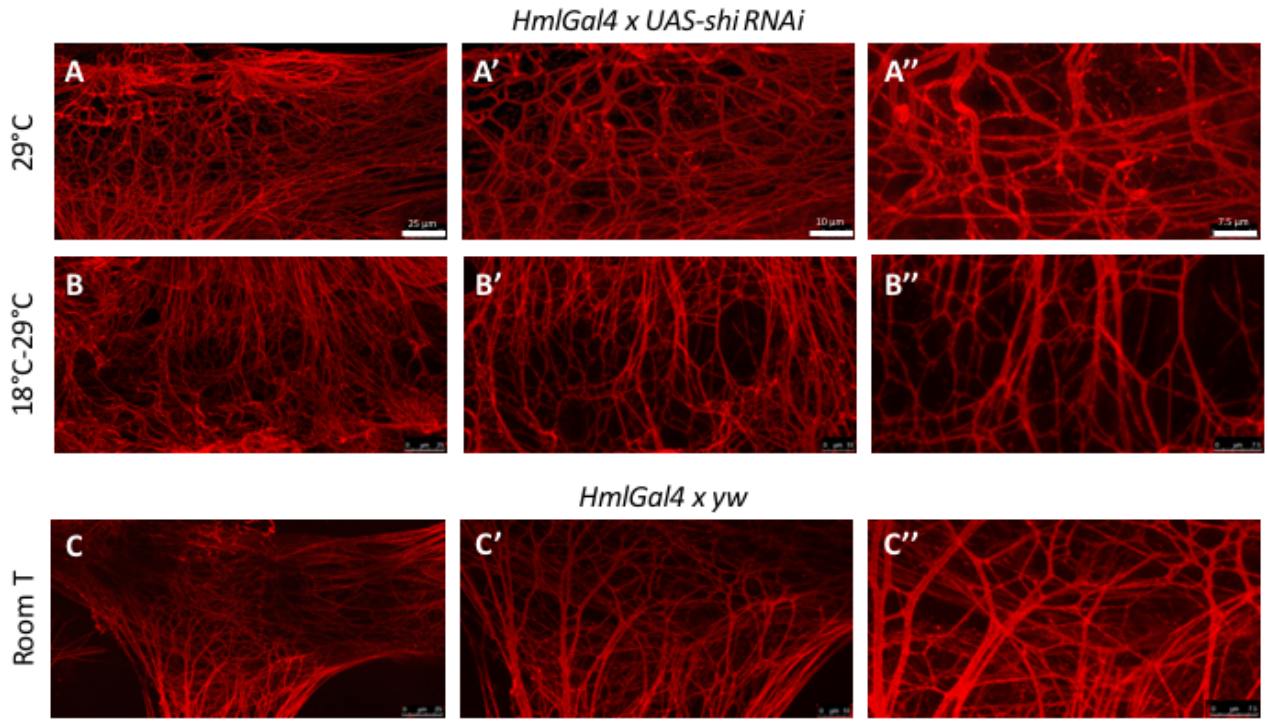

Figure 3.9: Hemocyte-specific expression of *shi RNAi* leads to sparser distribution of Pericardin fibers. (A) Prc network from *Hml-Gal4 x UAS-shi RNAi* third instar larvae raised at 29°C. The distribution of Prc fibers appeared sparser in animals raised at 29°C relative to controls (C). **(B)** Prc network from *Hml-Gal4 x UAS-shi RNAi* temperature shifted third instar larvae. In some larvae, the distribution of Prc fibers appeared sparser relative to control samples (C). In some samples the Prc network appeared normal and indistinguishable from controls. **(C)** Prc network from *Hml-Gal4 x yw* wildtype control raised at room temperature. Prc fibers naturally vary with regard to thickness, length, abundance, and directional orientation. Images taken on a Leica SP5 confocal microscope at 63X. Prime (‘) and double prime (‘’) images are 2x and 4x enlarged from the non-prime panels, respectively. Expression of *UAS-shi RNAi* was driven with the hemocyte specific driver *Hml-Gal4*. n=10 for all genotypes and temperature treatments.

3.2.3 Hemocyte-specific induction of apoptosis or impairment of membrane cycling results in disruption of the Vkg network

The *Drosophila* Collagen IV protein Viking is another key protein of most ECMs, including cardiac ECM. Antibody staining was performed to assess the distribution of Viking around the heart with induction of hemocyte apoptosis and with impairment of hemocyte motility and secretion. When *rpr* was overexpressed in hemocytes, the Vkg network appears to have formed considerably more clumps in the 29°C temperature treatment (Fig.3.10 A-A'') compared to controls (Fig.3.8 C-C''), but not in the temperature shift treatment (Fig3.10 B-B''). *rpr* overexpression also appeared to disrupt the uniformity of Vkg over the heart when compared to controls, particularly when larvae were raised at 29°C from embryogenesis (Fig.3.10 A-A''). Among *rpr* overexpression larvae raised at 29°C, an increase in holes was observed in the Vkg network, as well as the presence of bright puncta (Fig.3.10 A-A''), which is not consistent with the Vkg network in *rpr* overexpression temperature shifted larvae (Fig.3.10 B-B''. Because Viking is a major component of the basal lamina (BL), defects in its distribution or abundance likely lead to disruption of the basal lamina and consequently of the ECM as a whole (Sessions et al., 2017). When *shi-RNAi* was expressed in hemocytes, the Vkg network over the heart tube appears to have formed more clumps compared to controls, particularly in larvae raised at 29°C (Fig.3.12 A-A''). Vkg aggregates were occasionally observed in *shi-RNAi* temperature shifted individuals (Fig.3.12 B-B'') but were not as pervasive as in larvae raised at 29°C. There also appears to be decreased abundance of Vkg in *shi-RNAi* samples raised at 29°C relative to controls, as well as a less uniform distribution of the protein. Similar phenotypes were noted in larvae expressing the shi^{ts} allele (Fig.3.11). Vkg clumps were observed in shi^{ts} samples raised at 29°C (Fig.3.11 A-A''), but were not as abundant as in *shi-RNAi* samples raised at 29°C. The presence of holes in the Vkg network was another characteristic in temperature shifted larvae expressing shi^{ts} (Fig.3.11 B-B') compared to control animals. Again, decreased uniformity and abundance of Vkg was observed in shi^{ts} larvae from both temperature treatments. The Vkg protein network also appears more fibrous in temperature shifted samples expressing the shi^{ts} allele and in those expressing *shi RNAi* (Fig.3.11 B-B''), but not in those raised at 29°C (Fig.3.11 A-A''), compared to controls. Vkg is not a fibrous protein but rather forms a meshwork in the basal lamina, appears much smoother in controls (Lodish et al., 2000).

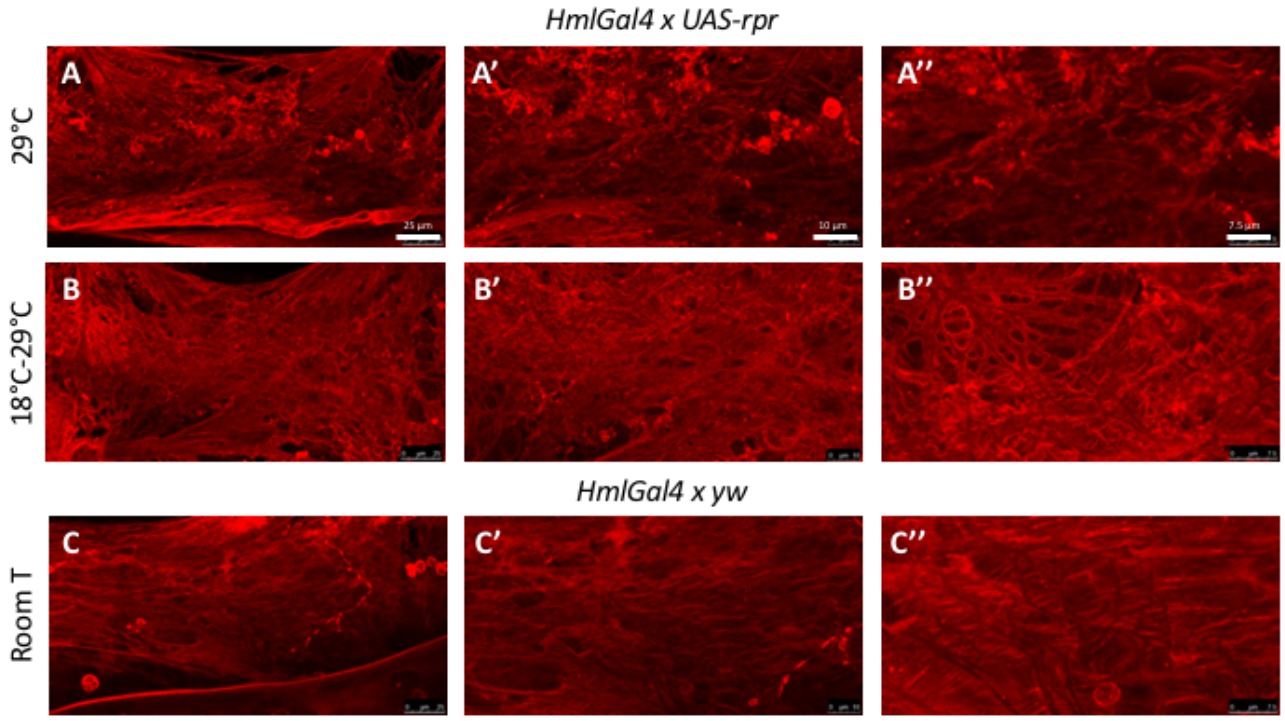

Figure 3.10: Overexpression of *rpr* in hemocyte leads to formation of Vkg aggregates and disrupted distribution of the Vkg (Collagen IV) network. (A) Vkg network from *Hml-Gal4 x UAS-rpr* third instar larvae raised at 29°C. Protein distribution is irregular and appears less abundant relative to control (C) animals. The presence of Vkg aggregates as well as smaller Vkg puncta is highly frequent in animals raised at 29°C. These structures were not observed in temperature shifted animals. Holes in the Vkg network are also common. **(B)** Vkg network from *Hml-Gal4 x UAS-rpr* temperature shifted larvae. Distribution of the Vkg network appears less consistent compared to control animals (C) but not to the extent seen in animals raised at 29°C (A). Holes in the network are also present but are not as abundant as in larvae raised at 29°C. **(C)** Vkg network from *Hml-Gal4 x yw* wildtype control raised at room temperature. A relatively smooth distribution of the Vkg protein can be seen in these animals. Images taken on a Leica SP5 confocal microscope at 63X. Prime (‘) and double prime (‘’) images are 2x and 4x enlarged from the non-prime panels, respectively. Expression of *UAS-rpr* was driven with the hemocyte specific driver *Hml-Gal4*. n=7 for all genotypes and temperature treatments.

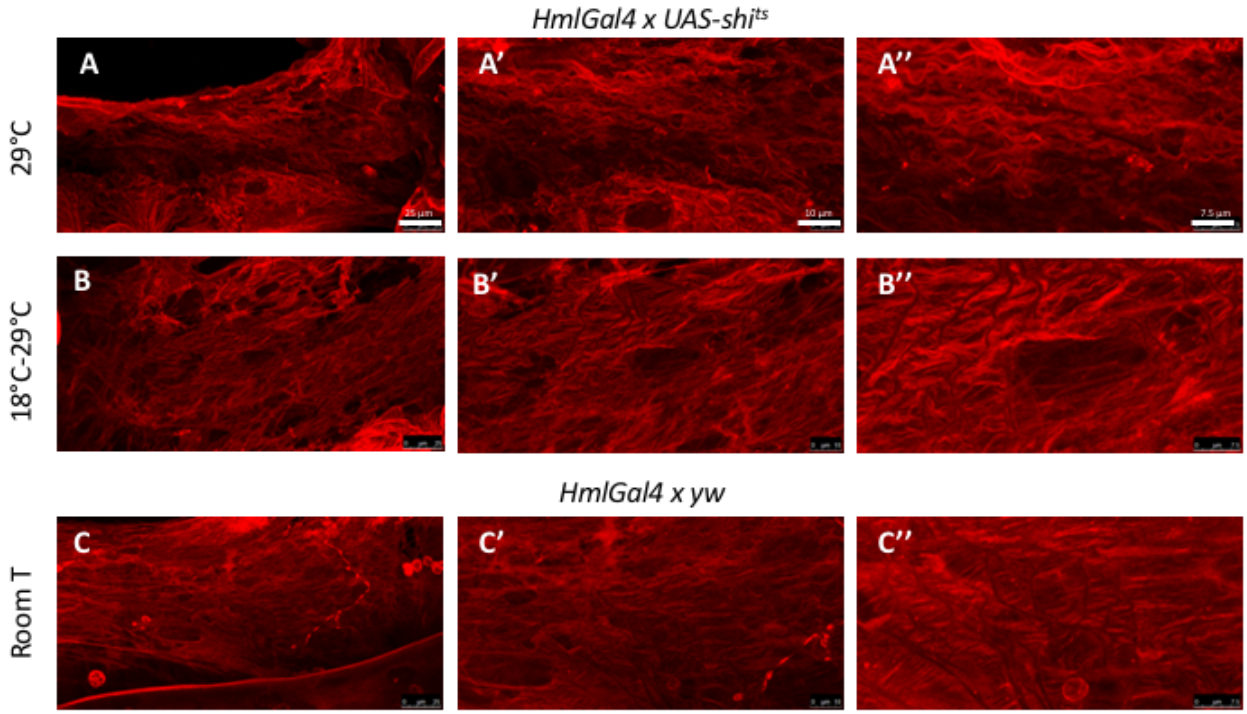

Figure 3.11: Expression of the temperature sensitive *shi^{ts}* allele in hemocyte leads to formation of holes and disrupted distribution of the Vkg (Collagen IV) network. (A) Vkg network from *Hml-Gal4 x UAS-shi^{ts}* third instar larvae raised at 29°C. Protein distribution seems irregular and is potentially less abundant relative to control (C) animals. The presence of Vkg aggregates is occasionally noted in animals raised at 29°C. Holes in the Vkg network are common. **(B)** Vkg network from *Hml-Gal4 x UAS-shi^{ts}* temperature shifted larvae. Distribution of the Vkg network appears less consistent compared to control animals (C) but not to the extent seen in animals raised at 29°C (A). Holes in the network are also present but are not as abundant as in larvae raised at 29°C. The Vkg network frequently appears more fibrous in temperature shifted animals, but not those raised at 29°C, relative to controls (C). **(C)** Vkg network from *Hml-Gal4 x yw* wildtype control raised at room temperature. A relatively smooth distribution of the Vkg protein can be seen in these animals. Images taken on a Leica SP5 confocal microscope at 63X. Prime (‘) and double prime (‘’) images are 2x and 4x enlarged from the non-prime panels, respectively. Expression of *UAS-shi^{ts}* was driven with the hemocyte specific driver *Hml-Gal4*. n=7 for all genotypes and temperature treatments.

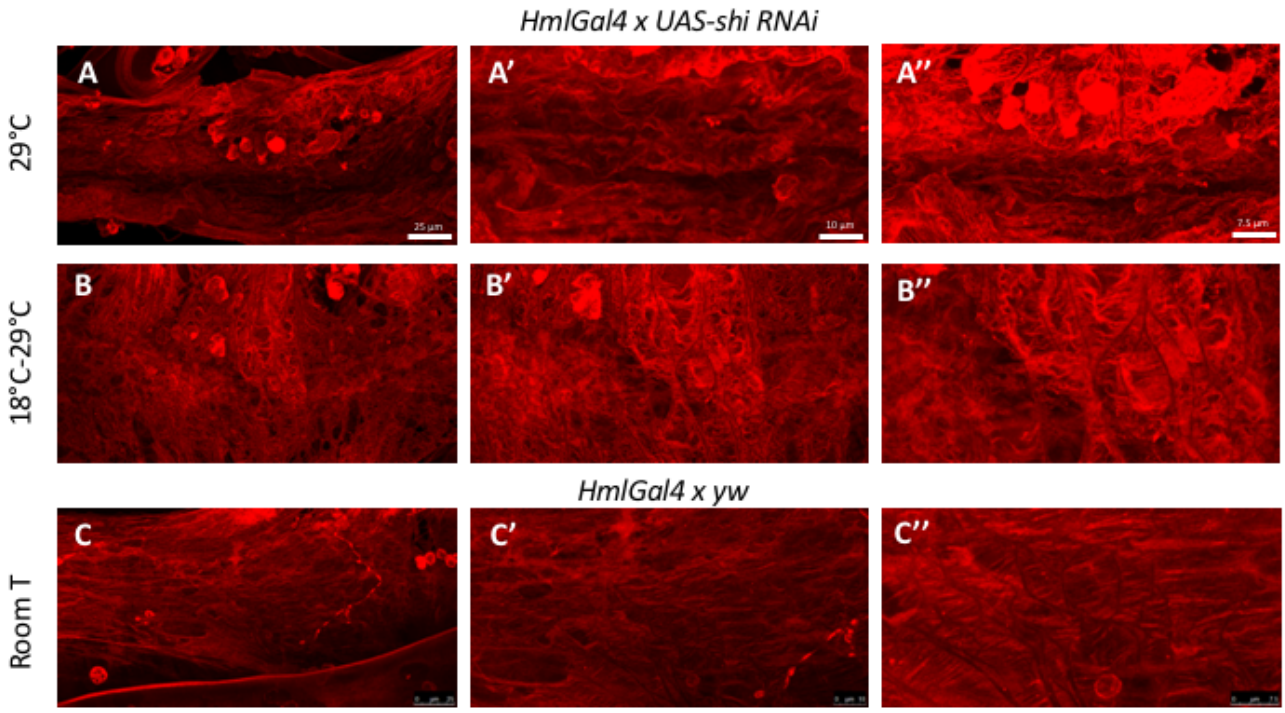

Figure 3.12: Knockdown of *shi* with *shi-RNAi* in hemocyte leads to the formation of Vkg aggregates and disrupted distribution of the Vkg (Collagen IV) network. (A) Vkg network from *Hml-Gal4 x UAS-shi RNAi* third instar larvae raised at 29°C. Protein distribution seems irregular and is potentially less abundant relative to control (C) animals. The presence of Vkg aggregates is noted particularly in animals raised at 29°C and also but to a lesser extent in temperature shifted larvae. **(B)** Vkg network from *Hml-Gal4 x UAS-shi RNAi* temperature shifted larvae. Distribution of the Vkg network appears less consistent compared to control animals but not to the extent seen in animals raised at 29°C. Vkg aggregates are also present but are not as abundant as in larvae raised at 29°C. **(C)** Vkg network from *Hml-Gal4 x yw* wildtype control raised at room temperature. A relatively smooth distribution of the Vkg protein can be seen in these animals. Images taken on a Leica SP5 confocal microscope at 63X. Prime (‘) and double prime (‘’) images are 2x and 4x enlarged from the non-prime panels, respectively. Expression of *UAS-shi RNAi* was driven with the hemocyte specific driver *Hml-Gal4*. n=7 for all genotypes and temperature treatments.

3.2.4 Hemocyte-specific induction of apoptosis or impairment of membrane cycling disturbs hemocyte abundance, shape, and association with the heart

Hemocytes were quantified using Volumest, an ImageJ plugin. Due to the typical tight clustering of hemocytes, counting individual cells is impossible. Therefore, the volume of hemocytes at or near the heart tube was determined using stacks of each sample assayed. Hemocyte quantities for all crosses and temperature treatment were compared to control samples raised at room temperature. Brown-Forsythe and Welch ANOVA tests (C.I. 95%) were performed to determine statistical significance between hemocyte volumes for all experimental groups vs. controls.

Table 3.2: Mean and median hemocyte volumes (n=10 for all groups).

Genotype	Temperature treatment	Mean hemocyte volume (μm^3)	Median hemocyte volume (μm^3)
Hml-Gal4 x UAS-rpr	18-29°C shift	5091.3	2655
	29°C	1966.5	630
Hml-Gal4 x UAS-shi RNAi	18-29°C shift	87572.3	63657.5
	29°C	80179.1	73170
Hml-Gal4 x UAS-shi^{ts}	18-29°C shift	50768	35730
	29°C	83574.9	47497.5
Hml-Gal4 x yw	Room temperature	65643.8	61924.5

The volume of hemocytes present at the heart appears drastically reduced in *rpr* overexpression samples raised both at 29°C (Fig.3.13 A-A'') as well as those shifted from 18°-29°C (Fig.3.13 B-B'') compared to controls (Fig.3.17 C-C''). Counting individual hemocytes is an unreliable quantification technique due to their tight clustering. The volume of hemocyte clusters (including individual cells, if applicable) around the heart was therefore calculated for each individual sample and averaged per experimental group.

Differences in volume between *rpr* overexpression samples and controls was in fact found to be statistically significant for both temperature groups (Fig. 3.15 D). *rpr* overexpression samples from both temperature treatments also appear to exhibit hemocyte clustering defects, as well as differences in cell shape when comparing hemocytes to those of control samples. Hemocytes found in *rpr* overexpression samples tend to exist as single cells or as clusters of very few cells. In contrast, hemocytes around the hearts of wildtype samples associate closely with one another in clusters such that individual cells often cannot be identified. Furthermore, hemocytes in wildtype third instars generally have irregular shapes, similar to the elongated forms of vertebrate fibroblasts. This phenotype seems to be lost in animals overexpressing *rpr,* where hemocytes are not only visibly smaller but maintain a rounder shape, which suggests that these cells are apoptotic and not migratory or active. This phenotype is more pronounced at 29°C (Fig.3.13 A-A'') than it is in temperature shifted samples (Fig.3.13 B-B''). The mean hemocyte volume for *rpr* overexpression individuals raised at 29°C was the lowest among all groups evaluated (Table 4). This group was also calculated to have the lowest median hemocyte volume.

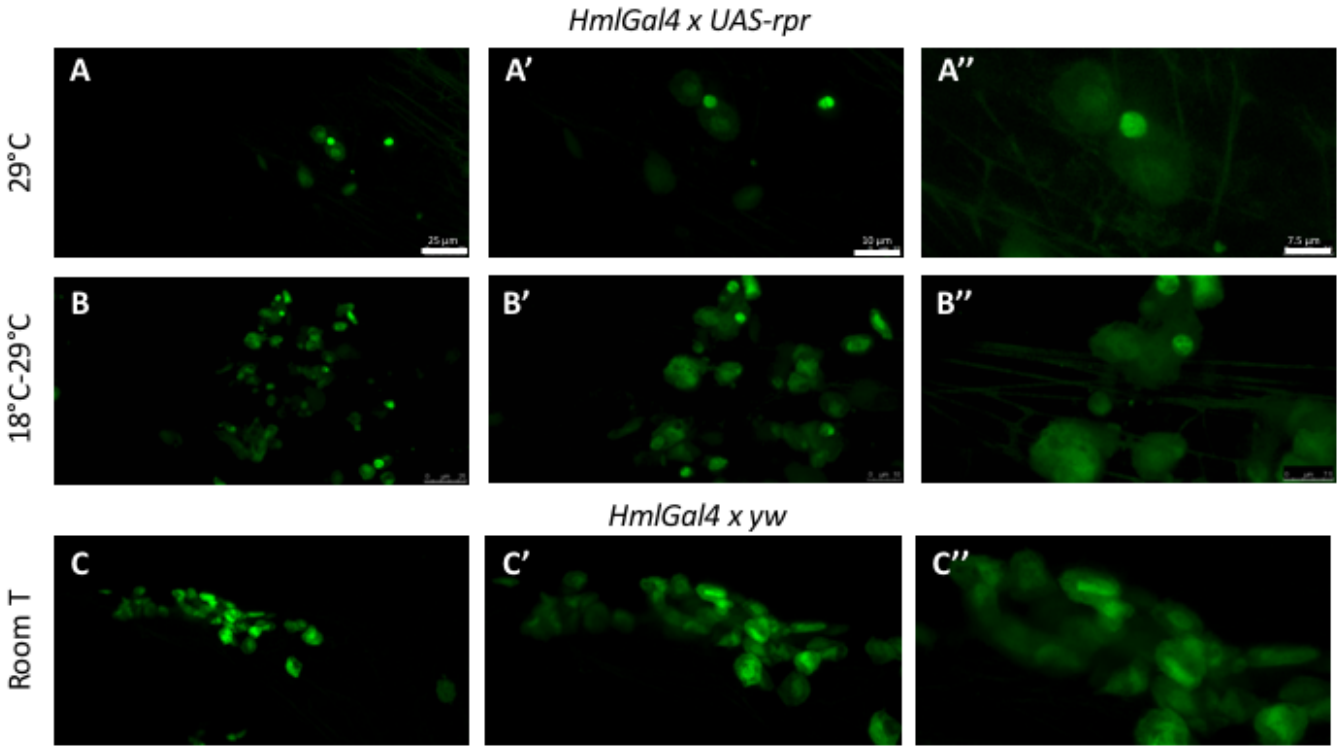

Figure 3.13: Overexpression of *rpr* leads to reduced hemocyte numbers and disruption of cell shape and cell clustering. (A) Hemocytes from *Hml-Gal4 x UAS-rpr* third instar larvae raised at 29°C. Cells are visibly smaller and rounder than control hemocytes. **(B)** Hemocytes from *Hml-Gal4 x UAS-rpr* temperature shifted larvae. Cells are more numerous than in larvae raised at 29°C from embryogenesis but are still rounder and smaller compared to hemocytes from control animals. Hemocytes from larvae overexpressing *rpr* also exhibit clustering defects relative to cells from control animals. This phenotype is particularly pronounced at 29°C and is present but to a lesser degree in temperature shifted animals. **(C)** Hemocytes from *Hml-Gal4 x yw* wildtype control raised at room temperature. Cells have an irregular shape and are often seen in close association with one another. Images taken on a Leica SP5 confocal microscope at 63X. Prime (‘) and double prime (‘’) images are 2x and 4x enlarged from the non-prime panels, respectively. Expression of *UAS-rpr* was driven with the hemocyte specific driver *Hml-Gal4*. n=10 for all genotypes and temperature treatments.

Hemocytes expressing the *shi-RNAi* appear to have a similar morphology compared to control cells (Fig.3.15). They do, however, frequently appear larger than control hemocytes in samples from both temperature treatments (e.g. Fig.3.15 B'). These large cells could be the result of hemocytes failing to divide due to the block in endocytosis from *shi* depletion. When looking at confocal images of the dissected heart, there often appear to be more hemocytes in *shi* knockdown larvae, or at least more hemocytes in close association with the pericardial cells flanking the heart tube (Fig.3.15 A-A'). Between *shi-RNAi* larvae temperature shifted from 18°-29°C and those raised at 29°C from embryogenesis, the mean hemocyte volume was higher in temperature shifted individuals (Table 3.2), however the median hemocyte volume was higher in *shi-RNAi* larvae raised at 29°C. Overall, there is a higher volume of hemocytes in larvae expressing *shi-RNAi* from both temperature treatments compared to controls raised at room temperature. Median values are also larger in *shi-RNAi* samples compared to controls.

When the shi^{ts} allele was expressed in hemocytes, cell shape closely resembled that of wildtype cells (Fig.3.14). One interesting observation is that hemocytes in samples expressing shi^{ts} and raised at 29°C (Fig.3.14 A-A'') exhibit more pronounced clustering of hemocytes compared to control dissections. This could be the result of impaired endocytosis and exocytosis. Vesicle trafficking allows for membrane cycling, which is required for cell motility. With reduced ability to endocytose and exocytose, hemocytes may not have been able to migrate and dissociated from each other as is seen in wildtype organisms. A related observation was that hemocytes in shi^{ts} temperature shifted individual (e.g. Fig.3.6 H) hemocytes are often found in closer association with the heart tube when compared to controls. This could be due to a migratory defect as described. Hemocytes

also appear not to associate as closely with the heart tube in individuals raised at 29°C (Fig. 3.4 A, B; Fig. 3.6 E, F) relative to the temperature shifted group (Fig.3.4 C, D; Fig.3.6 G, H), as many individual or small clusters of cells can be seen among the body wall muscle surrounding the heart. There is also significant variety (i.e. large standard deviation) in hemocyte volumes between *shi*^{ts} samples raised at 29°C compared to the *shi*^{ts} temperature shifted group as well as the control samples, which share similar variation (Table 3.2). Referring to the images of dissected *shi*^{ts} larvae (Fig. 3.4 A-D; Fig.3.6 E-H), in some instances there are very few hemocytes, whereas in other images from the same experiment, hemocytes are numerous. The mean for both temperature treatments of *shi*^{ts} larvae were smaller values compared to the mean hemocyte volume of controls (Table 3.2). Median hemocyte volumes of *shi*^{ts} larvae from both temperature treatments were also inferior to median control hemocyte volumes (Table 3.2).

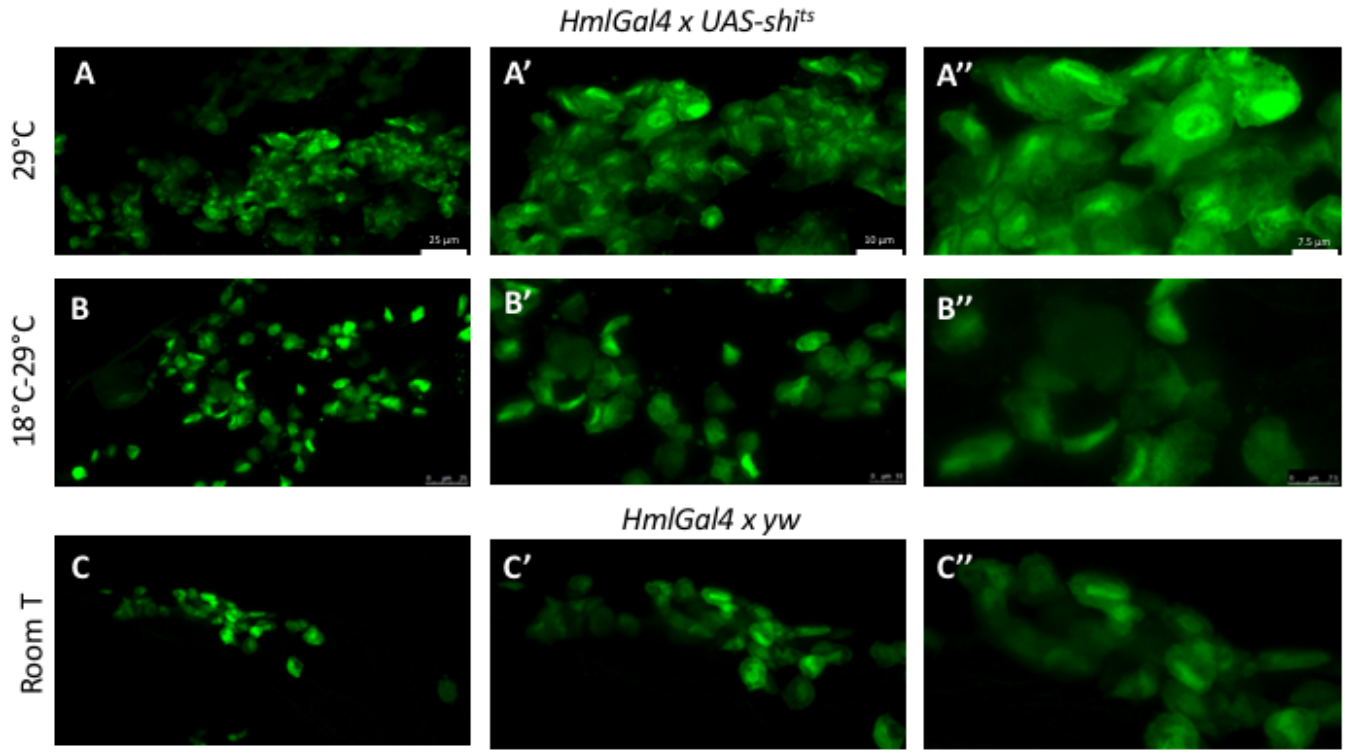

Figure 3.14: Hemocytes expressing the *shi^{ts}* allele do not exhibit morphological defects and closely resemble hemocytes from wildtype animals. (A) Hemocytes from *Hml-Gal4 x UAS-shi^{ts}* third instar larvae raised at 29°C. Hemocyte clustering is visibly more prominent in these larvae than it is in control larvae (C) as well as in temperature shifted larvae (B). **(B)** *Hemocytes from Hml-Gal4 x UAS-shi^{ts}* temperature shifted larvae. Cells are very similar in morphology and abundance to hemocytes from control larvae. **(C)** Hemocytes from *Hml-Gal4 x yw* wildtype control raised at room temperature. Cells have an irregular shape and are often seen in close association with one another. Images taken on a Leica SP5 confocal microscope at 63X. Prime (‘) and double prime (‘’) images are 2x and 4x enlarged from the non-prime panels, respectively. Expression of *UAS-shi^{ts}* was driven with the hemocyte specific driver Hml-Gal4. n=10 for all genotypes and temperature trea

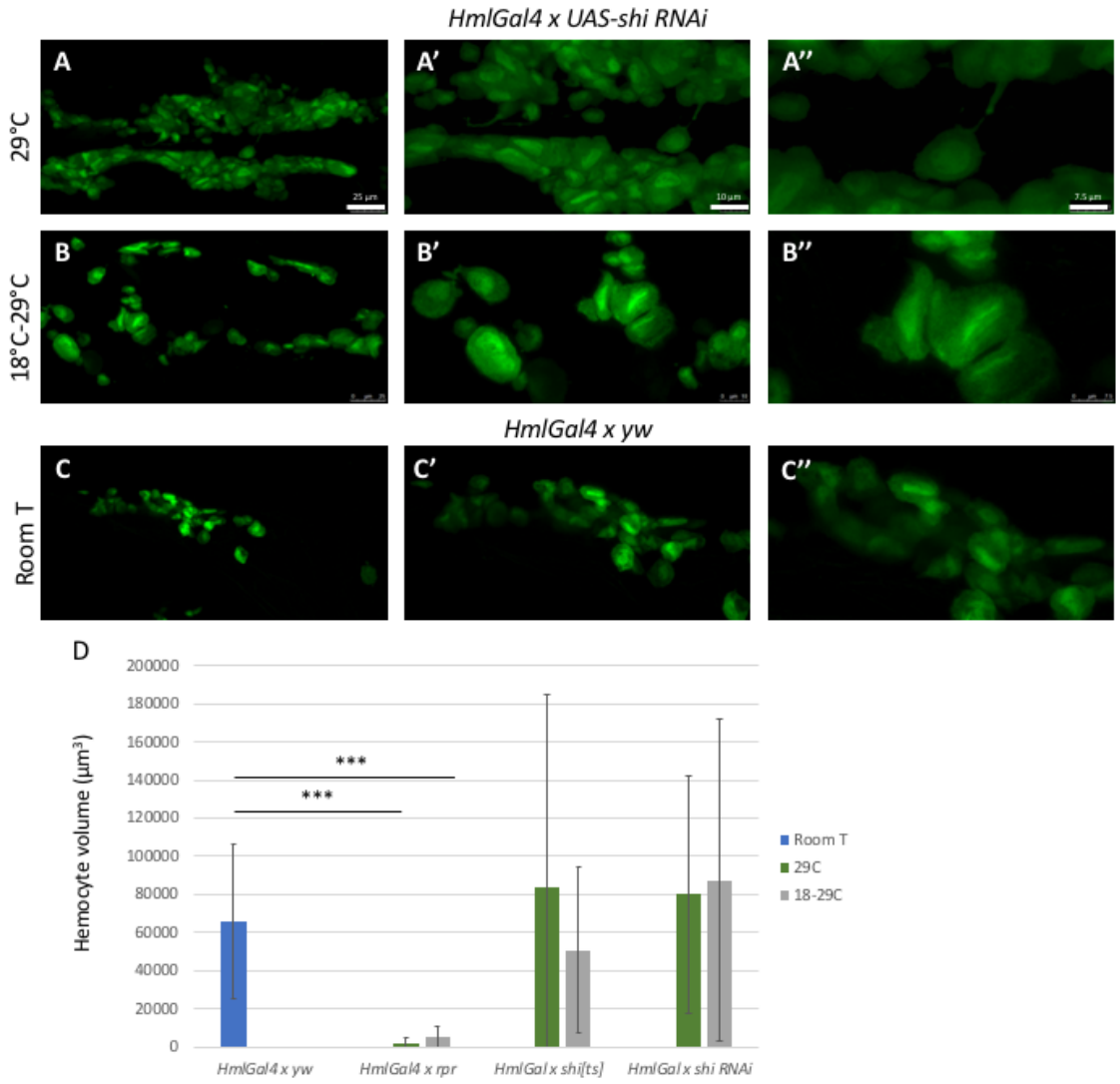

Figure 3.15: Hemocytes expressing *shi-RNAi* are larger than hemocytes from control animals. (A) Hemocytes from *Hml-Gal4 x UAS-shi RNAi* third instar larvae raised at 29°C. Hemocytes appear more numerous and are often larger relative to hemocytes from control larvae (C). **(B)** Hemocytes from *Hml-Gal4 x UAS-shi RNAi* temperature shifted larvae. Cells are larger and more numerous relative to control (C) larvae as well as those raised at 29°C. Larger cells could indicate a failure of cell division. **(C)** Hemocytes from *Hml-Gal4 x yw* wildtype control raised at room temperature. Cells have an irregular shape and are often seen in close association with one another. (D) Mean hemocyte volumes for all experimental groups and controls. n=10 for all groups. Error bars represent standard deviation. *** represents p-value: 0.0044 for *HmlGal4 x UAS-rpr* 29°C and p-value: 0.0064 for *HmlGal4 x UAS-rpr* 18-29°C. Images taken on a Leica SP5 confocal microscope at 63X. Prime (‘) and double prime (‘’) images are 2x and 4x enlarged from the non-prime panels, respectively. Expression of *UAS-shi RNAi* was driven with the hemocyte specific driver *Hml-Gal4*. n=10 for all genotypes and temperature treatments.

3.3 Recovery of fluorescence occurs in a time-dependent manner following photobleaching of Vkg-GFP

Fluorescence recovery after photobleaching (FRAP) is a technique most commonly used to assess the dynamics of protein diffusion *in vivo.* This consists of photobleaching a region of interest, usually within a cell's membrane or cytoplasm, via high intensity laser and subsequently monitoring the recovery of fluorescence in that region over time. Recovery of fluorescence in this case generally occurs within seconds or milliseconds and can in most cases be attributed to the diffusion of unbleached molecules from outside the ROI into the bleached region. FRAP was first developed as a way to measure mobility of single lipid molecule in a cell membrane but has since been adapted to track the diffusion of fluorescently-tagged proteins of interest (Axelrod et al., 1976). Even so, FRAP is generally used only in two-dimensional tissues or for a single cell layer. I have developed a novel adaptation of FRAP for photobleaching of the endogenous protein Viking (Collagen IV) in live, intact *Drosophila* larvae. The stock used comprises a Vkg-GFP protein trap, in which an exon encoding a GFP reporter is inserted directly into an intron separating two coding exons of the endogenous protein (Vkg) (Morin et al., 2001). The result is the production of a chimeric protein wherein GFP is fused to both termini of the 'trapped' Vkg protein (Morin et al., 2001).

In our system photobleached proteins exist in the extracellular space, and thus recovery of fluorescence is thought to be due to incorporation of newly synthesized protein (Hildick et al., 2012; Pincet et al., 2016). However, the possibility of lateral diffusion must also be considered (Mueller et al., 2012). The 'reversible' photobleaching of GFP is also

possible to some degree but is not thought to occur in our system due to the intensity of the laser used to perform the photobleaching (Hildick et al., 2012).

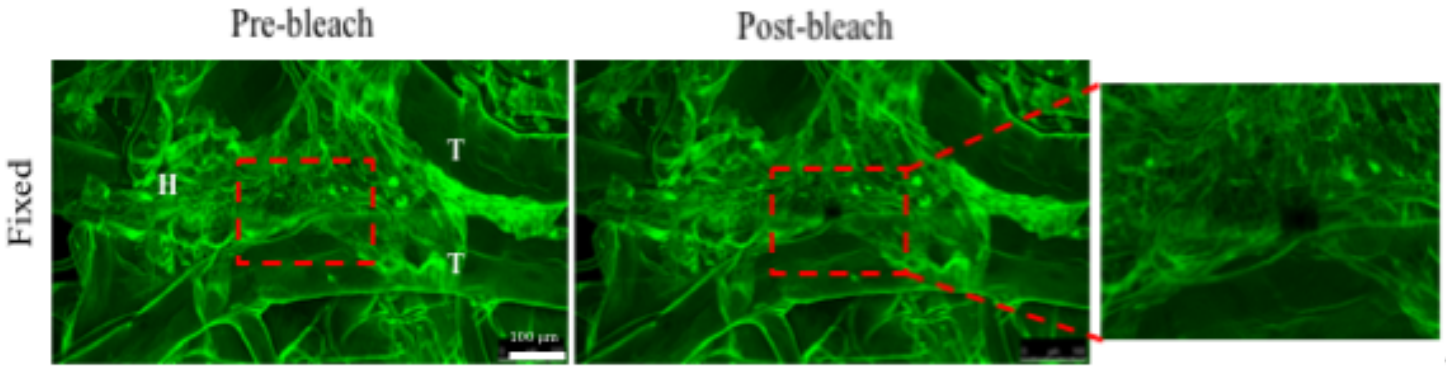

Figure 3.16: Photobleaching of (Viking-GFP) in a dissected third instar larva, with no recovery. Photobleaching of *Drosophila* Collagen IV (Viking) performed on dissected and fixed tissue. The bleached region is defined by a clear border, a characteristic of fixed tissue, which evidently did not undergo recovery of fluorescence. Green=Collagen IV; T=trachea; H=heart. Imaging was performed on a Leica DM6000CS SP5 confocal microscope. Genotype: Vkg-GFP (trap)

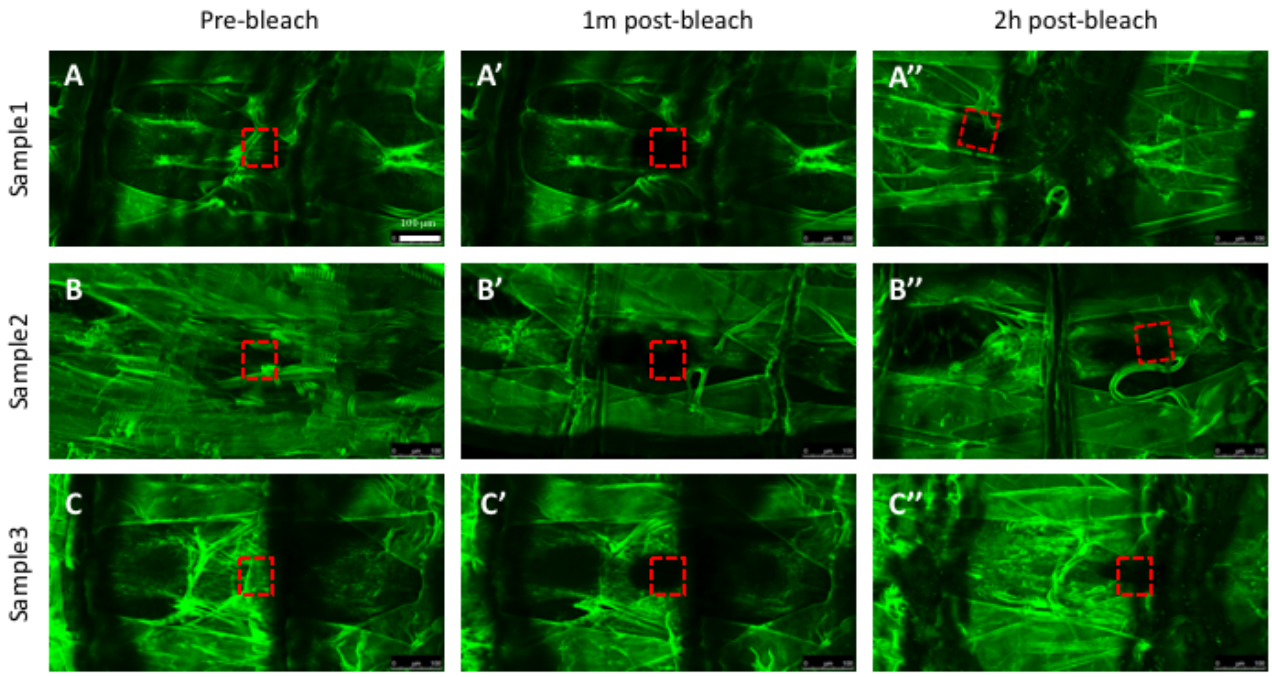

Figure 3.17: No recovery of fluorescence is observed in Vkg-GFP fluorescence 2h post-bleach in live, intact third instars. (A-A''; B-B''; C-C'') Three examples of anesthetized third instar larvae pre-bleach (A, B, C); immediately post-bleach (A', B', C'); and 2h post-bleach (A'', B'', C''). First, a pre-bleach stack of the heart was generated (A, B, C). An ROI was then selected and photobleached using the same stack generated for the pre-bleach image (A', B', C'). A stack was then taken 2h after photobleaching to determine the extent of recovery at the photobleached ROI (A'', B'', C''). Although the shape of the bleached ROI appears different in the same animal 2h postbleach (A'', B'', C''), no recovery of fluorescence is observed at this time point. Green=Vkg-GFP. ROIs in pre-, post- and 24h post-bleach are delineated by the red boxes. ROI dimensions: 66 x 66 µm. Photobleaching was performed on a Leica DM6000CS SP5 confocal microscope using the Argon laser to photobleach the GFP protein fused to Vkg. Genotype: Vkg-GFP (trap). n= 15.

Little is known about the time it takes for recovery to occur when bleaching is performed through several tissue layers. We opted to start with a very long recovery period, and to subsequently shorten the time between bleaching and determination of recovery. First, a 24h recovery period was allowed, at which point re-imaging of the bleached ROI was performed to determine the extent of Vkg-GFP recovery. Although in all cases the bleached ROI was still perceptible as a fainter region relative to the surrounding areas, marked recovery of Vkg-GFP was observed (Fig. 3.18). Photobleaching of Vkg-GFP was also performed in combination with hemocyte-specific *rpr* overexpression. After 24h, recovery of fluorescence was very minimal in *rpr* overexpression samples, suggesting that hemocytes are needed for turnover of Vkg at the cardiac ECM.

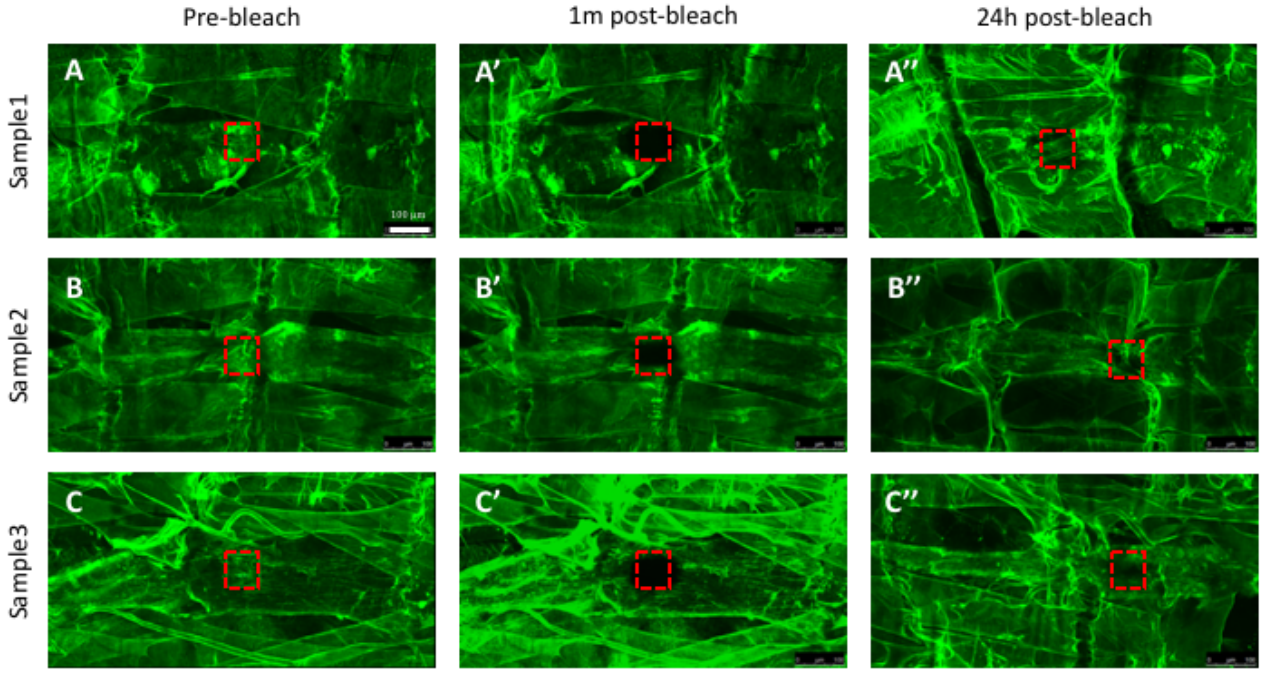

Figure 3.18: Significant recovery of Vkg-GFP fluorescence is observed 24h post-bleach in live, intact third instars. (A-A''; B-B''; C-C'') Three examples of anesthetized third instar larvae pre-bleach (A, B, C); immediately post-bleach (A', B', C'); and 24h post-bleach (A'', B'', C''). First, a pre-bleach stack of the heart was generated (A, B, C). An ROI was then selected and photobleached using the same stack generated for the pre-bleach image (A', B', C'). A stack was then taken 24h after photobleaching to determine the extent of recovery at the photobleached ROI (A'', B'', C''). The extent of recovery varies between individuals but generally it appears significant although incomplete. ROIs in pre-, post- and 24h post-bleach are delineated by the red boxes. ROI dimensions: 66 x 66 µm. Photobleaching was performed on a Leica DM6000CS SP5 confocal microscope using the Argon laser to photobleach the GFP protein fused to Vkg. Genotype: Vkg-GFP (trap). n= 4.

The next time point tested was a 12h recovery period. Due to the significant recovery of fluorescence seen with the 24h recovery period, we sought to determine if fluorescence recovery would be similar or minimal with a shorter recovery time. At 12h post-bleach, very minimal to no recovery was observed at the bleached region in both Vkg-GFP controls and in larvae exhibiting hemocyte-specific *rpr* overexpression (Fig.3.19 and 3.21, respectively). Recovery of fluorescence, and therefore turnover of Vkg protein seems to occur between 12h and 24h postbleach. This means that complete turnover of the Vkg protein does not occur within 24h. Lastly, re-imaging after a 2h recovery period was performed on Vkg-GFP controls only, to show the lack of fluorescence recovery relative to the other time point (Fig.3.17).

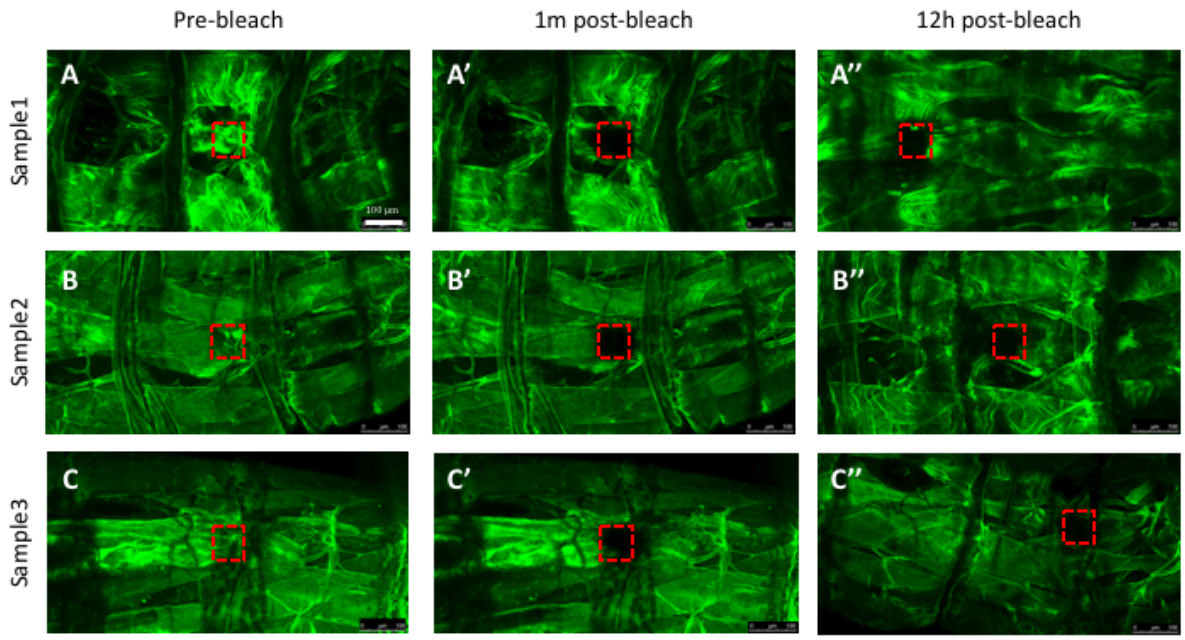

Figure 3.19: Minimal to no fluorescence recovery in Vkg-GFP intact, third instar larvae is observed 12h post-bleach. (A-A''; B-B''; C-C'') Three examples of anesthetized third instar larvae pre-bleach (A, B, C); immediately post-bleach (A', B', C'); and 12h post-bleach (A'', B'', C''). First, a pre-bleach stack of the heart was generated (A, B, C). An ROI was then selected and photobleached using the same stack generated for the pre-bleach image (A', B', C'). A stack was then taken 12h after photobleaching to determine the extent of recovery at the photobleached ROI (A'', B'', C''). The extent of recovery after 12h varies between individuals but generally appears very minimal or non-existent. ROIs in pre-, post- and 12h post-bleach are delineated by the red boxes. ROI dimensions: 66 x 66 µm. Photobleaching was performed on a Leica DM6000CS SP5 confocal microscope using the Argon laser to photobleach the GFP protein fused to Vkg. Genotype: Vkg-GFP (trap). n= 7.

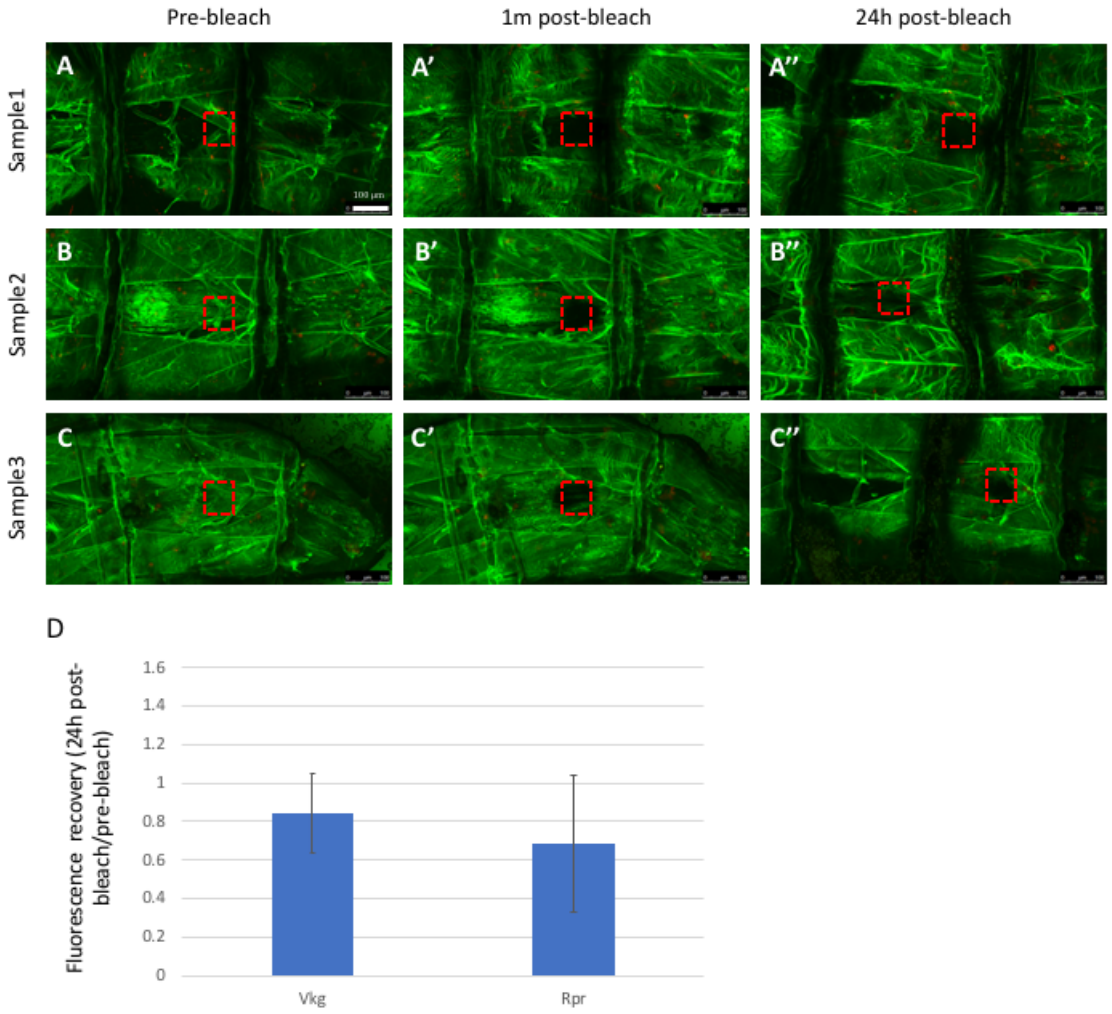

Figure 3.20: Hemocyte-specific *rpr* overexpression does appear to affect recovery of Vkg-GFP fluorescence 24h post-bleach in live, intact third instars. (A-A''; B-B''; C-C'') Three examples of anesthetized third instar larvae pre-bleach (A, B, C); immediately post-bleach (A', B', C'); and 24h post-bleach (A'', B'', C''). Larvae were raised at 29°C to increase the apoptotic effect of *rpr* overexpression. First, a pre-bleach stack of the heart was generated (A, B, C). An ROI was then selected and photobleached using the same stack generated for the pre-bleach image (A', B', C'). A stack was then taken 24h after photobleaching to determine the extent of recovery at the photobleached ROI (A'', B'', C''). The extent of recovery varies greatly between individuals. Recovery of fluorescence is minimal to nonexistent in samples 1 and 3 above but appears significant and similar to wildtype recovery at 24h postbleach in sample2. **(D)** Fluorescence recovery 24h post-bleach in wildtype (Vkg-GFP) and *rpr*-overexpressing individuals. Recovery is expressed at the gray value ratio from pre-bleach/24h post bleach ROI, normalized to an arbitrary pre-bleach value. Error bars represent standard deviation. Fluorescence recovery appears

superior in controls relative to *rpr* overexpression samples. Green=Vkg-GFP; red=hemocytes. Overexpression of *rpr* was driven with the hemocyte-specific driver Hml-Gal4. ROIs in pre-, post- and 24h post-bleach are delineated by the red boxes. ROI dimensions: 66 x 66 μm. Photobleaching was performed on a Leica DM6000CS SP5 confocal microscope using the Argon laser to photobleach the GFP protein fused to Vkg. Cross: *HmldsRed, Vkg-GFP/CyO; Hml-Gal4/TM3 x UAS-rpr*. Genotype: *HmldsRed, Vkg-GFP/+; Hml-Gal4/+; UAS-rpr*. n= 6.

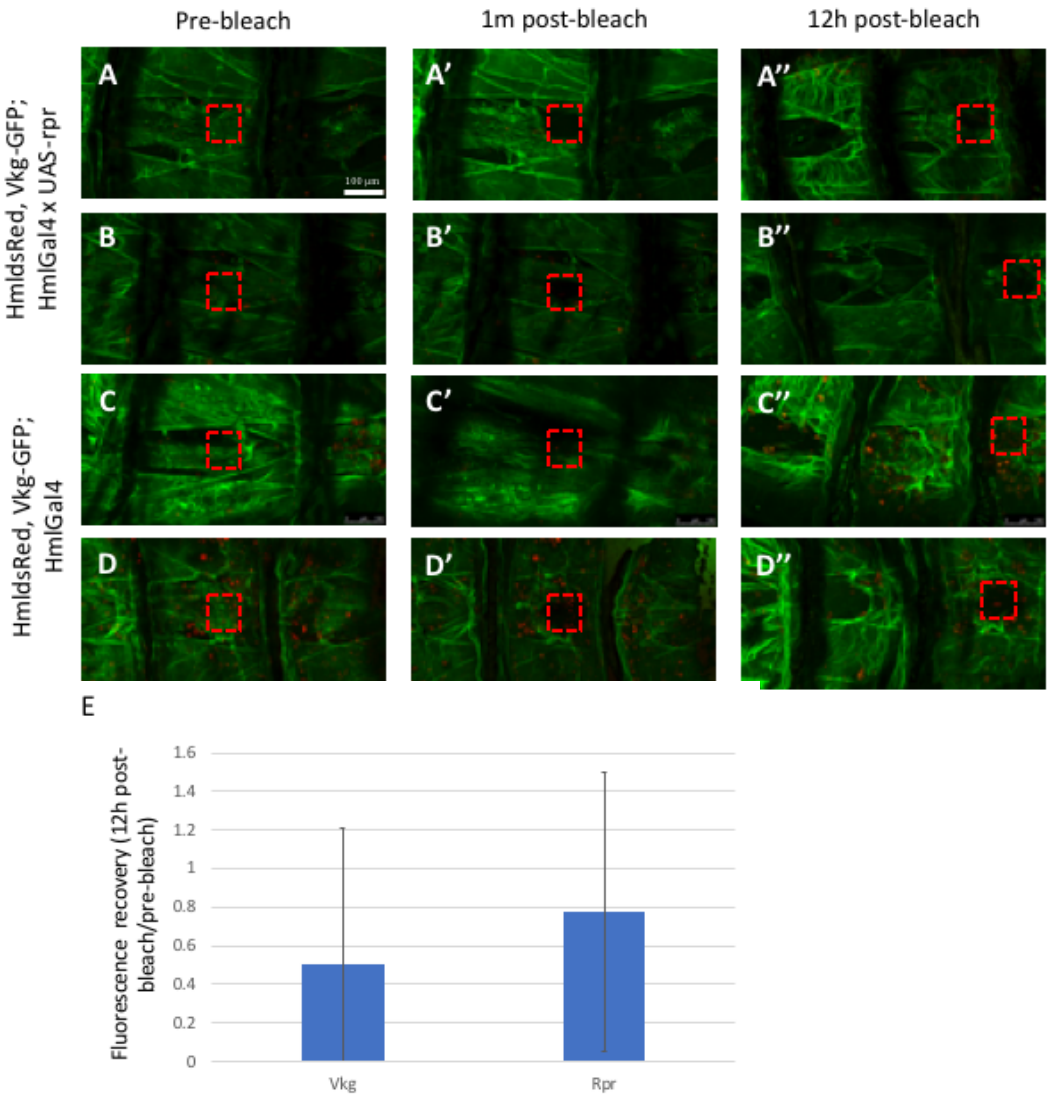

Figure 3.21: Hemocyte-specific *rpr* overexpression does not affect recovery of Vkg-GFP fluorescence 12h post-bleach in live, intact third instars. (A-A''; B-B''; C-C''; D-D'') Four examples of anesthetized third instar larvae pre-bleach (A, B, C, D); immediately post-bleach (A', B', C', D'); and 12h post-bleach (A'', B'', C'', D''). **(A-A'', B-B'')** Third instar larvae overexpressing *rpr* in hemocytes. **(C-C'', D-D'')** Third instar larvae in which *rpr* is not overespressed. First, a pre-bleach stack of the heart was generated (A, B, C). An ROI was then selected and photobleached using the same stack generated for the pre-bleach image (A', B', C'). Larvae were raised at 29°C to increase the apoptotic effect of *rpr* overexpression. A stack was then taken 12h after photobleaching to determine the extent of recovery at the photobleached ROI (A'', B'', C''). The extent of recovery varies between individuals but generally it appears very minimal or nonexistent. **(E)** Fluorescence recovery 12h post-bleach in wildtype (Vkg-GFP) and *rpr*-overexpressing individuals. Recovery is expressed at the gray value ratio from pre-bleach/12h post bleach

ROI, normalized to an arbitrary pre-bleach value. Recovery appears superior in *rpr* overexpression samples relative to controls. Green=Vkg-GFP; red=hemocytes. Overexpression of *rpr* was driven with the hemocyte-specific driver Hml-Gal4. ROIs in pre-, post- and 12h post-bleach are delineated by the red boxes. ROI dimensions: 66 x 66 μm. Photobleaching was performed on a Leica DM6000CS SP5 confocal microscope using the Argon laser to photobleach the GFP protein fused to Vkg. Cross: *HmldsRed, Vkg-GFP/CyO; Hml-Gal4/TM3 x UAS-rpr*. Genotype: *HmldsRed, Vkg-GFP/+; Hml-Gal4/+; UAS-rpr*. n= 8

For all recovery time points, changes in larval morphology and arrangement of internal structures took place between bleaching and re-imaging. These differences are likely also due to anesthesia, handling of larvae and normal growth. As a result, generating the same stack as used for bleaching, as well as locating the ROI was challenging. To demonstrate the extent to which morphology can differ between time points, I anesthetized, imaged, and 2h later re-imaged third instar Vkg-GFP larvae with no bleaching (no ROI) (Fig.3.22). Using the same stack parameters used at time 0, the images (3D projection) generated after re-imaging look remarkably different from the original projections.

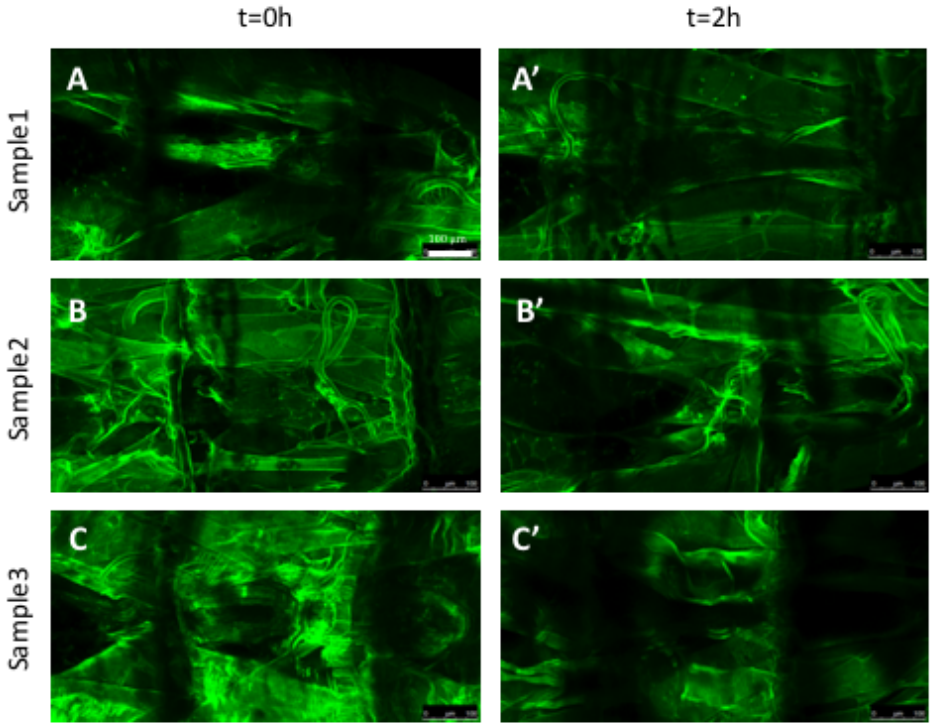

Figure 3.22: Significant morphological changes occur inherently in anesthetized, third instar larvae without photobleaching. (A-A'; B-B'; C-C') Anesthetized third instar larvae were imaged at time 0 (t=0h) and again 2h later (t=2h). Morphological changes are evident in the same animal 2h (A', B', C') after the initial stacks (A, B, C) were taken. This could be due to anesthesia, handling, or both. Green=Vkg-GFP. Imaging was performed on a Leica DM6000CS SP5 confocal microscope. Genotype: Vkg-GFP (trap). n=3.

Chapter 4: Discussion

4.1 Functionally impaired hemocytes fail to accumulate at discrete pockets near the *Drosophila* heart

Drosophila larval hemocytes are known to localize at discrete, segmentally repeated pockets along the dorsal midline. Perturbation of hemocyte function and behaviour can lead to defects in hemocyte association with these 'hematopoietic hubs' (Gyoergy et al., 2018; Letourneau et al., 2016). A powerful way to determine the effects of manipulating hemocyte function on their localization is to use the established Gal4-UAS system. Using the hemocyte-specific driver Hemolectin (*Hml)-Gal4*, I drove overexpression of the pro-apoptotic gene *rpr* as well as expression of *shi-RNAi* and the temperature sensitive allele shi^{ts} to reduce Dynamin expression in hemocytes and determine the consequences of killing or impairing endocytosis/exocytosis in these cells, respectively. With *rpr* overexpression, hemocyte abundance relative to control (*Hml-Gal4 x yw* raised at room temperature) larvae was reduced as expected. Hemocytes also did not appear to associate as closely with one another and were not organized in patches along the dorsal midline as they are in wildtype controls. These phenotypes were more pronounced at 29°C relative to larvae raised with temperature shift (18-29°C). Exposure to higher temperatures is a method used to increase the potency of Gal4 function (Schinko et al., 2010).

Defective localization along the dorsal midline was also observed when *shi* expression was knocked down. It is difficult to determine if hemocyte abundance was also reduced in these individuals due to the scattered distribution of these cells compared to the tight clustering of wildtype hemocytes. The disrupted localization along the dorsal midline in *shi*-impaired hemocytes was less pronounced than in *rpr* overexpression experiments.

Drosophila Dynamin, the protein encoded by *shi,* is needed for the clathrin-dependent endocytosis and exocytosis of vesicles (Menon & Schafer, 2013; van der Bliek & Meyerowitz, 1991). The impairment of vesicle trafficking and consequently membrane cycling, is known to paralyze cells (van der Bliek & Meyerowitz, 1991). Here, *shi*-impaired hemocytes may exhibit membrane cycling defects resulting in failure to migrate to hematopoietic pockets, resulting in disrupted localization. The phenotype caused by the knockdown of *shi* expression is therefore not as severe as the phenotype of *rpr* overexpression, which caused increased cell death.

4.2 Hemocyte-specific functional impairment does not lead to heart tube defects but does disrupt ECM proteins Prc and Vkg

Drosophila embryonic hemocytes have been shown to deposit ECM proteins as they migrate (Matsubayashi et al., 2017; Olofsson & Page, 2005; Sánchez-Sánchez et al., 2017). These proteins include the basement membrane components Laminin and Viking (Collagen IV). The contribution of hemocytes to ECM formation, organization, and integrity at later developmental stages, such as in larvae, is poorly understood. I present preliminary findings regarding hemocyte involvement in the formation of the larval cardiac ECM. Hemocytes were impaired as previously described. The consequent impacts on heart morphology, ECM integrity, and hemocyte behaviour were assessed.

It is important to note that the control used (*Hml-Gal4 x yw* raised at room temperature) only controls for genetic background effects. To control for gene expression as well as temperature-dependent effects, additional controls should be included in these experiments. For instance, the same crosses used to induce hemocyte-specific functional impairment should be set up at 18°C to limit potency of the Gal4 driver from

embryogenesis to L3. Progeny from the control cross should also be raised according to the same two temperature treatments used for hemocyte functional impairment crosses to control for any temperature-based differences between experimental groups. Lastly, all genotypes used in crosses (e.g. *Hml-Gal4, yw,* and all UAS lines) should be assessed individually (i.e. not outcrossed) based on the temperature treatments used to control for the effects of *Hml* and *UAS* on gene expression. The need for additional controls is in part due to the off-target binding of the Gal4 transcription factor. Although Gal4 is known to bind the short UAS enhancer sequence, it has also been shown to bind off-target sequences (Busson & Pret, 2007; Traven et al., 2006). It is therefore important to control for effects that the Gal4 transcription factor alone has on gene expression and phenotype. Furthermore, 'leaky' expression of genes or RNAis fused to UAS have been reported. As such, the effect of the activating sequence alone could result in constitutive activation of gene of interest (GOI) expression (Barwell et al., 2017).

4.2.1 Hemocyte-specific induction of apoptosis or impairment of membrane cycling does not result in heart formation defects

Knockdown of ECM proteins can lead to severe heart defects such as cardia bifida and fibrosis from increased Collagen deposition (Hughes & Jacobs, 2017). If hemocytes are implicated in larval cardiac ECM formation, I hypothesized that impairing hemocyte function would to lead to defects in the integrity of the heart tube. On the contrary, no major morphological heart defects were observed. Induction of hemocyte apoptosis with *rpr* overexpression or impairment of membrane cycling via expression of either *shi RNAi* or shi^{ts} did not result in morphological abnormalities of the heart tube or its alary muscles.

These results suggest that development of the heart tube and its supporting muscles occurs independent of hemocyte activity at the larval stage of development.

4.2.2 Hemocyte-specific induction of apoptosis or impairment of membrane cycling results in some disruption of the Prc network surrounding the heart

Although no defects in heart tube integrity were observed following manipulation of hemocyte function, I hypothesized that inducing hemocyte apoptosis and impairing their motility would lead to disruption in the organization and abundance of major ECM proteins at the third instar stage. One of the ECM components I examined was Pericardin, the *Drosophila* heart-specific Collagen IV protein (Drechsler et al., 2013; Rotstein & Paululat, 2016). Prc is a fibrous protein that forms a dynamic and complex network over the heart (Cevik et al., 2019; Rotstein & Paululat, 2016). In wildtype control samples there is extensive diversity in Prc fiber organization, thickness, and abundance. Therefore, there exists no clearly defined profile of a 'normal' Prc network. To reduce apparent diversity in fiber size, orientation, and arrangement, very precise staging of larvae within the third instar developmental stage should be performed. As such, imprecise staging of larvae could be eliminated as a cause of Prc network diversity. Due to the complex arrangement of Prc it can be difficult to discern fibers from one another and to determine the thickness of individual fibers or quantify their abundance.

Despite innate differences in Prc networks between individuals, decreased fiber abundance and density was apparent with hemocyte-specific expression of *rpr* and *shi RNAi*, particularly in individuals raised at 29°C compared to wildtype individuals. Hemocytes were hypothesized to play a role in alignment and deposition of Prc, similar to the way vertebrate fibroblasts behave in Collagen fiber organization (Alberts et al., 2002).

However, no clear Prc defects arose from hemocyte-specific expression of *shi*^{ts}. It is possible that the *shi RNAi* line is simply more effective in knocking down the function of *shi.* As such, hemocytes may still be implicated in the organization of Prc into a functional network, rather than in protein secretion. During embryogenesis, the pericardial cells are responsible for secretion of Prc (Wilmes et al., 2018). On the other hand, the majority of Prc in larvae is known to be secreted by the fat body from the first to second instar stages, although other cell types may contribute to a lesser degree to Prc secretion (Cevik, Acker, Michalski, et al., 2019; Wilmes et al., 2018). The importance of fat bodies in secretion of Prc makes them attractive targets to study the effects of Prc loss on ECM and heart formation. Loss of Prc or its ECM adaptor protein Lonely heart (Loh) is known to result in heart failure (Wilmes et al., 2018). Furthermore, knockdown of Sar1, a small COPII GTPase, in adipocytes prevents Prc secretion and consequently formation of a functional cardiac ECM (Saito et al., 2017; Wilmes et al., 2018). Without formation of a proper ECM to support it, the heart collapses (Wilmes et al., 2018).

Only a qualitative assessment of Prc network integrity under manipulation of hemocyte function was possible. These observations could be substantiated by quantification of Prc density and thickness of individual fibers. However, an objective, unbiased way to quantify fiber density and thickness has not yet been developed. Blind scoring is a candidate technique for the unbiased quantification of Prc fiber density and thickness. An automated approach would likely be best to assess differences in experimental groups with regard to fiber thickness and distance between fibers. An alternate technique that could allow for quantification of Prc fiber thickness and abundance is stereology. This involves examining two-dimensional objects as three-dimensional objects (Cakmak & Ragbetli, 2019).

Stereological techniques are commonly used to quantify objects in histological applications (West, 1999). Using this method, Prc fiber thickness and density could be quantified via stacks or three-dimensional projections of stacks (West, 1999). Quantification of Prc fibers would reveal the changes in Prc fiber distribution and quantity, and by extension the differences in ECM integrity, between experimental groups.

4.2.3 Hemocyte-specific induction of apoptosis or impairment of membrane cycling results in disruption of the Vkg network surrounding the heart

Viking, also known as *Drosophila* Collagen IV, is a significant structural protein of the ECM basement membrane. Embryonic *Drosophila* hemocytes have been shown to deposit Vkg as they migrate to colonize the embryo (Matsubayashi et al., 2017). Here I sought determine if hemocytes at the larval stage remain key players of Vkg secretion at the cardiac ECM. Induction of apoptosis in hemocytes was postulated to cause decreased abundance and defective distribution of Vkg. In fact, relative to control animals raised at room temperature, larvae overexpressing *rpr* in hemocytes exhibited increased clumping of Vkg as well as bright puncta at the cardiac ECM. The augmented presence of holes in the Vkg network was another characteristic of hemocyte-impaired individuals. Tremendous growth of the heart and its ECM occurs during larval stages. Tearing and clumping of protein networks is a product of such growth but nonetheless appears more prominent in larvae exhibiting hemocyte functional impairment. The Vkg defects observed with *rpr* overexpression imply that some threshold hemocyte volume is needed to produce or maintain uniform distribution of Vkg over the heart. As expected, animals raised at 29°C displayed more severe phenotypes compared to temperature shifted individuals for all genotypes. The uniformity of Vkg distribution over the heart as well as its abundance

appeared disrupted by all hemocyte impairments. Other defects observed in the Vkg network, such as the increased presence of holes and the fibrous appearance of Vkg suggest a role for hemocytes in maintaining the integrity of Vkg distribution at the larval stage. The Vkg phenotypes observed with hemocyte impairment are similar to defects observed in MMP mutants (C. Hughes, 2018). This further supports the theory that hemocytes are important in remodeling and turnover of Vkg in the cardiac ECM.

4.2.4 Hemocyte abundance, shape, and association with the heart are disturbed following hemocyte-specific induction of apoptosis or impairment of membrane cycling

The ECM related activities of hemocytes, including protein deposition and arrangement in the network may be revealed by altering their abundance or motility. I characterized change in the volume of hemocytes for all genotypes studied using the ImageJ plugin Volumest. The volume of hemocyte clusters at and around the heart was calculated per stack of images comprising one sample. Volume was chosen as the measure of hemocyte quantity because counting of individual hemocytes is impractical due to their tight clustering. Furthermore, measuring the area covered by hemocytes from a 3D projection is not an accurate assessment of their quantity because it does not represent all planes imaged. In accordance with the appearance of far fewer hemocytes in *rpr* overexpression samples, the difference in mean hemocyte volumes between the *rpr* overexpression group raised at 29°C and the control group was found to be statistically significant (p-value: 0.0001). The difference between the mean hemocyte volume of the *rpr* overexpression group shifted from 18-29°C and the control group was also statistically significant (p-value: 0.0002). This implies that first, *rpr* overexpression in hemocytes was the most powerful impairment of hemocyte function. Because *rpr* induces apoptosis, its overexpression in hemocytes was

expected to reduce their numbers more drastically than impairment of vesicle trafficking. In contrast, the augmented hemocyte volume calculated when *shi RNAi* was expressed in hemocytes could be a consequence of impaired motility. Impairing endocytosis and exocytosis reduces or eliminates membrane cycling, which is required for the polarization of plasma membrane proteins (van der Bliek & Meyerowitz, 1991). This, in turn is needed for cellular directed migration (Jones et al., 2006). For example, if cells have decreased ability to traffic vesicles, their migration is compromised, and they become paralyzed and/or unable to separate from each other or from some other extracellular surface such as pericardial cells or the ECM. The increase in total hemocyte volume occurred in tandem with a block in cytokinesis, as discussed further below. Conversely, hemocyte volumes in shi^{ts} experiments were inferior to control hemocyte volumes, which does not parallel the results seen with expression of *shi-RNAi* in hemocytes.

Whereas *rpr*-overexpressing hemocytes failed to cluster, cells with reduced *shi* function exhibited increased clustering around the heart, potentially from limited ability to migrate. Increased clustering could be the result of attractive cues drawing them towards the heart, similar to the attraction of hemocytes to hematopoetic pockets by peripheral nervous system (PNS) neurons (Makhijani et al., 2011). The ECM protein Prc has also been shown to facilitate to accumulation of hemocytes at the heart (Cevik, Acker, Michalski, et al., 2019). It is possible that reducing the expression of *shi* in hemocytes has a similar effect clustering of hemocytes near the heart.

In addition to determining hemocyte volume in impaired and unimpaired sample, cell shape and size was also qualitatively observed. The shape of a cell is also indicative of its function, stage in the cell cycle, and homeostatic state (Leitão & Sucena, 2015).

Plasmatocytes typically have a relatively irregular, elongated cell shape reminiscent of vertebrate fibroblasts (Hong et al., 2018; Leitão & Sucena, 2015). Plasmatocytes also produce cytoplasmic protrusions termed lamellipodia and filopodia, the latter of which extend beyond the leading edge of migrating cells, causing them to have a spindle-like shape (Hong et al., 2018; Sánchez-Sánchez et al., 2017). These structure serve to help the cell migrate along and adhere to surfaces such as the ECM, and are indicative of a motile cell interacting with external substrates (Hong et al., 2018; Matsubayashi et al., 2017). Hemocyte overexpressing *rpr* did not appear to exhibit the hallmark characteristics of motile plasmatocytes, suggesting that they are inactive and unable to migrate and/or adhere to extracellular substrates. It is interesting to note that although hemocyte numbers, shape, and adhesion were all drastically effected by *rpr* overexpression, severe heart defects were not observed. In fact, some animals in which hemocyte-specific *rpr* overexpression was induced survived to adulthood (data not shown). These findings imply that larval hemocytes are not needed for organismal survival.

Differences in cell size were also noted when hemocytes were functionally impaired, such as the small round cells observed with *rpr* overexpression. Hemocyte-specific expression of *shi RNAi* led to an increase in cell size, probably as a result of impaired cell division. Dynamin is a major link between membrane cycling and regulation of cytoskeletal dynamics, which are both required for cell division (Frémont & Echard, 2018; Konopka et al., 2006). The exact mechanisms through which Dynamin regulates cytokinesis and membrane trafficking is not completely understood, although Dynamin has been shown to mediate actin assembly and organization through interactions with F-actin

(Schafer, 2004). The ability of Dynamin to interact with the plasma membrane as well as the cytoskeleton render it a powerful player in the cell division and membrane cycling.

4.3 Recovery of fluorescence occurs in a time-dependent manner following photobleaching of Vkg-GFP

This work has provided some evidence that hemocytes play a role in ECM remodeling; the increased presence of holes and aggregates in the Vkg network seen with functional hemocyte impairment suggest some requirement for these cells in ECM integrity. The next step was to develop an *in vivo* approach to assess remodeling of Vkg at the cardiac ECM. An adaptation of fluorescence recovery after photobleaching (FRAP) was used to determine the recovery of GFP-labelled Vkg in live *Drosophila* third instar larvae. The concept of FRAP is not a novel one; its application in this system, however, is. FRAP is most often used to observe the movement of proteins as they diffuse in cells. This technique has not been applied on a larger scale to monitor recovery of fluorescently-labelled proteins through multiple tissue layers, such as the heart tube of a *Drosophila* larva. In this case, recovery of fluorescence is used as an indication of protein turnover at the ECM. Protein turnover can be defined as the balance between protein degradation and replacement via protein synthesis (Poortmans et al., 2012). Turnover of proteins is essential to maintain the integrity of the cardiac ECM (Hughes & Jacobs, 2017). Here I present preliminary results concerning the turnover of Vkg at the cardiac ECM in *Drosophila* third instars.

I developed an adaptation of FRAP to determine the extent to which the ECM protein Vkg is turned over at different time points. Due to the depth penetrated by the laser to effectively bleach a region of interest, and due to the strength of laser needed to bleach

through many tissue layers, I anticipated a very slow recovery of fluorescence. The first recovery time point tested was therefore 24h post-bleach. Significant recovery was observed when larvae were allowed to recover for 24h before re-imaging, although the bleached ROI was still identifiable as a fainter region relative to surrounding areas. This indicates that either more time is needed for full recovery of Vkg-GFP after photobleaching, or that Vkg-GFP is incapable of full recovery after photobleaching in this system. As discussed, the role of hemocytes in deposition of ECM proteins is not well understood at the *Drosophila* larval stage. The implications of these cells in protein turnover at the ECM at the larval stage is also not well documented. Here I sought to determine the consequences of reducing hemocyte abundance on recovery of Vkg-GFP relative to recovery in unimpaired individuals. To do this, *rpr* overexpression was induced in a hemocyte-specific manner and FRAP was performed as described. Animals expressing hemocyte-specific *rpr* overexpression do in fact appear to exhibit reduced recovery of Vkg-GFP relative to wildtype controls. Hemocytes may therefore be important players in turnover of ECM proteins in larvae. This work suggests that fluorescence recovery is likely not due to recovery of GFP activity. The intensity of laser power used for photobleaching is likely too strong to have permitted for spontaneous recovery of GFP fluorescence. In typical FRAP experiments, fluorescent molecules are irreversibly bleached using high intensity laser light (González-González et al., 2012; Sinnecker et al., 2005). Recovery of fluorescence can therefore be attributed to the movement of unbleached molecules into the ROI to replace bleached molecules (Goehring et al., 2010; Sinnecker et al., 2005). One indication that recovery of fluorescence was not the result of recovery of GFP activity is the changes in ROI geometry (Goehring et al., 2010). In our model, the changes in ROI

shape and dimensions observed are likely due to movement of the animal during the bleaching period. Although anesthetized via chloroform, a heartbeat could still be detected in most animals, which was thought to disrupt the borders of the ROI during photobleaching. At this point we cannot be certain that the recovery of fluorescence observed is due to innate protein turnover within the intact bleached tissue. It is also possible that photobleaching is damaging the tissue and that fluorescence recovery is the result of new ECM being laid down. One way to test this is to gradually decrease the laser intensity used to photobleach, and subsequently determine the extent of fluorescence recovery as well as the time required for recovery in the bleached region compared to samples bleached at a higher intensity.

Observing recovery at a time point after 24h would be interesting although challenging. The third instar stage lasts roughly 48h, at which point larvae begin to pupate and as a result are very difficult to image. Metamorphosis from larva to pupa is also characterized by removal of many ECM structures (Page-McCaw et al., 2003). This developmental constraint limits the time points at which recovery can be observed. Instead, I opted to assess recovery of Vkg-GFP at the shorter recovery time point of 12h. After observing substantial recovery of fluorescence at the 24h time point, some recovery was anticipated after 12h. Interestingly, very little to no recovery of fluorescence was observed at 12h post-bleach. Similarly, recovery in animals with induced hemocyte apoptosis also exhibited very limited to no recovery of Vkg-GFP after 12h. These results suggest that the recovery of Vkg-GFP seen at 24h post-bleach occurs between 12h and 24h post-bleach, the bulk of which does not take place before the 12h mark.

In order to test the theory that recovery of Vkg-GFP fluorescence is not regained quickly in third instar larvae, the recovery time point of 2h was tested. As expected, no recovery was observed at this time in any of the animals assayed. Clearly, recovery of fluorescence, and by association Vkg turnover does not occur within 2h of photobleaching. To demonstrate the apparent anatomical differences between pre- and post- bleach imaging, anesthetized third instar larvae were imaged without photobleaching, then again 2h later. The resulting structural differences in t=0h and t=2h are apparent in 3D projections from the same animal and are likely due to a combination of larval handling, anesthesia, mounting, laser exposure, and normal growth. The treatment of larvae for imaging often had deleterious effects on recovery and survival of the animals. Frequently (roughly 30-50%), individuals died following photobleaching, either as a result of anesthesia, mounting, bleaching, or a combination of the three.

An additional challenge associated with the use of this technique was the precise localization of the ROI at 2h, 12h, and 24h post-bleach. Although all ROIs were situated within segment A7 of the *Drosophila* heart chamber, changes in tissue conformation over time made precise targeting of the bleached zone difficult. Distinct morphological features, and visibility of the bleached ROI were used to assess the location of the bleached imaging hours after bleaching. Improving the precision in localization of the ROI is necessary to assure correct assessment of fluorescence recovery and by association protein turnover during photobleaching experiments.

The *Drosophila* Collagen IV Viking is an essential component of the cardiac ECM. Observing the recovery of fluorescently-labelled Vkg is a first step in understanding its innate turnover within the ECM. Investigating the recovery of other fluorescently tagged

ECM proteins such as Pericardin, Laminin, and Perlecan, should also be undertaken to gain a more complete picture of protein turnover at the cardiac ECM. Moreover, the technique developed here is based on the concept of FRAP but does not provide a perfectly accurate rate of protein turnover. The findings I present are more qualitative in nature than the results obtained from most traditional FRAP experiments. Common proteomic techniques used for the determination of protein turnover rates include pulse-chase and bleach-chase assays (Eden et al., 2011). Bleach-chase techniques are applicable to fluorescent proteins, whereby a fluorescent molecule is photobleached and subsequently monitored for recovery of fluorescence (Eden et al., 2011; Geva-Zatorsky et al., 2012). This method allows for the measurement of a protein's recovery half-life and provides an accurate and quantifiable rate of protein turnover (Geva-Zatorsky et al., 2012). Understanding the regulation of protein turnover at the cardiac ECM and the extent to which it occurs at different developmental stages is vital to comprehend ECM remodeling. This will help reveal the ECM dimension of many diseases, including cardiac fibrosis, arrhythmia, and cardiodilation, many of which can be modeled in *Drosophila* (Hughes & Jacobs, 2017).

4.4 Future directions and significance

The objective of much of the work reported here was to determine whether available tools could be applied to monitor turnover of the ECM *in vivo*, and whether a role for hemocytes could be revealed. This work has some success in both objectives, but both also require further investigation. Overexpression of the pro-apoptotic gene *rpr* and expression of *shi-RNAi* or shi^{ts} in hemocytes was performed to impair hemocyte function and determine the consequent effect on the heart ECM. The expression of myriad other genes can also be manipulated to alter hemocyte function and to reveal the role of those

genes in hemocyte behaviour, and by extension, in ECM formation. One candidate genes is *rhea*, which encodes the protein Talin, an essential component of the Integrin adhesion complex (Bogatan et al., 2015). Due to its importance in mediating Integrin adhesion to the ECM, Talin is also required for cardiomyocyte remodeling during heart growth and to position and expand the luminal domain of the *Drosophila* heart tube (Bogatan et al., 2015; Klapholz & Brown, 2017; Vanderploeg & Jacobs, 2015). Integrin, as a cell-surface receptor for BM proteins Laminin and Collagen, may also be vital to the adhesion of hemocytes to the ECM and could therefore be required for remodeling of ECM proteins (Klapholz & Brown, 2017). The Lysyl oxidase (*lox*) enzyme, which crosslinks ECM components Collagen and the mammalian protein Elastin, has a clear role in ECM remodeling (Vallet & Ricard-Blum, 2019). Because Lox is a secreted enzyme, it may also be implicated in hemocyte-mediated ECM protein turnover (Vallet & Ricard-Blum, 2019). The relationship between hemocytes, master ECM remodeling enzymes MMPs and TIMP, and ECM protein turnover also requires further investigation (Hughes, 2018).

In addition, many of the results obtained were qualitative, and often difficult to quantify objectively. For example, it was possible to determine the volume of hemocyte around the heart, however this does not allow for the counting of individual cells. This also prevents quantification of small versus larger cells. Impairment of hemocyte motility was only assessed using hemocyte volume, as well as observing hemocyte distribution and clumping. Assessing the effects of impaired *shi* expression on hemocyte membrane cycling and motility via larval dissection, confocal imaging, and subsequent calculation of hemocyte volume at the heart is a start but is indirect and imprecise. A useful technique to observe hemocyte motility is to record movement of fluorescently tagged hemocytes in

live, anesthetized larvae. Furthermore, an unbiased, random technique for the quantification of Pericardin fiber thickness and fiber density, or distance between fibers, has yet to be developed. The ability to quantify ECM fibers or protein abundance from confocal stacks would be an extremely useful tool to better understand matrix formation and integrity.

The *in vivo* photobleaching of intact larvae has never been reported in the literature. Although I have developed a protocol for the photobleaching of live, anesthetized larvae, this area of research is still poorly studied and understood. There remain many unaddressed parameters to in vivo photobleaching. One example is the assessment of fluorescent recovery between different developmental stages. The time constrains of this project allowed us to observe fluorescence recovery exclusively at the third instar stage. It is important to consider the developmental changes that occur between, for example, second and third instar stages, or from third instar to adulthood. It would also be beneficial to test the recovery of other major ECM proteins such as Pericardin and Laminin, and to determine the recovery of different ECM proteins under a variety of hemocyte impairments. Here I observed recovery of Vkg-GFP at three distinct time points following bleaching: 2h, 12h, 24h. Greater time resolution will better reveal the recovery of different ECM proteins at the *Drosophila* heart. Due to the lack of research concerning photobleaching in live tissue, it was a challenge to establish a minimum bleaching dose to avoid damage to the animal and/or bleaching of areas outside of the ROI. As a result, it is possible that the laser intensity selected for photobleaching experiments was too high, as some larvae did not survive bleaching experiments. In some cases, areas other than the ROI appear to have been affected by bleaching, because of laser intensity or displacement of

ECM. Lastly, a number of additional controls should be established and evaluated for fluorescence recovery of ECM proteins. For instance, an additional control could consist of anesthetizing and scanning a larva using a fluorescent channel other that the one used for bleaching. As such, photobleaching would not occur but otherwise the animal receives exactly the same treatment as a photobleached individual. This control would reveal the effects of manipulations, excluding photobleaching, on changes to larval morphology and survival.

Heart defects and associated illnesses affect a number of species, including countless humans worldwide. This work has revealed a possible role for hemocytes in turnover of Viking, a major ECM protein. Remodeling of the ECM is crucial to proper development of the heart and to ensuring the function of this organ over time. I have also developed a technique to study turnover of Vkg *in vivo* that is amenable to observe turnover of other fluorescently-labelled ECM proteins. Studying the molecular mechanisms underlying heart conditions using a simple genetic model like the fruit fly is a starting point to expanding our understanding of heart development, pathology, and will help generate improved tools and techniques to better prevent and mediate cardiac disorders.

References

Alberts, B., Johnson, A., Lewis, J., Raff, M., Roberts, K., & Walter, P. (2002). Fibroblasts and Their Transformations: The Connective-Tissue Cell Family. *Molecular Biology of the Cell. 4th Edition*. Retrieved from https://www.ncbi.nlm.nih.gov/books/NBK26889/

Axelrod, D., Koppel, D. E., Schlessinger, J., Elson, E., & Webb, W. W. (1976). Mobility measurement by analysis of fluorescence photobleaching recovery kinetics. *Biophysical Journal*, *16*(9), 1055–1069. https://doi.org/10.1016/S0006-3495(76)85755-4

Badylak, S. F., Freytes, D. O., & Gilbert, T. W. (2009). Extracellular matrix as a biological scaffold material: Structure and function. *Acta Biomaterialia*, *5*(1), 1–13. https://doi.org/10.1016/j.actbio.2008.09.013

Bandtlow, C. E., & Zimmermann, D. R. (2000). Proteoglycans in the developing brain: New conceptual insights for old proteins. *Physiological Reviews*, *80*(4), 1267–1290. https://doi.org/10.1152/physrev.2000.80.4.1267

Bangs, P., & White, K. (2000). Regulation and execution of apoptosis during Drosophila development. *Developmental Dynamics*, *218*(1), 68–79. https://doi.org/10.1002/(SICI)1097-0177(200005)218:1<68::AID-DVDY6>3.0.CO;2-9

Barwell, T., DeVeale, B., Poirier, L., Zheng, J., Seroude, F., & Seroude, L. (2017). Regulating the UAS/GAL4 system in adult Drosophila with Tet-off GAL80 transgenes. *PeerJ*, *5*. https://doi.org/10.7717/peerj.4167

Bataillé, L., Frendo, J.-L., & Vincent, A. (2015). Hox control of Drosophila larval anatomy; The Alary and Thoracic Alary-Related Muscles. *Mechanisms of Development*, *138*, 170–176. https://doi.org/10.1016/j.mod.2015.07.005

Bier, E. (2005). Drosophila, the golden bug, emerges as a tool for human genetics. *Nature Reviews. Genetics*, *6*(1), 9–23. https://doi.org/10.1038/nrg1503

Birk, D. E., Zycband, E. I., Woodruff, S., Winkelmann, D. A., & Trelstad, R. L. (1997). Collagen fibrillogenesis in situ: Fibril segments become long fibrils as the developing tendon matures. *Developmental Dynamics: An Official Publication of the American Association of Anatomists*, *208*(3), 291–298. https://doi.org/10.1002/(SICI)1097-0177(199703)208:3<291::AID-AJA1>3.0.CO;2-D

Bishop, J. R., Schuksz, M., & Esko, J. D. (2007). Heparan sulphate proteoglycans fine-tune mammalian physiology. *Nature*, *446*(7139), 1030–1037. https://doi.org/10.1038/nature05817

Bodmer, R., & Frasch, M. (2010). Chapter 1.2—Development and Aging of the Drosophila Heart. In N. Rosenthal & R. P. Harvey (Eds.), *Heart Development and Regeneration* (pp. 47–86). https://doi.org/10.1016/B978-0-12-381332-9.00002-5

Bogatan, S., Cevik, D., Demidov, V., Vanderploeg, J., Panchbhaya, A., Vitkin, A., & Jacobs, J. R. (2015). Talin Is Required Continuously for Cardiomyocyte Remodeling during Heart Growth in Drosophila. *PloS One*, *10*(6), e0131238. https://doi.org/10.1371/journal.pone.0131238

Bonnans, C., Chou, J., & Werb, Z. (2014). Remodelling the extracellular matrix in development and disease. *Nature Reviews. Molecular Cell Biology*, *15*(12), 786–801. https://doi.org/10.1038/nrm3904

Busson, D., & Pret, A.-M. (2007). GAL4/UAS targeted gene expression for studying Drosophila Hedgehog signaling. *Methods in Molecular Biology (Clifton, N.J.)*, *397*, 161–201. https://doi.org/10.1007/978-1-59745-516-9_13

Cakmak, G., & Ragbetli, M. C. (n.d.). A stereological analysis on the calculation of the volume values of thoracic segments in ducks. *Anatomia, Histologia, Embryologia*, *0*(0). https://doi.org/10.1111/ahe.12435

Cammarato, A., Dambacher, C. M., Knowles, A. F., Kronert, W. A., Bodmer, R., Ocorr, K., & Bernstein, S. I. (2007). Myosin Transducer Mutations Differentially Affect Motor Function, Myofibril Structure, and the Performance of Skeletal and Cardiac Muscles. *Molecular Biology of the Cell*, *19*(2), 553–562. https://doi.org/10.1091/mbc.e07-09-0890

Cevik, D. (2016). *Hemocyte-pericardial cell interaction during the growth of the dorsal vessel* (Thesis). Retrieved from https://macsphere.mcmaster.ca/handle/11375/19217

Cevik, D., Acker, M., Arefi, P., Ghaemi, R., Zhang, J., Ravi Selvaganapathy, P., … Roger Jacobs, J. (2019). Chloroform and Desflurane Immobilization with Recovery of Viable Drosophila Larvae for Confocal Imaging. *Journal of Insect Physiology*, 103900. https://doi.org/10.1016/j.jinsphys.2019.103900

Cevik, D., Acker, M., Michalski, C., & Jacobs, J. R. (2019). Pericardin, a Drosophila collagen, facilitates accumulation of hemocytes at the heart. *Developmental Biology*, *454*(1), 52–65. https://doi.org/10.1016/j.ydbio.2019.06.006

Chen, C., Wang, X., Jiang, H., & Hu, W. (2007). Direct observation of macromolecular structures of humic acid by AFM and SEM. *Colloids and Surfaces A: Physicochemical and Engineering Aspects*, *302*(1), 121–125. https://doi.org/10.1016/j.colsurfa.2007.02.014

Chen, P., Nordstrom, W., Gish, B., & Abrams, J. M. (1996). Grim, a novel cell death gene in Drosophila. *Genes & Development*, *10*(14), 1773–1782. https://doi.org/10.1101/gad.10.14.1773

Clavería, C., Albar, J. P., Serrano, A., Buesa, J. M., Barbero, J. L., Martínez-A, C., & Torres, M. (1998). Drosophila grim induces apoptosis in mammalian cells. *The EMBO Journal*, *17*(24), 7199–7208. https://doi.org/10.1093/emboj/17.24.7199

Cui, H., Freeman, C., Jacobson, G. A., & Small, D. H. (2013). Proteoglycans in the central nervous system: Role in development, neural repair, and Alzheimer's disease. *IUBMB Life*, *65*(2), 108–120. https://doi.org/10.1002/iub.1118

Das, D., Aradhya, R., Ashoka, D., & Inamdar, M. (2008). Post-embryonic pericardial cells of Drosophila are required for overcoming toxic stress but not for cardiac function or adult development. *Cell and Tissue Research*, *331*(2), 565–570. https://doi.org/10.1007/s00441-007-0518-z

de Castro Brás, L. E., Toba, H., Baicu, C. F., Zile, M. R., Weintraub, S. T., Lindsey, M. L., & Bradshaw, A. D. (2014). Age and SPARC change the extracellular matrix composition of the left ventricle. *BioMed Research International*, *2014*, 810562. https://doi.org/10.1155/2014/810562

Deepa, S. S., Carulli, D., Galtrey, C., Rhodes, K., Fukuda, J., Mikami, T., … Fawcett, J. W. (2006). Composition of perineuronal net extracellular matrix in rat brain: A different disaccharide composition for the net-associated proteoglycans. *The*

Journal of Biological Chemistry, *281*(26), 17789–17800. https://doi.org/10.1074/jbc.M600544200

Drechsler, M., Schmidt, A. C., Meyer, H., & Paululat, A. (2013). The Conserved ADAMTS-like Protein Lonely heart Mediates Matrix Formation and Cardiac Tissue Integrity. *PLOS Genetics*, *9*(7), e1003616. https://doi.org/10.1371/journal.pgen.1003616

Dulcis, D., & Levine, R. B. (2003). Innervation of the heart of the adult fruit fly, Drosophila melanogaster. *The Journal of Comparative Neurology*, *465*(4), 560–578. https://doi.org/10.1002/cne.10869

Eden, E., Geva-Zatorsky, N., Issaeva, I., Cohen, A., Dekel, E., Danon, T., … Alon, U. (2011). Proteome Half-Life Dynamics in Living Human Cells. *Science*, *331*(6018), 764–768. https://doi.org/10.1126/science.1199784

Evans, E. K., Kuwana, T., Strum, S. L., Smith, J. J., Newmeyer, D. D., & Kornbluth, S. (1997). Reaper-induced apoptosis in a vertebrate system. *The EMBO Journal*, *16*(24), 7372–7381. https://doi.org/10.1093/emboj/16.24.7372

Ezkurdia, I., Juan, D., Rodriguez, J. M., Frankish, A., Diekhans, M., Harrow, J., … Tress, M. L. (2014). Multiple evidence strands suggest that there may be as few as 19,000 human protein-coding genes. *Human Molecular Genetics*, *23*(22), 5866–5878. https://doi.org/10.1093/hmg/ddu309

Frantz, C., Stewart, K. M., & Weaver, V. M. (2010). The extracellular matrix at a glance. *Journal of Cell Science*, *123*(Pt 24), 4195–4200. https://doi.org/10.1242/jcs.023820

Frémont, S., & Echard, A. (2018). Membrane Traffic in the Late Steps of Cytokinesis. *Current Biology: CB*, *28*(8), R458–R470. https://doi.org/10.1016/j.cub.2018.01.019

Geva-Zatorsky, N., Issaeva, I., Mayo, A., Cohen, A., Dekel, E., Danon, T., … Eden, E. (2012). Using bleach-chase to measure protein half-lives in living cells. *Nature Protocols*, *7*(4), 801–811. https://doi.org/10.1038/nprot.2012.028

Ghosh, S., Mandal, S., & Mandal, L. (2018). Detecting proliferation of adult hemocytes in Drosophila by BrdU incorporation and PH3 expression in response to bacterial infection. *Wellcome Open Research*, *3*. https://doi.org/10.12688/wellcomeopenres.14560.2

Goehring, N. W., Chowdhury, D., Hyman, A. A., & Grill, S. W. (2010). FRAP Analysis of Membrane-Associated Proteins: Lateral Diffusion and Membrane-Cytoplasmic Exchange. *Biophysical Journal*, *99*(8), 2443–2452. https://doi.org/10.1016/j.bpj.2010.08.033

González-González, I. M., Jaskolski, F., Goldberg, Y., Ashby, M. C., & Henley, J. M. (2012). Measuring Membrane Protein Dynamics in Neurons Using Fluorescence Recovery after Photobleach. *Methods in Enzymology*, *504*, 127–146. https://doi.org/10.1016/B978-0-12-391857-4.00006-9

Gougeon, M.-L., Garcia, S., Heeney, J., Tschopp, R., Lecoeur, H., Guetard, D., … Montagnier, L. (1993). Programmed Cell Death in AIDS-Related HIV and SIV Infections. *AIDS Research and Human Retroviruses*, *9*(6), 553–563. https://doi.org/10.1089/aid.1993.9.553

Gu, C., Yaddanapudi, S., Weins, A., Osborn, T., Reiser, J., Pollak, M., … Sever, S. (2010). Direct dynamin-actin interactions regulate the actin cytoskeleton. *The EMBO Journal*, *29*(21), 3593–3606. https://doi.org/10.1038/emboj.2010.249

Guha, A., Sriram, V., Krishnan, K. S., & Mayor, S. (2003). Shibire mutations reveal distinct dynamin-independent and -dependent endocytic pathways in primary cultures of Drosophila hemocytes. *Journal of Cell Science*, *116*(Pt 16), 3373–3386. https://doi.org/10.1242/jcs.00637

Gyoergy, A., Roblek, M., Ratheesh, A., Valoskova, K., Belyaeva, V., Wachner, S., … Siekhaus, D. E. (2018). Tools Allowing Independent Visualization and Genetic Manipulation of Drosophila melanogaster Macrophages and Surrounding Tissues. *G3: Genes, Genomes, Genetics*, g3.300452.2017. https://doi.org/10.1534/g3.117.300452

Hay, E. D. (1993). Extracellular matrix alters epithelial differentiation. *Current Opinion in Cell Biology*, *5*(6), 1029–1035. https://doi.org/10.1016/0955-0674(93)90088-8

Hein, S., Gaasch, W. H., & Schaper, J. (2002). Giant molecule titin and myocardial stiffness. *Circulation*, *106*(11), 1302–1304. https://doi.org/10.1161/01.cir.0000031760.65615.3b

Heymans, S. (2006). Inflammation and cardiac remodeling during viral myocarditis. *Ernst Schering Research Foundation Workshop*, (55), 197–218.

Hildick, K. L., González-González, I. M., Jaskolski, F., & Henley, Jeremy. M. (2012). Lateral Diffusion and Exocytosis of Membrane Proteins in Cultured Neurons Assessed using Fluorescence Recovery and Fluorescence-loss Photobleaching. *Journal of Visualized Experiments : JoVE*, (60). https://doi.org/10.3791/3747

Hinkson, I. V., & Elias, J. E. (2011). The dynamic state of protein turnover: It's about time. *Trends in Cell Biology*, *21*(5), 293–303. https://doi.org/10.1016/j.tcb.2011.02.002

Hong, M., Hwang, D., & Cho, S. (2018). Hemocyte Morphology and Cellular Immune Response in Termite (Reticulitermes speratus). *Journal of Insect Science*, *18*(2). https://doi.org/10.1093/jisesa/iey039

Honti, V., Csordás, G., Kurucz, É., Márkus, R., & Andó, I. (2014). The cell-mediated immunity of Drosophila melanogaster: Hemocyte lineages, immune compartments, microanatomy and regulation. *Developmental & Comparative Immunology*, *42*(1), 47–56. https://doi.org/10.1016/j.dci.2013.06.005

Hughes, C. (2018). *The Larval Requirement for Matrix Metalloproteinase-Mediated Remodelling of the Cardiac Extracellular Matrix in Drosophila melanogaster* (Thesis). Retrieved from https://macsphere.mcmaster.ca/handle/11375/22878

Hughes, C. J. R., & Jacobs, J. R. (2017). Dissecting the Role of the Extracellular Matrix in Heart Disease: Lessons from the Drosophila Genetic Model. *Veterinary Sciences*, *4*(2). https://doi.org/10.3390/vetsci4020024

Hulmes, David J. S. (2002). Building collagen molecules, fibrils, and suprafibrillar structures. *Journal of Structural Biology*, *137*(1–2), 2–10. https://doi.org/10.1006/jsbi.2002.4450

Hulmes, D.J.S. (2008). Collagen Diversity, Synthesis and Assembly. In P. Fratzl (Ed.), *Collagen* (pp. 15–47). https://doi.org/10.1007/978-0-387-73906-9_2

Humphrey, J. D., Dufresne, E. R., & Schwartz, M. A. (2014). Mechanotransduction and extracellular matrix homeostasis. *Nature Reviews. Molecular Cell Biology*, *15*(12), 802–812. https://doi.org/10.1038/nrm3896

Hynes, R. O. (1992). Integrins: Versatility, modulation, and signaling in cell adhesion. *Cell*, *69*(1), 11–25. https://doi.org/10.1016/0092-8674(92)90115-S

Ivy, J. R., Drechsler, M., Catterson, J. H., Bodmer, R., Ocorr, K., Paululat, A., & Hartley, P. S. (2015). Klf15 Is Critical for the Development and Differentiation of Drosophila Nephrocytes. *PloS One*, *10*(8), e0134620. https://doi.org/10.1371/journal.pone.0134620

Jagla, K., Frasch, M., Jagla, T., Dretzen, G., Bellard, F., & Bellard, M. (1997). Ladybird, a new component of the cardiogenic pathway in Drosophila required for diversification of heart precursors. *Development (Cambridge, England)*, *124*(18), 3471–3479.

Jakeman, L. B., Williams, K. E., & Brautigam, B. (2014). In the presence of danger: The extracellular matrix defensive response to central nervous system injury. *Neural Regeneration Research*, *9*(4), 377–384. https://doi.org/10.4103/1673-5374.128238

Johnson, K. G., Ghose, A., Epstein, E., Lincecum, J., O'Connor, M. B., & Van Vactor, D. (2004). Axonal heparan sulfate proteoglycans regulate the distribution and efficiency of the repellent slit during midline axon guidance. *Current Biology: CB*, *14*(6), 499–504. https://doi.org/10.1016/j.cub.2004.02.005

Jones, M. C., Caswell, P. T., & Norman, J. C. (2006). Endocytic recycling pathways: Emerging regulators of cell migration. *Current Opinion in Cell Biology*, *18*(5), 549–557. https://doi.org/10.1016/j.ceb.2006.08.003

Kalluri, R. (2003). Basement membranes: Structure, assembly and role in tumour angiogenesis. *Nature Reviews. Cancer*, *3*(6), 422–433. https://doi.org/10.1038/nrc1094

Kim, E. H., Galchev, V. I., Kim, J. Y., Misek, S. A., Stevenson, T. K., Campbell, M. D., … Westfall, M. V. (2016). Differential protein expression and basal lamina remodeling in human heart failure. *Proteomics. Clinical Applications*, *10*(5), 585–596. https://doi.org/10.1002/prca.201500099

Kim, S. N., Jeibmann, A., Halama, K., Witte, H. T., Wälte, M., Matzat, T., … Klämbt, C. (2014). ECM stiffness regulates glial migration in Drosophila and mammalian glioma models. *Development (Cambridge, England)*, *141*(16), 3233–3242. https://doi.org/10.1242/dev.106039

King, J. G., & Hillyer, J. F. (2012). Infection-Induced Interaction between the Mosquito Circulatory and Immune Systems. *PLOS Pathogens*, *8*(11), e1003058. https://doi.org/10.1371/journal.ppat.1003058

Klapholz, B., & Brown, N. H. (2017). Talin—The master of integrin adhesions. *Journal of Cell Science*, *130*(15), 2435–2446. https://doi.org/10.1242/jcs.190991

Knudson, C. B., & Knudson, W. (2001). Cartilage proteoglycans. *Seminars in Cell & Developmental Biology*, *12*(2), 69–78. https://doi.org/10.1006/scdb.2000.0243

Kohfeldt, E., Sasaki, T., Göhring, W., & Timpl, R. (1998). Nidogen-2: A new basement membrane protein with diverse binding properties. *Journal of Molecular Biology*, *282*(1), 99–109. https://doi.org/10.1006/jmbi.1998.2004

Konopka, C. A., Schleede, J. B., Skop, A. R., & Bednarek, S. Y. (2006). Dynamin and Cytokinesis. *Traffic (Copenhagen, Denmark)*, *7*(3), 239–247. https://doi.org/10.1111/j.1600-0854.2006.00385.x

Kreis, T., & Vale, R. (1999). *Guidebook to the Extracellular Matrix, Anchor, and Adhesion Proteins*. Oxford University Press.

Krzemien, J., Oyallon, J., Crozatier, M., & Vincent, A. (2010). Hematopoietic progenitors and hemocyte lineages in the Drosophila lymph gland. *Developmental Biology*, *346*(2), 310–319. https://doi.org/10.1016/j.ydbio.2010.08.003

Kwok, J. C. F., Dick, G., Wang, D., & Fawcett, J. W. (2011). Extracellular matrix and perineuronal nets in CNS repair. *Developmental Neurobiology*, *71*(11), 1073–1089. https://doi.org/10.1002/dneu.20974

LaBeau, E. M., Trujillo, D. L., & Cripps, R. M. (2009). Bithorax complex genes control alary muscle patterning along the cardiac tube of Drosophila. *Mechanisms of Development*, *126*(5–6), 478–486. https://doi.org/10.1016/j.mod.2009.01.001

Lamiable, O., Arnold, J., Faria, I. J. da S. de, Olmo, R. P., Bergami, F., Meignin, C., … Imler, J.-L. (2016). Analysis of the Contribution of Hemocytes and Autophagy to Drosophila Antiviral Immunity. *Journal of Virology*, *90*(11), 5415–5426. https://doi.org/10.1128/JVI.00238-16

Lebestky, T. (2000). Specification of Drosophila Hematopoietic Lineage by Conserved Transcription Factors. *Science*, *288*(5463), 146–149. https://doi.org/10.1126/science.288.5463.146

Lehmacher, C., Abeln, B., & Paululat, A. (2012). The ultrastructure of Drosophila heart cells. *Arthropod Structure & Development*, *41*(5), 459–474. https://doi.org/10.1016/j.asd.2012.02.002

Leitão, A. B., & Sucena, É. (2015). Drosophila sessile hemocyte clusters are true hematopoietic tissues that regulate larval blood cell differentiation. *ELife*, *4*, e06166. https://doi.org/10.7554/eLife.06166

Letourneau, M., Lapraz, F., Sharma, A., Vanzo, N., Waltzer, L., & Crozatier, M. (2016). Drosophila hematopoiesis under normal conditions and in response to immune stress. *FEBS Letters*, *590*(22), 4034–4051. https://doi.org/10.1002/1873-3468.12327

Lieber, S. C., Aubry, N., Pain, J., Diaz, G., Kim, S.-J., & Vatner, S. F. (2004). Aging increases stiffness of cardiac myocytes measured by atomic force microscopy nanoindentation. *American Journal of Physiology. Heart and Circulatory Physiology*, *287*(2), H645-651. https://doi.org/10.1152/ajpheart.00564.2003

Lockhart, M., Wirrig, E., Phelps, A., & Wessels, A. (2011). Extracellular Matrix and Heart Development. *Birth Defects Research. Part A, Clinical and Molecular Teratology*, *91*(6), 535–550. https://doi.org/10.1002/bdra.20810

Lodish, H., Berk, A., Zipursky, S. L., Matsudaira, P., Baltimore, D., & Darnell, J. (2000). Collagen: The Fibrous Proteins of the Matrix. *Molecular Cell Biology. 4th Edition*. Retrieved from https://www.ncbi.nlm.nih.gov/books/NBK21582/

Lu, P., Takai, K., Weaver, V. M., & Werb, Z. (2011). Extracellular matrix degradation and remodeling in development and disease. *Cold Spring Harbor Perspectives in Biology*, *3*(12). https://doi.org/10.1101/cshperspect.a005058

Maeda, N., Ishii, M., Nishimura, K., & Kamimura, K. (2011). Functions of chondroitin sulfate and heparan sulfate in the developing brain. *Neurochemical Research*, *36*(7), 1228–1240. https://doi.org/10.1007/s11064-010-0324-y

Makhijani, K., Alexander, B., Rao, D., Petraki, S., Herboso, L., Kukar, K., … Brückner, K. (2017). Regulation of *Drosophila* hematopoietic sites by Activin-β from active sensory neurons. *Nature Communications*, *8*, 15990. https://doi.org/10.1038/ncomms15990

Makhijani, K., Alexander, B., Tanaka, T., Rulifson, E., & Brückner, K. (2011). The peripheral nervous system supports blood cell homing and survival in the Drosophila larva. *Development (Cambridge, England)*, *138*(24), 5379–5391. https://doi.org/10.1242/dev.067322

Mandal, L., Dumstrei, K., & Hartenstein, V. (2004). Role of FGFR signaling in the morphogenesis of the Drosophila visceral musculature. *Developmental Dynamics*, *231*(2), 342–348. https://doi.org/10.1002/dvdy.20088

Martin, G. R., & Timpl, R. (1987). Laminin and Other Basement Membrane Components. *Annual Review of Cell Biology*, *3*(1), 57–85. https://doi.org/10.1146/annurev.cb.03.110187.000421

Matsubayashi, Y., Louani, A., Dragu, A., Sánchez-Sánchez, B. J., Serna-Morales, E., Yolland, L., … Stramer, B. M. (2017). A Moving Source of Matrix Components Is Essential for De Novo Basement Membrane Formation. *Current Biology*, *27*(22), 3526-3534.e4. https://doi.org/10.1016/j.cub.2017.10.001

McCarthy, J. V., & Dixit, V. M. (1998). Apoptosis induced by Drosophila reaper and grim in a human system. Attenuation by inhibitor of apoptosis proteins (cIAPs). *The Journal of Biological Chemistry*, *273*(37), 24009–24015. https://doi.org/10.1074/jbc.273.37.24009

McNeal, D. W., Brandner, D. D., Gong, X., Postupna, N. O., Montine, T. J., Dirk Keene, C., & Back, S. A. (2016). Unbiased Stereological Analysis of Reactive Astrogliosis to Estimate Age-Associated Cerebral White Matter Injury. *Journal of Neuropathology & Experimental Neurology*, *75*(6), 539–554. https://doi.org/10.1093/jnen/nlw032

Mecham, R. P. (2001). Overview of extracellular matrix. *Current Protocols in Cell Biology*, *Chapter 10*, Unit 10.1. https://doi.org/10.1002/0471143030.cb1001s00

Menon, M., & Schafer, D. A. (2013). Chapter Three - Dynamin: Expanding Its Scope to the Cytoskeleton. In K. W. Jeon (Ed.), *International Review of Cell and Molecular Biology* (Vol. 302, pp. 187–219). https://doi.org/10.1016/B978-0-12-407699-0.00003-0

Molina, M. R., & Cripps, R. M. (2001). Ostia, the inflow tracts of the Drosophila heart, develop from a genetically distinct subset of cardial cells. *Mechanisms of Development*, *109*(1), 51–59.

Morin, X., Daneman, R., Zavortink, M., & Chia, W. (2001). A protein trap strategy to detect GFP-tagged proteins expressed from their endogenous loci in Drosophila. *Proceedings of the National Academy of Sciences*, *98*(26), 15050–15055. https://doi.org/10.1073/pnas.261408198

Mouw, J. K., Ou, G., & Weaver, V. M. (2014). Extracellular matrix assembly: A multiscale deconstruction. *Nature Reviews. Molecular Cell Biology*, *15*(12), 771–785. https://doi.org/10.1038/nrm3902

Mueller, F., Morisaki, T., Mazza, D., & McNally, J. G. (2012). Minimizing the Impact of Photoswitching of Fluorescent Proteins on FRAP Analysis. *Biophysical Journal*, *102*(7), 1656–1665. https://doi.org/10.1016/j.bpj.2012.02.029

Myllyharju, J., & Kivirikko, K. I. (2004). Collagens, modifying enzymes and their mutations in humans, flies and worms. *Trends in Genetics: TIG*, *20*(1), 33–43. https://doi.org/10.1016/j.tig.2003.11.004

Naba, A., Clauser, K. R., Hoersch, S., Liu, H., Carr, S. A., & Hynes, R. O. (2012). The matrisome: In silico definition and in vivo characterization by proteomics of normal and tumor extracellular matrices. *Molecular & Cellular Proteomics: MCP*, *11*(4), M111.014647. https://doi.org/10.1074/mcp.M111.014647

Nappi, A. J., & Vass, E. (1998). Hydrogen Peroxide Production in Immune-Reactive Drosophila melanogaster. *The Journal of Parasitology*, *84*(6), 1150–1157. https://doi.org/10.2307/3284664

Ocorr, K., Perrin, L., Lim, H.-Y., Qian, L., Wu, X., & Bodmer, R. (2007). Genetic control of heart function and aging in Drosophila. *Trends in Cardiovascular Medicine*, *17*(5), 177–182. https://doi.org/10.1016/j.tcm.2007.04.001

O'Leary, L. E. R., Fallas, J. A., Bakota, E. L., Kang, M. K., & Hartgerink, J. D. (2011). Multi-hierarchical self-assembly of a collagen mimetic peptide from triple helix to nanofibre and hydrogel. *Nature Chemistry*, *3*(10), 821–828. https://doi.org/10.1038/nchem.1123

Olofsson, B., & Page, D. T. (2005). Condensation of the central nervous system in embryonic Drosophila is inhibited by blocking hemocyte migration or neural activity. *Developmental Biology*, *279*(1), 233–243. https://doi.org/10.1016/j.ydbio.2004.12.020

Page-McCaw, A., Serano, J., Santé, J. M., & Rubin, G. M. (2003). Drosophila Matrix Metalloproteinases Are Required for Tissue Remodeling, but Not Embryonic Development. *Developmental Cell*, *4*(1), 95–106. https://doi.org/10.1016/S1534-5807(02)00400-8

Paulsson, M. (1992). Basement membrane proteins: Structure, assembly, and cellular interactions. *Critical Reviews in Biochemistry and Molecular Biology*, *27*(1–2), 93–127. https://doi.org/10.3109/10409239209082560

Pelouch, V., Dixon, I. M., Golfman, L., Beamish, R. E., & Dhalla, N. S. (1993). Role of extracellular matrix proteins in heart function. *Molecular and Cellular Biochemistry*, *129*(2), 101–120. https://doi.org/10.1007/bf00926359

Pincet, F., Adrien, V., Yang, R., Delacotte, J., Rothman, J. E., Urbach, W., & Tareste, D. (2016). FRAP to Characterize Molecular Diffusion and Interaction in Various Membrane Environments. *PLOS ONE*, *11*(7), e0158457. https://doi.org/10.1371/journal.pone.0158457

Poortmans, J. R., Carpentier, A., Pereira-Lancha, L. O., & Lancha, A. (2012). Protein turnover, amino acid requirements and recommendations for athletes and active populations. *Brazilian Journal of Medical and Biological Research*, *45*(10), 875–890. https://doi.org/10.1590/S0100-879X2012007500096

Raza, Q., & Jacobs, J. R. (2016). Guidance signalling regulates leading edge behaviour during collective cell migration of cardiac cells in Drosophila. *Developmental Biology*, *419*(2), 285–297. https://doi.org/10.1016/j.ydbio.2016.09.005

Rienks, M., Papageorgiou, A.-P., Frangogiannis, N. G., & Heymans, S. (2014). Myocardial extracellular matrix: An ever-changing and diverse entity. *Circulation Research*, *114*(5), 872–888. https://doi.org/10.1161/CIRCRESAHA.114.302533

Rienks Marieke, Papageorgiou Anna-Pia, Frangogiannis Nikolaos G., & Heymans Stephane. (2014). Myocardial Extracellular Matrix. *Circulation Research*, *114*(5), 872–888. https://doi.org/10.1161/CIRCRESAHA.114.302533

Rizki, T. M. (1978). Circulatory system and associated cells and tissues. *Genetics and Biology of Drosophila*. Retrieved from http://agris.fao.org/agris-search/search.do?recordID=US201301393040

Rotstein, B., & Paululat, A. (2016). On the Morphology of the Drosophila Heart. *Journal of Cardiovascular Development and Disease*, *3*(2), 15. https://doi.org/10.3390/jcdd3020015

Rotstein, B., Post, Y., Reinhardt, M., Lammers, K., Buhr, A., Heinisch, J. J., … Paululat, A. (2018). Distinct domains in the matricellular protein Lonely heart are crucial for cardiac extracellular matrix formation and heart function in Drosophila. *The Journal of Biological Chemistry*, *293*(20), 7864–7879. https://doi.org/10.1074/jbc.M117.817940

Rowe, R. G., & Weiss, S. J. (2008). Breaching the basement membrane: Who, when and how? *Trends in Cell Biology*, *18*(11), 560–574. https://doi.org/10.1016/j.tcb.2008.08.007

Rozario, T., & DeSimone, D. W. (2010). The extracellular matrix in development and morphogenesis: A dynamic view. *Developmental Biology*, *341*(1), 126–140. https://doi.org/10.1016/j.ydbio.2009.10.026

Saito, K., Maeda, M., & Katada, T. (2017). Regulation of the Sar1 GTPase Cycle Is Necessary for Large Cargo Secretion from the Endoplasmic Reticulum. *Frontiers in Cell and Developmental Biology*, *5*. https://doi.org/10.3389/fcell.2017.00075

Sánchez-Sánchez, B. J., Urbano, J. M., Comber, K., Dragu, A., Wood, W., Stramer, B., & Martín-Bermudo, M. D. (2017). Drosophila Embryonic Hemocytes Produce Laminins to Strengthen Migratory Response. *Cell Reports*, *21*(6), 1461–1470. https://doi.org/10.1016/j.celrep.2017.10.047

Sanes, J. R. (2003). The basement membrane/basal lamina of skeletal muscle. *The Journal of Biological Chemistry*, *278*(15), 12601–12604. https://doi.org/10.1074/jbc.R200027200

Schaefer, L., & Schaefer, R. M. (2010). Proteoglycans: From structural compounds to signaling molecules. *Cell and Tissue Research*, *339*(1), 237–246. https://doi.org/10.1007/s00441-009-0821-y

Schafer, D. A. (2004). Regulating actin dynamics at membranes: A focus on dynamin. *Traffic (Copenhagen, Denmark)*, *5*(7), 463–469. https://doi.org/10.1111/j.1600-0854.2004.00199.x

Schaub, C., März, J., Reim, I., & Frasch, M. (2015). Org-1-Dependent Lineage Reprogramming Generates the Ventral Longitudinal Musculature of the Drosophila Heart. *Current Biology*, *25*(4), 488–494. https://doi.org/10.1016/j.cub.2014.12.029

Schinko, J. B., Weber, M., Viktorinova, I., Kiupakis, A., Averof, M., Klingler, M., … Bucher, G. (2010). Functionality of the GAL4/UAS system in Tribolium requires

the use of endogenous core promoters. *BMC Developmental Biology*, *10*(1), 53. https://doi.org/10.1186/1471-213X-10-53

Sellin, J., Albrecht, S., Kölsch, V., & Paululat, A. (2006). Dynamics of heart differentiation, visualized utilizing heart enhancer elements of the Drosophila melanogaster bHLH transcription factor Hand. *Gene Expression Patterns: GEP*, *6*(4), 360–375. https://doi.org/10.1016/j.modgep.2005.09.012

Sessions, A. O., Kaushik, G., Parker, S., Raedschelders, K., Bodmer, R., Van Eyk, J. E., & Engler, A. J. (2017). Extracellular matrix downregulation in the Drosophila heart preserves contractile function and improves lifespan. *Matrix Biology: Journal of the International Society for Matrix Biology*, *62*, 15–27. https://doi.org/10.1016/j.matbio.2016.10.008

Shah, A. P., Nongthomba, U., Kelly Tanaka, K. K., Denton, M. L. B., Meadows, S. M., Bancroft, N., … Cripps, R. M. (2011). Cardiac remodeling in Drosophila arises from changes in actin gene expression and from a contribution of lymph gland-like cells to the heart musculature. *Mechanisms of Development*, *128*(3–4), 222–233. https://doi.org/10.1016/j.mod.2011.01.001

Sigle, L. T., & Hillyer, J. F. (2016). Mosquito hemocytes preferentially aggregate and phagocytose pathogens in the periostial regions of the heart that experience the most hemolymph flow. *Developmental & Comparative Immunology*, *55*, 90–101. https://doi.org/10.1016/j.dci.2015.10.018

Sigle, L. T., & Hillyer, J. F. (2018). Mosquito Hemocytes Associate With Circulatory Structures That Support Intracardiac Retrograde Hemolymph Flow. *Frontiers in Physiology*, *9*. https://doi.org/10.3389/fphys.2018.01187

Simon Davis, D. A., & Parish, C. R. (2013). Heparan sulfate: A ubiquitous glycosaminoglycan with multiple roles in immunity. *Frontiers in Immunology*, *4*, 470. https://doi.org/10.3389/fimmu.2013.00470

Singh, P., Carraher, C., & Schwarzbauer, J. E. (2010). Assembly of fibronectin extracellular matrix. *Annual Review of Cell and Developmental Biology*, *26*, 397–419. https://doi.org/10.1146/annurev-cellbio-100109-104020

Sinnecker, D., Voigt, P., Hellwig, N., & Schaefer, M. (2005). Reversible Photobleaching of Enhanced Green Fluorescent Proteins. *Biochemistry*, *44*(18), 7085–7094. https://doi.org/10.1021/bi047881x

Stamenkovic, I. (2003). Extracellular matrix remodelling: The role of matrix metalloproteinases. *The Journal of Pathology*, *200*(4), 448–464. https://doi.org/10.1002/path.1400

Tepass, U., Fessler, L. I., Aziz, A., & Hartenstein, V. (1994). Embryonic origin of hemocytes and their relationship to cell death in Drosophila. *Development*, *120*(7), 1829–1837.

Timpl, R., & Brown, J. C. (1994). The laminins. *Matrix Biology: Journal of the International Society for Matrix Biology*, *14*(4), 275–281.

Timpl, Rupert. (1996). Macromolecular organization of basement membranes. *Current Opinion in Cell Biology*, *8*(5), 618–624. https://doi.org/10.1016/S0955-0674(96)80102-5

Tögel, M., Pass, G., & Paululat, A. (2008). The Drosophila wing hearts originate from pericardial cells and are essential for wing maturation. *Developmental Biology*, *318*(1), 29–37. https://doi.org/10.1016/j.ydbio.2008.02.043

Traven, A., Jelicic, B., & Sopta, M. (2006). Yeast Gal4: A transcriptional paradigm revisited. *EMBO Reports*, *7*(5), 496–499. https://doi.org/10.1038/sj.embor.7400679

Tutor, A. S., Prieto-Sánchez, S., & Ruiz-Gómez, M. (2014). Src64B phosphorylates Dumbfounded and regulates slit diaphragm dynamics: Drosophila as a model to study nephropathies. *Development*, *141*(2), 367–376. https://doi.org/10.1242/dev.099408

Vallet, S. D., & Ricard-Blum, S. (2019). Lysyl oxidases: From enzyme activity to extracellular matrix cross-links. *Essays in Biochemistry*, *63*(3), 349–364. https://doi.org/10.1042/EBC20180050

van der Bliek, A. M., & Meyerowitz, E. M. (1991). Dynamin-like protein encoded by the Drosophila shibire gene associated with vesicular traffic. *Nature*, *351*(6325), 411–414. https://doi.org/10.1038/351411a0

Vanderploeg, J., & Jacobs, J. R. (2015). Talin is required to position and expand the luminal domain of the Drosophila heart tube. *Developmental Biology*, *405*(2), 189–201. https://doi.org/10.1016/j.ydbio.2015.04.024

Viswanathan, M. C., Kaushik, G., Engler, A. J., Lehman, W., & Cammarato, A. (2014). A Drosophila melanogaster model of diastolic dysfunction and cardiomyopathy based on impaired troponin-T function. *Circulation Research*, *114*(2), e6-17. https://doi.org/10.1161/CIRCRESAHA.114.302028

Volk, T., Wang, S., Rotstein, B., & Paululat, A. (2014). Matricellular proteins in development: Perspectives from the Drosophila heart. *Matrix Biology: Journal of the International Society for Matrix Biology*, *37*, 162–166. https://doi.org/10.1016/j.matbio.2014.03.006

Wade, A., McKinney, A., & Phillips, J. J. (2014). Matrix regulators in neural stem cell functions. *Biochimica Et Biophysica Acta*, *1840*(8), 2520–2525. https://doi.org/10.1016/j.bbagen.2014.01.017

Wang, D., & Fawcett, J. (2012). The perineuronal net and the control of CNS plasticity. *Cell and Tissue Research*, *349*(1), 147–160. https://doi.org/10.1007/s00441-012-1375-y

Wang, J. H.-C. (2006). Mechanobiology of tendon. *Journal of Biomechanics*, *39*(9), 1563–1582. https://doi.org/10.1016/j.jbiomech.2005.05.011

Wang, T.-H., Hsia, S.-M., & Shieh, T.-M. (2017). Lysyl Oxidase and the Tumor Microenvironment. *International Journal of Molecular Sciences*, *18*(1), 62. https://doi.org/10.3390/ijms18010062

Wasserthal, L. T. (2007). Drosophila flies combine periodic heartbeat reversal with a circulation in the anterior body mediated by a newly discovered anterior pair of ostial valves and "venous" channels. *The Journal of Experimental Biology*, *210*(Pt 21), 3707–3719. https://doi.org/10.1242/jeb.007864

Weavers, H., Prieto-Sánchez, S., Grawe, F., Garcia-López, A., Artero, R., Wilsch-Bräuninger, M., … Denholm, B. (2009). The insect nephrocyte is a podocyte-like cell with a filtration slit diaphragm. *Nature*, *457*(7227), 322–326. https://doi.org/10.1038/nature07526

Wess, T. J. (2005). Collagen fibril form and function. *Advances in Protein Chemistry*, *70*, 341–374. https://doi.org/10.1016/S0065-3233(05)70010-3

West, M. J. (1999). Stereological methods for estimating the total number of neurons and synapses: Issues of precision and bias. *Trends in Neurosciences*, *22*(2), 51–61. https://doi.org/10.1016/s0166-2236(98)01362-9

White, E. (1996). Life, death, and the pursuit of apoptosis. *Genes & Development*, *10*(1), 1–15. https://doi.org/10.1101/gad.10.1.1

White, K., Grether, M. E., Abrams, J. M., Young, L., Farrell, K., & Steller, H. (1994). Genetic control of programmed cell death in Drosophila. *Science*, *264*(5159), 677–683. https://doi.org/10.1126/science.8171319

Wilmes, A. C., Klinke, N., Rotstein, B., Meyer, H., & Paululat, A. (2018). Biosynthesis and assembly of the Collagen IV-like protein Pericardin in Drosophila melanogaster. *Biology Open*, *7*(4). https://doi.org/10.1242/bio.030361

Wiradjaja, F., DiTommaso, T., & Smyth, I. (2010). Basement membranes in development and disease. *Birth Defects Research. Part C, Embryo Today: Reviews*, *90*(1), 8–31. https://doi.org/10.1002/bdrc.20172

Wolf, M. J., Amrein, H., Izatt, J. A., Choma, M. A., Reedy, M. C., & Rockman, H. A. (2006). Drosophila as a model for the identification of genes causing adult human heart disease. *Proceedings of the National Academy of Sciences of the United States of America*, *103*(5), 1394–1399. https://doi.org/10.1073/pnas.0507359103

Wu, M., & Crane, J. S. (2019). Biochemistry, Collagen Synthesis. In *StatPearls*. Retrieved from http://www.ncbi.nlm.nih.gov/books/NBK507709/

Yamaguchi, Y. (2000). Lecticans: Organizers of the brain extracellular matrix. *Cellular and Molecular Life Sciences: CMLS*, *57*(2), 276–289. https://doi.org/10.1007/PL00000690

Yurchenco, P. D. (2011). Basement membranes: Cell scaffoldings and signaling platforms. *Cold Spring Harbor Perspectives in Biology*, *3*(2). https://doi.org/10.1101/cshperspect.a004911

Yurchenco, P. D., & Furthmayr, H. (1984). Self-assembly of basement membrane collagen. *Biochemistry*, *23*(8), 1839–1850. https://doi.org/10.1021/bi00303a040

Zaffran, S., Astier, M., Gratecos, D., Guillen, A., & Sémériva, M. (1995). Cellular interactions during heart morphogenesis in the Drosophila embryo. *Biology of the Cell*, *84*(1–2), 13–24.

Zhang, F., Zhao, Y., & Han, Z. (2013). An in vivo functional analysis system for renal gene discovery in Drosophila pericardial nephrocytes. *Journal of the American Society of Nephrology: JASN*, *24*(2), 191–197. https://doi.org/10.1681/ASN.2012080769

Zhang, L. (2010). Glycosaminoglycan (GAG) biosynthesis and GAG-binding proteins. *Progress in Molecular Biology and Translational Science*, *93*, 1–17. https://doi.org/10.1016/S1877-1173(10)93001-9

Zhuang, S., Shao, H., Guo, F., Trimble, R., Pearce, E., & Abmayr, S. M. (2009). Sns and Kirre, the Drosophila orthologs of Nephrin and Neph1, direct adhesion, fusion and formation of a slit diaphragm-like structure in insect nephrocytes. *Development*, *136*(14), 2335–2344. https://doi.org/10.1242/dev.031609